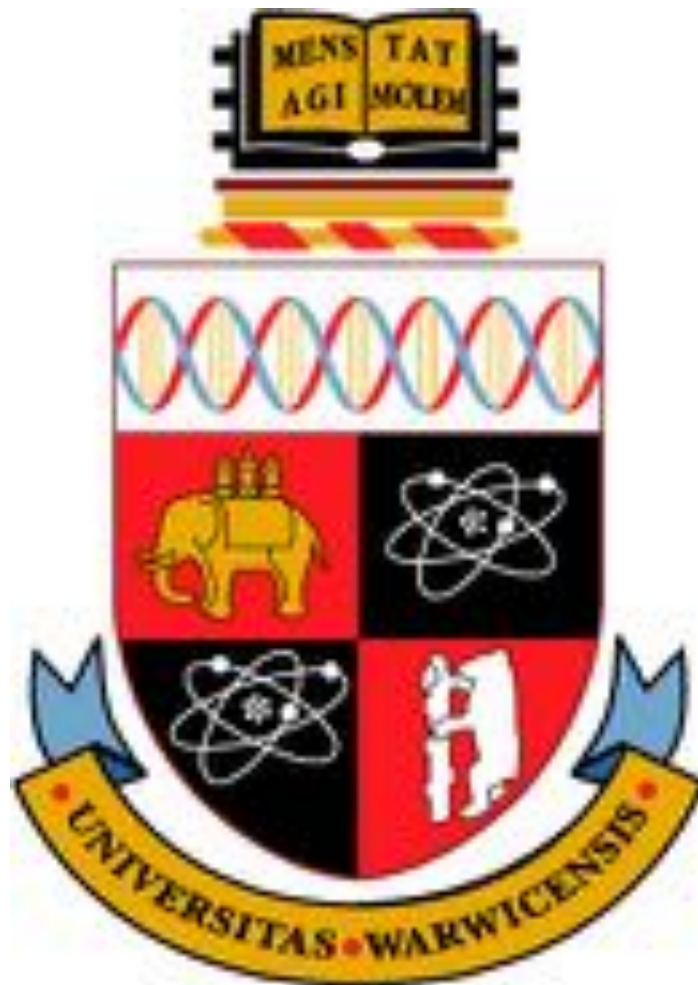


Cationic polymers and novel gold nanoparticle conjugate compounds: prospective antimicrobials?



Klea Isufi 1209538

MBio, Biomedical Sciences

Life Sciences, University of Warwick

Supervisor: Dr Elizabeth Fullam

May 2016

Abstract

Some strains of *Mycobacterium tuberculosis*, the etiologic agent of tuberculosis, have developed resistance to first-line antibiotics, rifampicin and isoniazid. Other drug-resistant bacteria, such as strains of *Escherichia coli*, have grown in prevalence in hospitals, causing a variety of infections no longer treatable by antibiotic agents. The development of new antimicrobial compounds is more paramount than ever. The use and manipulation of inorganic gold nanoparticles (AuNPs) by surface modifications with various ligands has become an innovative avenue for drug discovery and development. We synthesized gold nanoparticles with dimensions of 2nm, 5nm, 16nm and 36nm using a standard HAuCl₄/citrate reduction method. We aimed to modify these gold nanoparticles with combinations of two polymers, poly(2-dimethylamino)ethyl methacrylate (pDMAEMA) and poly(*N*-hydroxyethyl acrylamide) (pHEA) to form novel polymer-AuNP conjugate compounds with improved antimicrobial activity and stability against model microorganisms, *Mycobacterium smegmatis*, *E. coli* and *Pseudomonas putida*. Resazurin microtiter assays (REMA) revealed that pDMAEMA alone was most effective at inhibiting the growth of *M. smegmatis* (minimum inhibitory concentration = 0.025mg/mL) compared to *E. coli* and *P. putida*. Stability testing revealed that pHEA increases the stability of the AuNP conjugates in growth media but REMA showed it reduces antimicrobial activity. Immobilization of pDMAEMA onto the 2nm AuNPs increases their activity against *E. coli* and *P. putida*, lowering MIC values by up to a factor of 25 compared to pDMAEMA alone. This enhanced activity was not observed against *M. smegmatis*. Blood toxicity testing revealed that neither polymers nor AuNP conjugates are cytotoxic to mammalian erythrocytes. Overall, our data shows that immobilization of pDMAEMA onto gold nanoparticles is a good technique to enhance antimicrobial activity against *E. coli* and *P. putida*, and potentially against other Gram-negative bacteria. The novel conjugate compounds and pDMAEMA are good candidates for the development of future therapeutics to treat diseases caused by challenging bacterial pathogens.

Acknowledgements

I would like to express my gratitude to my supervisor, Dr Elizabeth Fullam, whose expertise, patience and guidance has been extremely valuable in the development of this project and in the development of my research skills and experience. I am very grateful to Professor Matthew Gibson for his collaboration and the opportunity to co-work with his lab team. I would like to give special thanks to Dr Sarah-Jane Richards. Her continuous support, advice and uncanny knowledge of chemistry have been vital to the coordination of the chemistry aspects of this project. She has been a great mentor and lab partner throughout.

I would like to express my deepest appreciation for the rest of the Fullam Lab team; Dr Chris Furze, Dr Collette Guy and Dr Marie Gyprioti. Their feedback, constructive criticism and friendly advice have been crucial to the improvement of my work and scientific approach. I would like to thank Dr Lucienne Otten. Her advice, pragmatic approach and witty humour made working in chemistry that much more fun.

Finally, I am extremely grateful to my family, friends and boyfriend for their inexhaustible support and continuous, unfailing encouragement through the year and especially in the lead-up to the completion of this thesis.

Table of Contents

Abstract.....	2
Acknowledgements.....	3
List of Figures.....	6
List of Tables.....	7
List of Abbreviations.....	8

Chapter	Page Number
1 Introduction	9
1.1 Background on Tuberculosis.....	9
1.2 Epidemiology of Tuberculosis.....	10
1.3 TB Disease and Diagnosis.....	13
1.4 <i>Mycobacterium tuberculosis</i>	16
1.5 TB treatment.....	20
1.6 Antimicrobial Resistance.....	22
1.7 Developing novel antimicrobials.....	27
1.8 Aims and Objectives.....	30
2 Materials and Methods	31
2.1 Suppliers.....	31
2.2 Bacteria.....	31
2.3 Growth media.....	31
2.4 Antibiotic Stock.....	31
2.5 Growth Conditions.....	32
2.6 Buffers and Reagents.....	32
2.7 Preparation of bacterial glycerol stocks.....	33
2.8 Preparation of frozen aliquots of <i>M. smegmatis</i> for REMA.....	33
2.9 Synthesis of AuNPs.....	33
2.10 Nanoparticle Characterisation.....	34
2.11 Synthesis of polymer-coated nanoparticles.....	35
2.12 Stability Testing.....	36
2.13 Synthesis of 2nm polymer-coated AuNPs.....	37
2.14 REMA Assays.....	37
2.15 Determining CFU/mL.....	39

2.16 Blood Toxicity Assays.....	40
2.17 2nm compounds: further testing.....	41
3 Results and Discussion	44
3.1 Establishing viable bacteria and antibiotic activity.....	44
3.2 Polymers and nanoparticles.....	46
3.3 Stability.....	50
3.4 Results from REMA.....	53
3.5 2nm compounds: other results.....	56
3.6 Blood toxicity results.....	60
3.7 Summary of results.....	64
4 Conclusion	66
4.1 Summary.....	66
4.2 Future Recommendations.....	67
References.....	69
Appendices.....	79
Appendix A.....	79
Appendix B.....	82
Appendix C.....	83

List of Figures

Figure		Page Number
1.1	Estimated TB incidence rates, 2014	10
1.2	Estimated HIV prevalence and relapse TB cases in 2014	11
1.3	Aims of the End TB Strategy	13
1.4	TB pathogenesis	14
1.5	X-Ray of patient with pulmonary TB	16
1.6	<i>Mycobacterium tuberculosis</i> bacilli	17
1.7	Mycobacterial cell wall components	18
1.8	Circular map of the chromosome of <i>Mycobacterium tuberculosis</i> H37Rv strain	19
1.9	Global Epidemiology of MDR-TB and XDR-TB, 2014	23
1.10	Chemical structure of pDMAEMA	29
2.1	Representative 96-well plate format for screening compounds to determine minimum inhibitory concentration	38
3.1	Conversion of resazurin to resorufin by metabolically active cells	46
3.2	Chemical structures of (A) pDMAEMA and (B) pHEA	47
3.3	Colouration of gold nanoparticles with different dimensions	48
3.4	UV-Visible Spectra	49
3.5	Stability of polymer-gold nanoparticle compounds in LB and 7H9GT	52
3.6	Time-kill curves	58
3.7	Turbidity of bacteria treated with antibiotics, ampicillin or tetracycline	59
3.8	Turbidity of bacteria treated with 2nm AuNP conjugate compounds	59
3.9	Haemagglutination assay results	61
3.10	Percentage haemolysis of ovine blood exposed to pDMAEMA and pHEA	62
3.11	Percentage haemolysis of ovine blood exposed to 5nm and 2nm AuNP conjugate compounds.	62
3.12	Visual haemolysis	63

List of Tables

Table		Page Number
1.1	The mechanism of action of five well-known anti-TB drugs	21
1.2	Minor and major adverse side effects of a selection of antituberculosis drugs	22
1.3	Genetics of drug resistance in <i>Mycobacterium tuberculosis</i>	24
2.1	40 x MIC of 2nm AuNP conjugate compounds	41
3.1	MIC and CFU/mL values for <i>E. coli</i> , <i>P. putida</i> and <i>M. smegmatis</i> treated with known antibiotics	45
3.2	Citrate-stabilised gold nanoparticles used in this project and determination of size	50
3.3	Antimicrobial activity of pDMAEMA polymers DP 10, 25, 50 and 100	54
3.4	Antimicrobial activity of 8 different polymer-AuNP conjugate compounds	55
3.5	Minimum bactericidal concentration (MBC) of 2nm AuNP conjugate compounds	57
3.6	Summary of results from REMA and blood toxicity testing for pDMAEMA and pHEA polymers	64
3.7	Summary of results from REMA and blood toxicity testing for 2nm and 5nm gold nanoparticle conjugate compounds	65

List of Abbreviations

AMR	Antimicrobial Resistance
AgNP	Silver Nanoparticle
AuNP	Gold Nanoparticle
BCG	Bacille Calmette-Guerin
CFU	Colony-Forming Unit
DLS	Display Light Scattering
DOTS	Directly Observed Treatment, Short-Course
DMSO	Dimethyl Sulfoxide
DP	Degree of Polymerisation
EMB	Ethambutol
FDA	Food and Drug Association
GT	Glycerol-Tween
HIV	Human Immunodeficiency Virus
ICP-MS	Inductively Coupled Plasma Mass Spectrometry
IFN- γ	Interferon-Gamma
IGRA	Interferon-Gamma Release Assay
INH	Isoniazid
LAM	Lipoarabinomannan
LB	Luria-Bertani
LSPR	Localized Surface Plasmon Resonance
MBC	Minimum Bactericidal Concentration
MDGs	Millennium Development Goals
MDR-TB	Multidrug-resistant tuberculosis
MIC	Minimum Inhibitory Concentration
MRSA	Methicillin-Resistant <i>Staphylococcus aureus</i>
Mtb	<i>Mycobacterium tuberculosis</i>
NP	Nanoparticle
OD	Optical Density
PBS	Phosphate-Buffered Saline
PEG	Polyethylene glycol
PEI	Polyethyleneimine
PKC	Protein Kinase C
pDMAEMA	Poly(2-dimethylamino)ethyl methacrylate
pHEA	Poly(<i>N</i> -hydroxyethyl acrylamide)
PPD	Purified Protein Derivative
PZA	Pyrazinamide
RAFT	Reversible-Addition Fragmentation Chain Transfer
REMA	Resazurin Microtiter Assay
RIF	Rifampicin
RNA	Ribonucleic Acid
ROS	Reactive Oxygen Species
SDG	Sustainable Development Goal
SM	Streptomycin
SPR	Surface Plasmon Resonance
TB	Tuberculosis
TSB	Tryptic soy broth
TBT	Tuberculin Skin Test
TEM	Transmission Electron Microscopy
TCN	Tetracycline
TGA	Thermogravimetric Analysis
XDR-TB	Extensively drug-resistant tuberculosis

1. Introduction

1.1 Background on Tuberculosis

Tuberculosis (TB) is not a new disease; in fact it is one of the oldest recorded human diseases, dating back approximately 15,000 years. During 5th century BCE TB was known as phthisis and was typically fatal (1). Although the disease can manifest itself in different parts of the human body such as bone and the central nervous system, it is primarily a pulmonary disease (2). The causative agent in most cases is the bacterial pathogen *Mycobacterium tuberculosis*. In 1882, Robert Koch identified the tubercle bacilli using a specific stain called the Ziehl-Neelson stain also known as the acid-fast stain (3). TB is highly contagious, airborne and is very much influenced by the immunocompetency of the host and environmental factors such as population density. When a person with active TB coughs, sneezes or even talks, mucus and saliva loaded with the infectious microorganism are propelled into the air (4). A single sneeze will release millions of mycobacteria in the air spreading the infection; one person with active TB can go on to infect 10-15 people throughout the year (4).

In the 1920s the first human trials of the vaccine Bacille Calmette-Guerin (BCG), an attenuated version of *Mycobacterium bovis*, which causes TB-like disease in cattle, were launched. *M. bovis* was attenuated by 230 passages in broth, during the course of which the bacteria lost its virulence for animals and was first shown to be harmless and protective in a child in 1921 (5). Later in 1953 a survey of 50,000 children demonstrated an 80% reduction in infection rate following the BCG vaccination but research on the efficacy of the BCG vaccine proved contradictory (6). Although relatively safe and protective against severe forms of childhood TB, the BCG vaccine fails to afford protection against adolescent and adult pulmonary TB (7).

The number of TB cases reached epidemic proportions in Europe and North America during the 18th and 19th centuries; at this time it was called 'consumption' (8). Poor housing, bad sanitation, over-crowding and malnutrition facilitated the spread of TB during this era (5). Following the late 19th century TB declined but reemerged as a major public health emergency continuing into the 21st century as one of the biggest medical health concerns.

1.2 Epidemiology of Tuberculosis

1.2.1 Global Burden

Despite the discovery of effective and affordable chemotherapy more than 50 years ago TB remains a major cause of death worldwide with 1.3 million TB deaths in 2012 alone (9). There are 22 countries that collectively account for 80% of the tuberculosis cases in the world and are known as high-burden (10). These countries include India, China, Nigeria and South Africa. Approximately one-third of the world's population has been estimated to have been exposed to TB bacteria and thus potentially infected according to statistics attained from The World Health Organisation (WHO) in 2013 (9). More recently in 2014 9.6 million individuals had fallen ill with TB, 1.5 million died and 480,000 people worldwide developed multidrug-resistant tuberculosis (MDR-TB) (11). MDR-TB is a type of tuberculosis that does not respond to at least isoniazid and rifampicin, two of the most potent and commonly prescribed TB drugs. The estimated TB incidence rates for 2014 are shown by Fig. 1.1, these rates vary widely among countries worldwide.

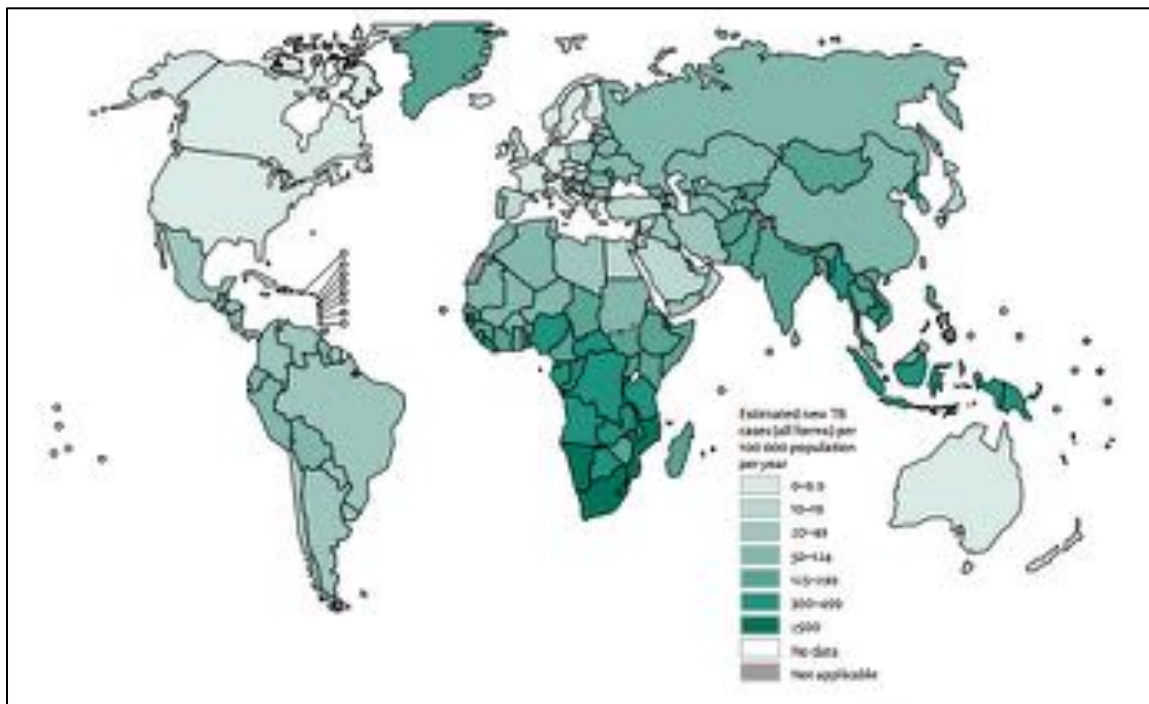


Figure 1.1. Estimated TB incidence rates, 2014. Estimated new TB cases for all forms of TB are shown per 100,000 population per year (11).

The global prevalence has been declining globally since the 1990s and the incident rate declined slowly from 1997 to 2001 with a 1.3% per year reduction rate observed since 2002 (12). The Stop TB Partnership was established in 2000 with the aim of eliminating TB

as a public health concern. One main aim of this initiative and its 1000 partner organizations was to halve TB prevalence by 2015 compared with the baseline of 1990 (9). This target was met well in advance in the region of the Americas by around 2004 but only 9 of the 22 high-burden countries have met the 50% reduction from 1990 levels (11).

1.2.2 HIV co-infection and other vulnerable populations

The Human Immunodeficiency Virus (HIV) significantly increases the risk of latent TB progression into active TB disease (13). This is due to lower CD4 counts and general overall immunosuppression in individuals with HIV. TB in this case is opportunistic and it is one of the most common opportunistic infection that affects HIV-seropositive individuals worldwide (14). The region with the highest proportion of TB cases co-infected with HIV is the African Region, with >50% of TB cases co-infected with HIV in southern Africa alone (Fig. 1.2) (9). In 2014, it was estimated that 1.2 million (12%) of the 9.6 million people who developed TB worldwide were HIV-positive and the African Region accounted for 74% of the estimated number of HIV-positive incident TB cases (11).

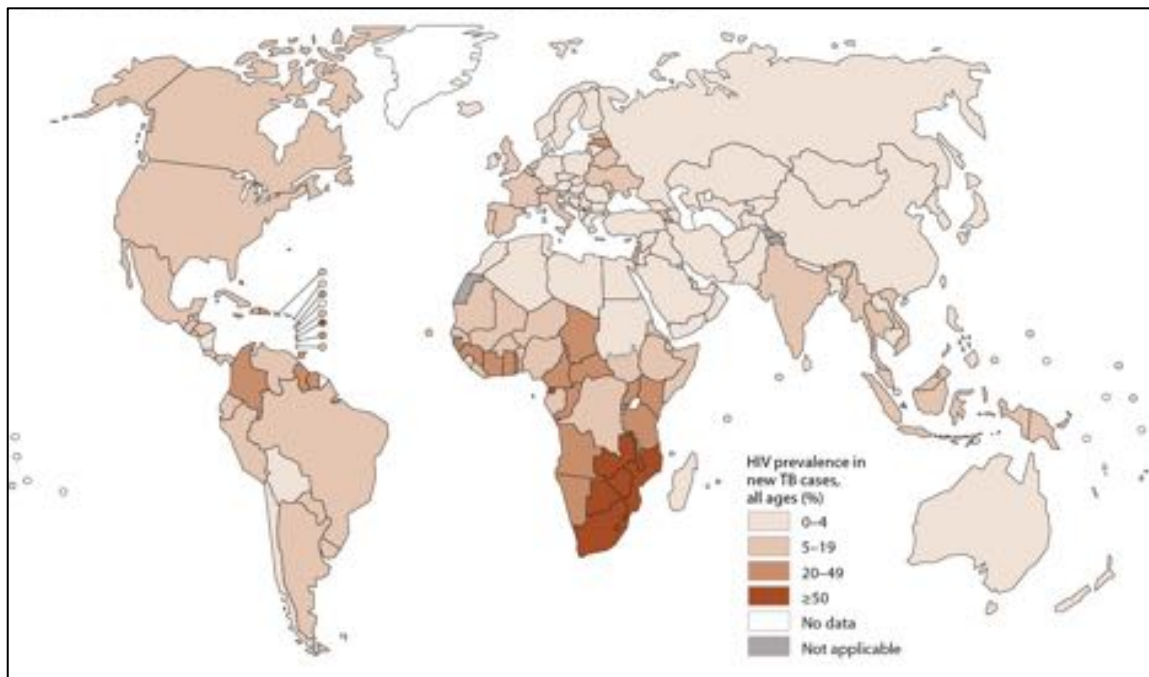


Figure 1.2. Estimated HIV prevalence and relapse TB cases in 2014. Estimated HIV prevalence in TB cases for all ages of the population (%) (11).

HIV-seropositive individuals are one group of many other vulnerable populations. Other vulnerable groups include immigrants, prisoners, and the socially and economically deprived. Poor housing and environmental conditions, poor access to healthcare services and unfavorable psycho-social circumstances are some major determinants of TB infection

and treatment capability (12). Another determinant highlighted in TB: Return of the Plague, a documentary produced by True Vision Productions, is the stigmatization associated with TB infection, in particular in regions of Africa such as Swaziland (shown in the documentary) (15). This often discourages people from seeking medical care and talking about their condition, which in turn further facilitates the spread of TB. Furthermore, increased populations movements due to global air travel and immigration have also aided the spread of TB, especially in more developed countries such as the UK and North America.

1.2.3 TB control strategies

Over the last twenty years global strategies for controlling TB worldwide have been proposed for adoption and adaptation in all countries (12). The first of these strategies was Directly Observed Treatment, Short-Course (DOTS) and it comprises five key elements: 1) political commitment with increased and sustained financing, 2) case detection through quality-assured bacteriology, 3) standardized treatment, with supervision and patient support, 4) an effective drug supply and management system, and 5) monitoring and evaluation system, and impact measurement (16). The DOTS strategy encompasses the logistical, operational, political and technical aspects of TB management and control that can be applied globally. The DOTS approach was launched in the mid-1990s by WHO and was successful in countries such as Peru, China, Bangladesh and countries of Western Africa (17,18).

Since DOTS, more recent newer strategies have been developed. These include the Stop TB Strategy, End TB Strategy, Millennium Development Goals (MDGs) and the most recent Sustainable Development Goals (SDGs). From 2016, the End TB Strategy is to be implemented, with targets linked to the newly adopted SDGs (11). The End TB Strategy (Fig. 1.3) is the post-2015 global strategy aiming to end the global tuberculosis epidemic by expanding the scope and reach for interventions for TB care and prevention, eliciting full benefits of health and development policies and systems, and pursuing new scientific knowledge and innovations (19).

In order to reach the targets outline by the End TB strategy, the annual decline in TB incidence rates must accelerate and additional investment in new tools must be made in order to sustain progress beyond 2025 (Fig. 1.3). The pursuit of new scientific knowledge encompasses, in part, the development of novel antimicrobial agents to treat TB. This is an extremely crucial aspect in reaching the goals set out by the End TB strategy.

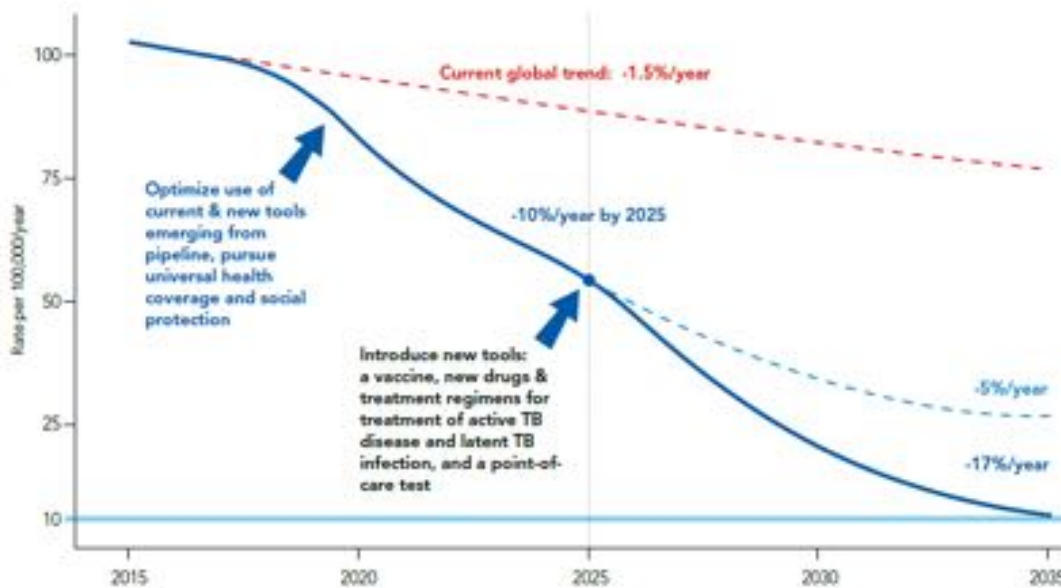


Figure 1.3. Aims of the End TB Strategy. Graph shows the projected acceleration of the decline in global TB incidence rates (solid and dotted blue lines). This involves the optimization of current tools combined with progress towards universal health coverage and social protection from 2015 and the additional impact of new tools by 2025 (arrows). The current global trend is shown by the red dotted line. Solid pale blue line indicates the optimum incident rate (10 per 100,000/year). (19)

1.3 TB Disease and Diagnosis

1.3.1 Transmission and disease development

TB is a highly infectious disease transmitted by small respiratory droplet nuclei expelled by infected individuals and inhaled by the new host. These droplets can remain suspended in the air for several hours (20). The infectious dose is 1-200 bacilli although each droplet can contain 1-400 bacilli (21). Once inhaled by an individual the droplet nuclei move into the upper respiratory tract via the mouth or nasal passages, and eventually reach the alveoli of the lungs. There are many factors that determine the risk of transmission and these include: population density, if the person transmitting is infectious, length of exposure to infectious individual(s) and hyper-susceptibility to infection i.e. in patients with HIV.

Once the bacterial droplets are inhaled they are deposited in the alveoli where they are taken up by non-specific alveolar macrophages (Fig. 1.4); these cells are *Mtb*'s preferred niche (22). Macrophages are not activated and are unable to destroy the bacteria in this 'inactive' state. Approximately 7-21 days after infection *Mtb* multiplies unrestricted within non-activated macrophages until these cells burst. Once this happens other macrophages

are recruited to the site and engulf Mtb. Once again these remain inactivated but present TB antigenic molecules on their surface that are recognized by T lymphocytes resulting in their activation and the release of cytokines including interferons. As a consequence, macrophages are activated and release lytic enzymes and reactive intermediates. Tubercles form but in these tubercles Mtb is unable proliferate but can persist indefinitely; in this case TB is latent (Fig. 1.4).

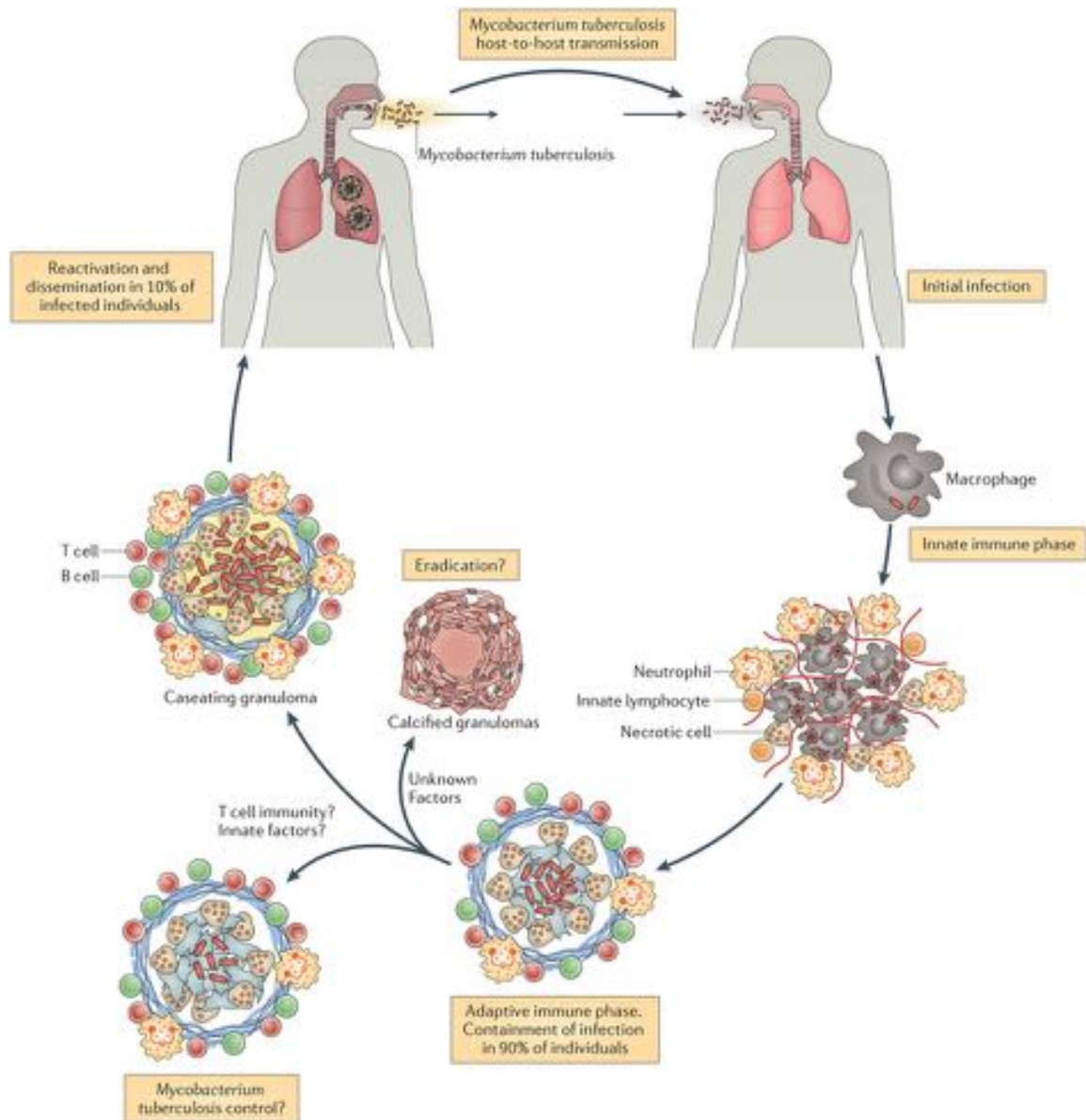


Figure 1.4. TB pathogenesis. Disease onset occurs in the alveoli. The initial stages are characterized by the innate immune responses that recruit inflammatory cells to the lungs. In the later stages, the adaptive immune responses are activated leading to the recruitment of T cells as well as activated macrophages. Most individuals will remain in a 'latent' state of infection with no clinical representation. A small percentage of these people will develop active TB disease that can lead to the release of *M. tuberculosis* from the granulomas. (22)

M. tuberculosis can use surrounding macrophages to replicate causing the tubercle to grow. Growing tubercles can invade the bronchi, arteries or other components of the respiratory system causing infections as a result. These infections may then spread to other parts of the body forming secondary lesions in the bones, peritoneum and lymph nodes. Finally, the caseous centres of the tubercles liquefy aiding the growth of TB and rapid extracellular multiplication. This then causes the walls of the nearby bronchi to become necrotic and rupture resulting in cavity formation that allows TB to spread into other parts of the lungs and also beyond the respiratory system.

The human immune system is capable of controlling the infection (Fig. 1.4) but ultimately the management of TB is not the same as eradication. The 10% of individuals whom develop active TB are capable of disseminating the bacteria and infecting other individuals. Primary TB develops as a result of the initial infection whereas secondary TB occurs due to the reactivation of the latent primary infection or reinfection with Mtb (23).

1.3.2 Diagnosis

TB diagnostic tests can determine whether someone has latent TB or active TB and TB disease. Latent TB is the presence of TB in the body of an individual but who do not exhibit any symptoms and do not feel unwell. When the TB bacteria are spreading and causing damage to tissue and the infected person exhibits symptoms such as a persistent coughing and constant fatigue, they are considered to have active TB (24). The Mantoux tuberculin skin test (TBT) is a method used to diagnose infection with TB via injection of purified protein derivative (PPD) into the inside of the forearm. A positive result forms a red and swollen circle at the site of infection measuring 10mm or more (25). TB blood tests are also referred to as interferon-gamma release assays (IGRAs). This measures a person's immune response to the bacteria that causes TB, in particular detecting the interferon gamma cytokine, an activator of macrophages (26).

Chest x-ray and sputum tests can be carried out to help determine whether an individual has active TB. Sputum smear microscopy has been the most commonly used method of diagnosing pulmonary TB in low and middle income countries (27). It is a rapid, relatively inexpensive and simple technique. In areas with high prevalence of TB sputum smear microscopy is highly specific and widely applicable (27). However, there are limitations to this diagnostic method. When the bacterial load is less than 10,000 organisms/mL sputum sample, the sensitivity of the diagnostic method is heavily compromised (27). Fluorescent microscopy was introduced as a way of improving the accuracy of sputum smear

microscopy by using fluorochrome dyes to stain the smear. In 2011, WHO issued a policy statement recommending that conventional fluorescence microscopy should be replaced by LED microscopy (26).

Chest x-rays can identify inflammation of the lungs caused by Mtb (Fig. 1.5), however a normal chest x-ray result does not exclude extra pulmonary TB (26).

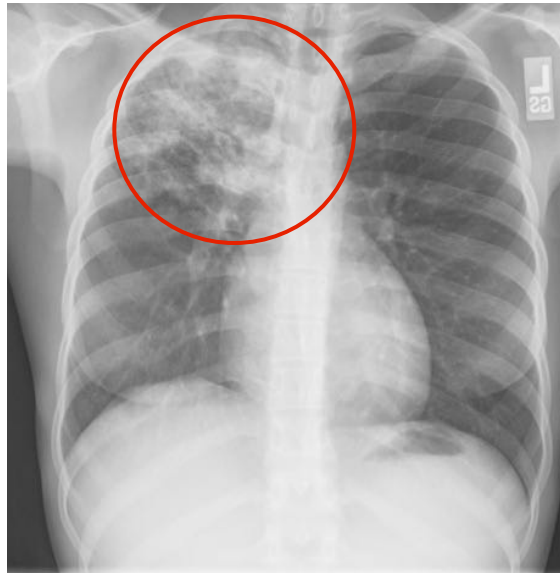


Figure 1.5. X-Ray of patient with pulmonary TB. Patient presented with a month of cough, fever and weight loss, all symptoms of TB disease. X-Ray shows multifocal opacities in the right upper lobe (red circle) with thickening and upward shift of the minor fissure. The findings from the X-Ray were consistent and confirmed to be pulmonary tuberculosis (28).

Other tests used to diagnose TB include culturing bacteria, serological tests, and TB drug susceptibility testing to identify individuals infected with drug-resistant *M. tuberculosis*. TB tests may have low sensitivity and/or low specificity so it is important to carry out several tests in order to make a full and accurate diagnosis.

1.4 *Mycobacterium tuberculosis*

1.4.1 Microbiological characteristics

M. tuberculosis (Mtb) is an obligate aerobic, non-motile, acid-fast intracellular pathogen. Mtb cells are bacilli in the form of thin straight rods (Fig. 1.6) approximately 2-4 μ m in length and 0.2-0.5 μ m in width (29).

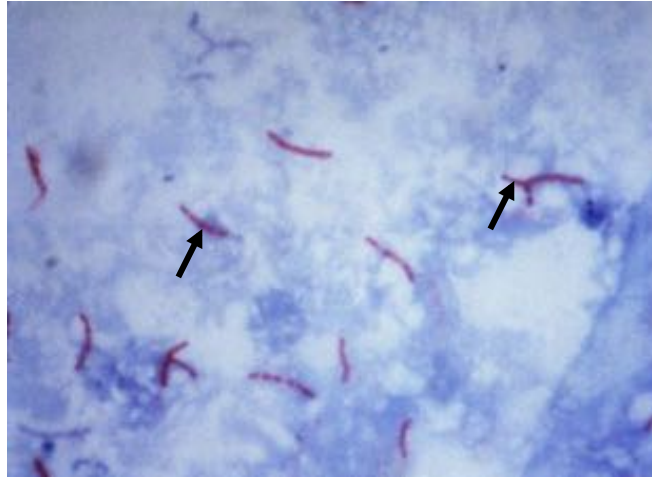


Figure 1.6. *Mycobacterium tuberculosis* bacilli. The photomicrograph reveals *M. tuberculosis* bacterial rods using the acid-fast Ziehl-Neelsen stain (image - 1000x magnification). The bacteria appear red (highlighted by the black arrows) (30).

M. tuberculosis requires high levels of oxygen which is one of the reasons why it primarily affects the mammalian respiratory system. The lungs provide an abundant supply of oxygen. Mtb possesses an unusual, waxy coating on the cell surface due to a high lipid content in its cell wall. This renders the bacteria impervious to Gram-staining so acid-fast techniques are employed for mycobacterial identification. The Ziehl-Neelsen stain is the most commonly used acid-fast technique. Mtb stains pink as it retains the carbol-fuchsin dye and is not de-stained by the acid-alcohol used in this method of staining, hence the bacteria is “acid-fast” (Fig. 1.6).

The mycobacterium cell envelope (Fig. 1.7) is very distinctive as it contains an extra layer, beyond the typical bacterial peptidoglycan layer, extensively rich in unusual lipids, glycolipids and polysaccharides (31). The bacterium uniquely expresses mycolic acids on its cell wall and these molecules play a critical role in the structure and function of the cell wall (32). Mycolic acids are long, strongly hydrophobic α -alkyl, β -hydroxy fatty acids, the composition and quantity of which affects the virulence, colony morphology, growth rate and permeability of Mtb (33). Mycolic acids are extremely impermeable to hydrophilic molecules, such as antibiotic compounds and chemotherapeutic molecules, and are therefore an important factor in antibiotic resistance (34).

Other major components of the Mtb cell wall include: trehalose dimycolate (cord factor), arabinogalactan and lipoarabinomannan (LAM) (Fig. 1.7).

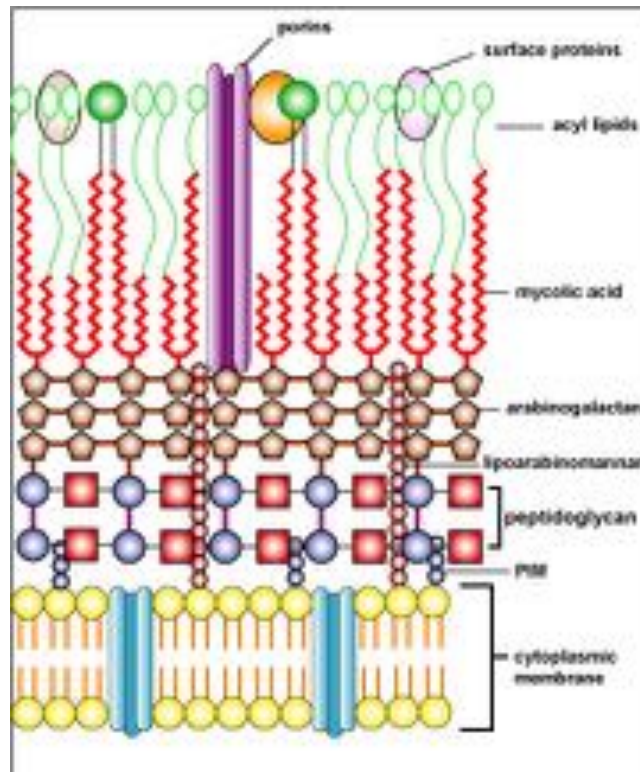


Figure 1.7. Mycobacterial cell wall components. A schematic diagram of the layout of the *M. tuberculosis* cell envelope. Key cell components include: mycolic acid, lipoarabinomannan, peptidoglycan and arabinogalactan (35).

Arabinogalactan is composed predominantly of arabinose and galactose. In Mtb approximately 10-12% of the *N*-glycolylmuramic acid (MurNGly) residues of peptidoglycan are covalently attached to arabinogalactan (36). Arabinogalactan is therefore essential in connecting the peptidoglycan layer with the outer mycolic acid layer of Mtb to form a network. LAM is a phosphatidylinositol anchored lipoglycan abundant in the inner and outer membranes of Mtb and plays a key role in modulating the host immune response during infection (36). Cord factor is the most abundant glycolipid in the Mtb cell wall and is toxic to mammalian cells (37). Cord factor consists of trehalose, which is attached to hydrophobic components of the mycobacterial cell wall and is a key virulence factor affecting the host immune system (37).

1.4.2 Genome

The genome of the *M. tuberculosis* strain H37Rv has been deciphered (Fig. 1.8). It is approximately $\sim 4.4 \times 10^6$ base pairs and contains approximately 4000 genes (2). The G+C content of the Mtb genome is 65.6% and is relatively constant throughout the genome (31). Many of the genes encode enzymes and other proteins associated with the metabolism and biosynthesis of fatty acids.

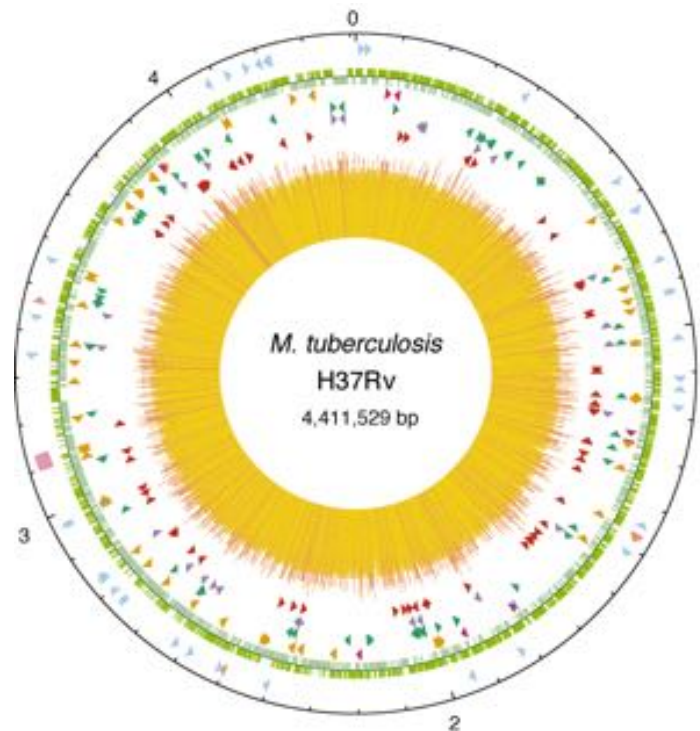


Figure 1.8. Circular map of the chromosome of *Mycobacterium tuberculosis* H37Rv strain. The outer circle shows the scale in Mb whereby 0 represents the origin of replication. The first ring from the exterior denotes the positions of the stable RNA genes. The second ring shows the coding sequence by strand, the third ring depicts repetitive DNA sequences and the fourth ring shows the members of the PPE family members. The fifth ring shows the PE family members and the sixth ring shows the PGRS sequences (31).

Approximately 10% of the genes in Mtb are associated with the production of two families of glycine-rich proteins, proline-glutamine motifs and proline-proline-glutamine motifs (38). The function of these two families is generally unknown but it has been suggested that they are involved in the antigenic variation of Mtb during infection thereby contributing to its pathogenicity (2).

1.4.3 Bacterial pathogenesis

The pathogenicity of *M. tuberculosis* is determined by a number of factors including the immunocompetency of the host and bacterial virulence factors. Immunocompromised individuals such as those with HIV are more susceptible to TB infection and disease. Virulence factors help the bacteria to invade the host, cause disease and evade host defenses (39). They can be divided into two groups: proteins and cell wall components (32). Firstly, the high lipid profile of the Mtb cell wall acts as a barrier to antibiotic drugs, lysozyme attack and acidic/alkaline compounds in the intracellular and extracellular environment (40). Secondly, cell wall components such as LAM, cord factor and secreted

proteins such as protein kinase G, and transcriptional regulators such as PhoP/PhoR, all contribute to the pathogenicity of *M. tuberculosis*.

Cord factor causes *M. tuberculosis* to grow in serpentine cords in the lungs and it is the primary cause of chronic granulomatous inflammation. Cord factor stimulates macrophages to produce proinflammatory and type 1 help T-cell-inducing cytokines such as tumour necrosis factor alpha, interleukin-1, interleukin-12 and chemotactic factors (41). Cord factor is also an important compound for the survival of *M. tuberculosis* in the host's phagosomes by inhibiting the process of phagosome-lysosome fusion (42).

LAM is highly immunogenic and known to inhibit macrophage activation and trigger cytotoxic activity, thereby allowing the persistence of Mtb within mononuclear phagocytes (43). In murine models of TB, the addition of LAM to murine macrophages blocks the expression of interferon-gamma-induced genes by depressing interferon-gamma (IFN- γ) production (2). In addition to this, LAM has the ability to scavenge oxygen radicals in the lungs and inhibits the host protein kinase C (PKC), a family of kinases involved in the regulation of numerous cellular responses including the inflammatory response, cell proliferation and protein secretion (44). One particular isoform of PKC, PKC θ , is a key modulator of T cell receptor signaling and an essential regulator of T cell activation and survival (45). LAM inhibition of PKC aids in protecting Mtb from T-cell attack.

Protein kinase G has been shown to modulate phagosome-lysosome fusion thus blocking the intracellular degradation of mycobacteria in lysosomes (46). The PhoP/PhoR two-component signal transduction system controls the expression of approximately 2% of the bacterial genome and is another major contributor to Mtb pathogenicity (47). Many of the genes that are up-regulated by PhoP are involved in general lipid metabolism, substrate transport across the plasma membrane and the synthesis of regulators (47). Inactivation of PhoP would disrupt these processes and affect the lipid content of the Mtb cell wall making it more permeable to chemotherapeutic agents. There are many other virulence factors beyond the ones that have been discussed here, such as oxidative stress proteins, ESX-1 (type VII) secretion system and 19-kDa protein which induces macrophage apoptosis (48).

1.5 TB treatment

Effective regimens for treating TB comprises multiple drugs and can last from 6-9 months. First-line TB drugs are: rifampicin (RIF), isoniazid (INH), pyrazinamide (PZA) and

ethambutol (EMB) as well as streptomycin (SM). Four of these drugs are combined in multiple-drug therapy to treat TB. Second-line antibiotics include fluoroquinolones, kanamycin, amikacin and capreomycin. Table 1.1 shows a selection of well-known TB antibiotics and their mechanisms of antibiotic action against *M. tuberculosis*.

Table 1.1. The mechanism of action of five well-known anti-TB drugs.

Antibiotic	Mechanism of action
Rifampicin	Targets the β -subunit of Mtb RNA polymerase, it binds to this subunit and inhibits the elongation of messenger RNA. Active against actively growing and slowly metabolizing (non-growing) bacilli (49).
Isoniazid	A pro-drug that must be activated by a bacterial catalase-peroxidase enzyme in Mtb. Mechanism of action is not entirely clear although its activation results in the inhibition of mycolic acids and InhA, the enoyl reductase for Mtb (50,51).
Pyrazinamide	Has an ability to inhibit semi-dormant bacilli residing in acidic environments (49). Inhibits multiple targets such as energy production and pyrazinoic acid, the active moiety of pyrazinamide, is able to disrupt membrane energetics and inhibit membrane transport in Mtb (52,53) .
Ethambutol	Affects arabinogalactan biosynthesis through inhibition of cell wall arabinan polymerization (54).
Streptomycin	An aminoglycoside that binds “irreversibly” to specific 30S-subunit proteins and 16S ribosomal RNA (55).

Antibiotics to treat TB must be taken over lengthy periods of time ranging from 6-30 months including follow-up treatment. Antibiotics must be taken several times a week and the treatment regimen strictly adhered to. These regimens have an initial phase of 2 months followed by a continuation phase. The initial phase includes four of the first-line anti-TB drugs and is crucial for preventing the emergence of drug-resistance (56). The continuation phase can vary depending on whether patients have uncomplicated, drug-susceptible TB or extensive pulmonary TB disease with a positive sputum culture after the initial phase (56). In the latter case the continuation phase lasts longer i.e. >6 months.

Patients can exhibit a variety of debilitating side effects to TB medications (Table 1.2). These adverse reactions can vary in severity between individuals and are related to a number of factors. The principle determinants of these reactions to antituberculosis drugs are the dose and time of day at which the medication is administered, patient age and nutritional status, alongside the presence of preexisting diseases or dysfunctions such as alcoholism, impaired liver and/or kidney function, and HIV co-infection (57).

Table 1.2. Minor and major adverse side effects of a selection of antituberculosis drugs.

Antibiotic	Minor side effects	Major side effects
Rifampicin	Nausea, abdominal pain Orange coloured tears, sweat and urine Pruritus, fatigue, dizziness dyspnea and ataxia (57)	Hepatotoxicity and exanthema Leukopenia, hemolytic anaemia, eosinophilia, vasculitis and septic shock (57)
Isoniazid	Nausea and vomiting Arthralgia Head, insomnia, euphoria (57)	Psychosis, convulsive seizures, mental confusion Peripheral neuropathy and clinical hepatitis (57)
Pyrazinamide	Nausea, vomiting Dermatitis, pruritus (57)	Rhabdomyolysis and kidney failure Acute arthritis Hepatotoxicity (57)
Ethambutol	Abdominal pain, nausea, dizziness and vomiting (57)	Retrobulbar neuritis, myocarditis and neutropenia (57)
Second-line drugs: capreomycin, cycloserine, kanamycin	Nausea and vomiting Loss of appetite	Auditory, vestibular and renal toxicity Psychosis, convulsions and rash (58)

Newer anti-TB drugs have been developed and investigated. These include nitroimidazoles, SQ109, TMC207, phenothiazines and benzothiazinones. Nitroimidazole compounds PA-284 and OPC-67683 have shown activity against *M. tuberculosis* strains that are susceptible and resistant to the class anti-TB drugs (49). In particular, PA-284 has been found to inhibit the synthesis of lipids and proteins of the Mtb cell wall, although this is probably not the only mechanism of action (49). Conversely, the mode of action of TMC207 is through the inhibition of mycobacterial ATP synthase while phenothiazines and benzothiazinones appear to target other proteins and enzymes such as calmodulin-like protein and decaprenylphosphoryl- β -o-ribose 2'-epimerase, respectively (49).

1.6 Antimicrobial Resistance

Antimicrobial resistance (AMR) is the ability of microbes to stop responding to antibiotic treatments to which they were previously susceptible. Many different species of bacteria have and are developing mechanisms of resistance that are rendering even the most novel of antibiotics futile. AMR is a massive global health problem and will continue to

become an increasingly bigger problem unless effective strategies are developed and implemented to combat AMR.

1.6.1 MDR-TB and XDR-TB

Multidrug-resistant TB (MDR-TB) is caused by *M. tuberculosis* that is resistant to at least isoniazid and rifampicin, two of the most potent TB drugs. Extensively drug-resistant TB (XDR-TB) is a form of TB that is resistant to any fluoroquinolone and at least one of the three injectable second-line drugs (kanamycin, amikacin and capreomycin), in addition to rifampicin and isoniazid. MDR-TB and XDR-TB are two of the biggest threats to controlling TB globally as well as treating TB on an individual basis. Globally, in 2014 the percentage of new cases of MDR-TB was estimated to be 3.3% (Fig. 1.9A) (11).

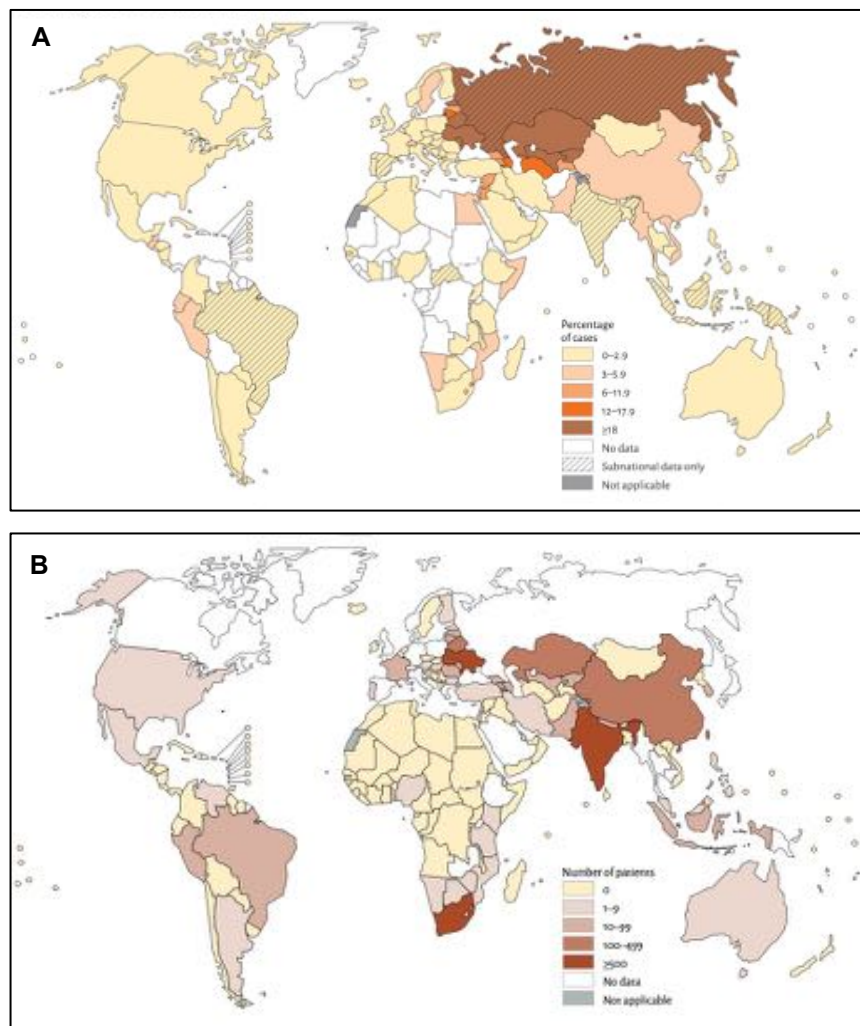


Figure 1.9. Global Epidemiology of MDR-TB and XDR-TB, 2014. (A) Percentage of new cases of MDR-TB in 2014. **(B)** Number of patients laboratory-confirmed XDR-TB started on treatment in 2014 (11).

Additionally in 2014, 49 countries and territories reported treating people with XDR-TB (Fig. 1.9B) and 4,044 patients with XDR-TB were enrolled on treatment worldwide (11). By 2015, XDR-TB had been reported by 105 countries and an estimated 9.7% of people with MDR-TB have XDR-TB (11).

There are many reasons for the development of MDR-TB and XDR-TB. Patients must take multiple drugs over very long periods of time. Poor or slack adherence to designated drug regimens as well as improper use of the drugs can result in the development of drug-resistant TB. Patient compliance can often be poor due to the debilitating side effects associated with taking TB medication over extended periods of time. Furthermore, in low-income countries, TB medication might not be as easily supplied or the drugs that are administered have been poorly formulated. Improperly formulated drugs will not be as effective in killing the TB bacteria as well as high quality drug formulations.

The development of drug-resistant Mtb strains results from spontaneous and random mutations in the bacterial chromosome (Table 1.3) that result in reduced susceptibility to current antibiotic treatments (58).

Table 1.3. Genetics of drug resistance in *Mycobacterium tuberculosis* (58).

Drug	Gene(s) implicated in resistance
Rifampicin	<i>rpoB</i> ; b-subunit of RNA polymerase
Isoniazid	<i>katG</i> : catalase-peroxidase <i>oxyR-ahpC</i> : alkylhydrokinase reductase <i>inhA</i> : enoyl-ACP reductase
Pyrazinamide	<i>pncA</i> : pyrazinamidase
Ethambutol	<i>embCAB</i> : Arabinosyl transferase
Fluoroquinolones	<i>gyrA</i> : DNA gyrase

Mutations in several Mtb genes including *katG*, *ahpC*, *inhA*, *kasA* and *ndh* have all been associated with specific resistance to isoniazid (49). Conversely, a large majority of rifampicin resistant Mtb clinical isolates show mutations in genes *rpoB* that β-subunit of the Mtb RNA polymerase resulting in a conformational change (49). Given that rifampicin specifically targets the β-subunit of the mycobacterial polymerase, the conformational change brought about by the mutation lowers the affinity of the drug for its target. This then results in the development of resistance to rifampicin. Other mutations in different genes

(Table 1.3) have been found to lead to resistance to other TB drugs such as pyrazinamide, ethambutol and fluoroquinolones.

In order to tackle drug-resistant TB specific drugs have been repurposed such as linezolid and two new anti-TB drugs approved, bedaquiline and delamanid. Linezolid is a first-generation oxalidione that has demonstrated clinical effectiveness in the most difficult to treat TB drug-resistant cases however, its long-term use is limited the frequency and severity of adverse reactions such as optic neuropathy and gastrointestinal disorders (59). Bedaquiline belongs to the diarylquinoline class of antibiotics and selectively targets the proton pump of ATP synthesis, necessary for bacterial metabolism (59). Delamanid is a nitroimidazole that inhibits the synthesis of mycolic acids and has shown high activity in adult cases affected by pulmonary TB both *in vitro* and *in vivo* (59).

Three phase IIb clinical trials were conducted using delamanid: trials 204, 208 and 116, with trial 204 providing the main evidence for the efficacy and safety of delamanid (60). Overall, patients who received delamanid for 2 months had a higher rate of a 2-month sputum-culture conversion than patients who received the placebo, and mortality was lower among patients treated with delamanid for 6 months or more in comparison to patients treated with delamanid for 2 months or less (Trial 204) (61). The safety and effectiveness of bedaquiline were established in 440 patients in phase-2 clinical trials and on December 28th 2012 the U.S. Food and Drug Administration (FDA) granted accelerated approval for the use of bedaquiline to treat drug-resistant TB (62). However, preclinical and clinical studies have demonstrated that bedaquiline may cause hyperuricemia, headaches, chest pain and joint pain (63).

The development of drugs like bedaquiline and delamanid gives promise to tackling drug-resistant TB. It is of note that to tackle drug-resistant TB, drug discovery has primarily involved the synthesis of novel small-molecule antimicrobials and repurposing already known drugs such as linezolid. The safety and efficacy of novel anti-TB drug candidates must be supported across many clinical trials before they become clinically available.

1.6.2 Other drug-resistant bacteria

Drug-resistant *M. tuberculosis* is not the only bacterial species causing great concerns in terms of AMR. The acronymically dubbed ESKAPE pathogens encompassing six pathogens with growing resistance to antibacterial drugs: *Enterococcus faecium*, *Staphylococcus aureus*, *Klebsiella pneumoniae*, *Acinetobacter baumannii*, *Pseudomonas*

aeruginosa and *Enterobacter* species. These six pathogens are responsible for a significant percentage of nosocomial infections in the modern hospital and represent the vast majority of bacterial isolates whose drug-resistance poses many therapeutic dilemmas for healthcare professionals (64). Rates of infection due to methicillin-resistant *S. aureus* (MRSA), vancomycin-resistant *E. faecium*, and fluoroquinolone-resistant *P. aeruginosa* are rapidly increasing (65).

With respect to TB a significant portion of low/middle income countries are responsible for the high burden of MDR-TB and XDR-TB. There are considerable variations in patterns of AMR globally however; AMR is a considerable problem for all countries across the world irrespective of their income. For instance, in 2013, more than 10% of bloodstream *S. aureus* infections were caused by MRSA strains in 15 European countries, with several of these countries seeing resistance rates closer to 50% (66). Antibiotic resistant *Escherichia coli* is another bacterial species that has received attention due to the fact that drug-resistant *E. coli* infections are becoming increasingly problematic. For example, a study carried out by a university in the U.S. analyzed patient records at 26 community hospitals in the U.S. They discovered that the rate of drug-resistant extended-spectrum β -lactamase-producing *E. coli* infections had doubled between 2009 and 2014; 5.28 infections per 100,000 patients in 2009 and 10.5 infections per 100,000 in 2014 (67).

With drug-resistant bacteria causing infections ranging from urinary tract infections (UTI) to life-threatening pneumonias and bloodstream infections, novel drug therapies are more paramount than ever in tackling AMR (68). In 2014 two new glycopeptides and one new oxazolidinone were licensed but these drugs were only deemed effective against Gram-positive bacteria whereas most of the ESKAPE pathogens and other drug-resistant bacteria are generally Gram-negative (68). Since December 2014, two new cephalosporin/ β -lactamase inhibitor combinations have been licensed by the Food and Drug Administration (FDA) and these have been shown to have antimicrobial activity against Gram-negative bacterial strains (68). What is of note is that the development of new drugs often stems from the modification of already available drugs or drug types/classes, rather than the synthesis of completely novel compounds.

The discovery and development of novel therapeutics at the laboratory stage to combat AMR is vital but clinical trials will need to be carried out to ensure drug safety, tolerance and efficacy in patients with drug-resistant diseases.

1.7 Developing novel antimicrobials

There is an urgent need for new drugs and new methods of treating disease to combat bacteria that are resistant to conventional antibiotics. Focus has shifted away from classical small-molecule antibiotic towards the use of organic and inorganic nano-molecules in antimicrobial drug discovery.

1.7.1 Nanotechnology and gold nanoparticles

Nanotechnology, the use of materials with dimensions on the atomic or molecular scale, has become increasingly used in medical applications and has acquired a lot of scientific interest (69). Nanoparticles (NPs) are particles with lengths that range from 1-100nm in two or three dimensions according to the American Society Testing and Materials standard definition (70).

Gold nanoparticles (AuNPs), nanometer-sized particles of gold, have gained significant interest and have already been established in a wide variety of applications including electronics, biological imaging and materials science (71). Their popularity can be attributed to a number of distinctive characteristics. These include: high stability, biological compatibility, unusual optical and electronic properties, easy surface functionalization, and controllable morphology and size dispersion (72). Furthermore, gold nanoparticles can be readily functionalized with various biological molecules such as antibodies, enzymes and nucleotides (73). Silver nanoparticles (AgNPs) are widely used commercially as antibacterial agents in the health industry, food storage, textile coatings and in various environmental applications (74). However, in contrast to AuNPs, AgNPs are less biocompatible and display cytotoxicity to mammalian cells (75).

Among many other applications, gold nanoparticles serve as versatile platforms for therapeutic drug development and drug discovery. Gold nanoparticles have demonstrated antibacterial activities and have shown potential applications as anti-TB compounds in one particular study carried out by Zhou *et al.* (76). Antibacterial activity and the mechanism of action of the AuNPs are dependent upon their composition and surface modifications.

Modification of the gold nanoparticle surface with various compounds can result in the formation of novel conjugate compounds with potential antimicrobial activity. For example, Gifford *et al.* modified gold nanoparticles with thiol groups to form novel conjugate compounds. They showed that some of the new compounds they synthesized were

capable of inhibiting the growth of *Mycobacterium smegmatis* (a surrogate for Mtb used in scientific research) (77). Additionally, they demonstrated that the activity of one particular conjugate compound called LAL-3346 was specific for *M. smegmatis* growth inhibition vs. other bacteria tested including *E. coli* and *S. aureus* (77).

There are advantages to using gold nanoparticles in the ways mentioned above vs. conventional small-molecule drugs. Firstly, the ability to modify and manipulate the nanoparticle scaffold with a variety of ligands can result in the formation of nanoparticle conjugate compounds with multifunctional activities. Secondly, classical small-molecule drugs often have specific microbial target and can be easily expelled from the bacterial by efflux pumps (78). Due to their slightly larger diameter than drug efflux pumps, gold nanoparticles may be able to avoid antibiotic resistance more effectively than the aforementioned small-molecule drugs (78).

1.7.2 Cationic polymers

Cationic polymers are molecules with a net positive charge. Some cationic polymers are biocides; they display antimicrobial activity. Cationic biocides are widely used in domestic and public hygiene as well as to control microbial contamination in biofouling and in industry (79). More recently, antimicrobial polymers have been developed and successfully used as alternatives to existing antibiotics (80). In particular, cationic polymers have displayed selectivity for bacterial cells over mammalian cells by their ability to disrupt bacterial cytoplasmic membranes but not eukaryotic cytoplasmic membranes (80). Cationic polymers contain a hydrophobic segment in their alkyl chains that is compatible with the lipid bilayers of cytoplasmic membranes (80). They can form electrostatic complexes with anionic biomolecules, proteins and nucleic acids (81).

Cationic polymers can be used to functionalize gold nanoparticles by surface modification of the gold nanoparticle surface with polymer. Gifford *et al.* used thiol cationic ligands to functionalize gold nanoparticles in a set of ligand exchange reactions to synthesize gold nanoparticle conjugates with antimicrobial activity (77). Widely studied cationic polymers include natural polymers such as chitosan and synthetic polymers such as poly(2-dimethylamino)ethyl methacrylate (pDMAEMA) and poly-L-(lysine) (81). The pDMAEMA cationic polymer (Fig. 1.10) contains tertiary amino groups, is pH responsive and water-soluble (81). In previous literature, pDMAEMA polymers have been used for gene transfection as non-viral gene vectors (81,82). The combination of their biocompatibility,

relatively easy synthesis, and possibility of being able to functionalize the polymers have made them suitable candidates for gene delivery studies (83).

In 2014 by Mei *et al.* synthesized pDMAEMA and quaternized the pDMAEMA chains with 1-bromobutane to serve as templates in the preparation of antimicrobial particles (80). The antibacterial properties of these new particles were tested against *P. aeruginosa* and *S. aureus* using a growth inhibitory assay, a zone of inhibition test, and a LIVE/DEAD bacterial viability assay (80). This particular study was successful in synthesizing a new antimicrobial compound by conjugation of gold nanoparticles with the pDMAEMA polymer. However there are limitations to this study; firstly, only one type, one size pDMAEMA was used, secondly, there was no variation in the AuNPs that were used and thirdly, the antimicrobial activity of the compounds was only tested against *S. aureus* and *P. aeruginosa*.

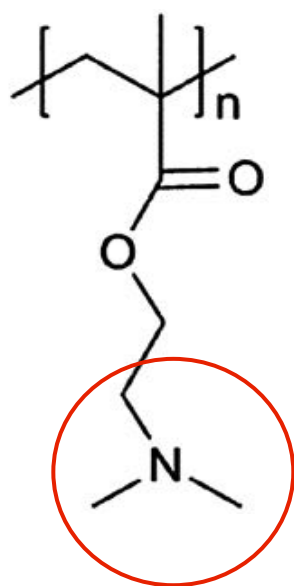


Figure 1.10. Chemical structure of pDMAEMA. Tertiary amino group is highlighted by red circle. n = chain length (81).

To date, most scientific reports with pDMAEMA as an antimicrobial agent have used a quaternized derivative or used pDMAEMA as a part of a copolymer with other polymers (84). The testing of these agents has been primarily against Gram-negative or Gram-positive bacterial species, in particular Gram-negatives. Currently, no cationic polymer-nanoparticle conjugate compounds have been synthesized, using pDMAEMA and gold nanoparticles, for specific antimicrobial testing against *M. smegmatis*, a surrogate for *M. tuberculosis* in scientific studies.

1.8 Aims and Objectives

The overall aim of this project was to improve the antimicrobial activity of pDMAEMA polymers, vs. polymers alone, against *M. smegmatis*, *Escherichia coli* and/or *Pseudomonas putida* by immobilization onto gold nanoparticles to form novel polymer-AuNP conjugate compounds. Our primary focus was on *M. smegmatis* while using *E. coli* and *P. putida* to draw comparisons between the activities of the novel compounds against the mycobacteria to those against the Gram-negatives.

Key Objectives:

1. Synthesize different sized gold nanoparticles and functionalize them with pDMAEMA and pHEA polymers to form novel conjugate compounds.
2. Investigate the stability of these newly synthesized compounds in saline and in different growth media.
3. Investigate the antimicrobial activity of the novel conjugate compounds against *M. smegmatis*, *E. coli* and *P. putida*.
4. Test the potential toxicity of the compounds against mammalian cells, using sheep erythrocytes as a model, by carrying out blood toxicity assays.

2. Materials and Methods

2.1 Suppliers

Luria-Bertani (LB) broth, LB agar plates, antibiotics; rifampicin, ampicillin, tetracycline and isoniazid (from Sigma-Aldrich) were provided by the Warwick Life Sciences media prep room.

The original poly(2-dimethylamino)ethyl methacrylate (pDMAEMA) and poly(*N*-hydroxyethyl acrylamide) (pHEA) polymers were previously synthesized and supplied by Dr Sarah-Jane Richards from Professor Gibson's Laboratory, Chemistry Department at the University of Warwick.

2.2 Bacteria

Escherichia coli TOP 10 was provided by Invitrogen and used for all experiments involving *E. coli* throughout the research project. *Mycobacterium smegmatis* MC² 155 was taken from ATCCTM 700084 culture collection and used throughout the whole research project. *Pseudomonas putida* strain KT2440 was provided by Professor E. Sim. This strain was cultured and used for all assays involving *P. putida* throughout the research project.

2.3 Growth media

LB media was used to grow cultures of *E. coli* and *P. putida*. Tryptic Soy Broth (TSB) + 0.05% Tween 80 was used to grow culture of *M. smegmatis*.

7H9 + 20% glycerol + 0.05% Tween 80 was prepared by dissolving 1.04g of Middlebrook 7H9 powder (BD Difco) in 200mL sterile water. 111µL of 20% Tween 80 and 0.4mL of 80% glycerol were added to the solution. The mixture was then autoclaved.

2.4 Antibiotic Stock

10µg/mL rifampicin (RIF), 100µg/mL isoniazid (INH), 25µg/mL ampicillin (AMP) and 100µg/mL tetracycline (TCN) antibiotic working stocks were used throughout this project.

Isoniazid and ampicillin were prepared in sterile water. Rifampicin was prepared in 10% dimethyl sulphoxide (DMSO). Tetracycline was prepared in LB media.

2.5 Growth Conditions

2.5.1 *E. coli*

E. coli was grown in LB media at 37°C, using either static incubation or incubation with shaking. Overnight cultures of *E. coli* were prepared by dissolving a sample of frozen *E. coli* glycerol stock in 4mL of LB media in a round-bottomed falcon tube. This was transferred to an incubator with shaking at 37°C and left overnight.

2.5.2 *P. putida*

P. putida was grown in LB media at 30°C, using either static incubation or incubation with shaking. Overnight cultures of *P. putida* were prepared by dissolving a sample of *P. putida* frozen glycerol stock in 4mL LB in a round-bottomed falcon tube. This was transferred to an incubator with shaking at 37°C and left overnight.

2.5.3 *M. smegmatis*

M. smegmatis was grown at 37°C, in static incubation or incubation with shaking. Fresh culture of *M. smegmatis* was grown in TSB media + 0.05% Tween 80 and incubated with shaking for 24 hours at 37°C. For all other assays 7H9GT media was used.

2.6 Buffers and Reagents

2.6.1 Phosphate-buffered saline (PBS) + Tween 80

0.955mL of 20% Tween 80 was added to 382mL of PBS. The mixture was the autoclaved.

2.6.2 Resazurin

One tablet of Resazurin was dissolved in 30mL PBS + Tween 80 in a 50mL falcon tube. The solution was sterile filtered into a new 50mL falcon tube. The tube was wrapped in tin foil and transferred to the fridge ready to use in resazurin microtiter assays (REMA).

2.7 Preparation of bacterial glycerol stocks

E. coli and *P. putida* were grown in 4mL LB media overnight in 37°C and 30°C incubators with shaking, respectively. After overnight growth, 500µL of each culture was added to 50mL LB media in two separate conical flasks (one for *E. coli* and one for *P. putida*). The newly setup cultures were then grown to an OD₆₀₀ (optical density) of ~0.4. 1.2mL of each culture was then pipetted into a separate 2mL cryovial. 400µL of sterile 80% glycerol was added to each cryovial and then mixed by pipetting. The cryovials were labeled and transferred to the -80°C freezer.

M. smegmatis was grown in TSB + Tween 80 in a 37°C incubator with shaking for ~24 hrs. 500µL of the overnight culture was added to 50mL 7H9GT in a conical flask. *M. smegmatis* was grown to an OD₆₀₀ of ~0.6. 1.2mL of the overnight culture was then pipetted into a 2mL cryovial. 400µL of sterile 80% glycerol was added to the culture in the cryovial and mixed by pipetting. The cryovial was labeled and transferred to the -80°C freezer.

2.8 Preparation of frozen aliquots of *M. smegmatis* for REMA

A sample of *M. smegmatis* glycerol stock was added to 10mL of TSB + Tween 80 and incubated with shaking at 37°C for 24 hours. 100mL of TSB + Tween 80 was added to a conical flask. To this, 5mL of the *M. smegmatis* overnight culture was added. The mixture was incubated at 37°C with shaking. The OD₆₀₀ was measured every hour until the bacteria had grown to an OD₆₀₀ of ~0.6. The 100mL culture was then separated into two 50mL falcon tubes. These were centrifuged for 10 minutes at 4°C, 4000 r.p.m. Following centrifugation the supernatant was removed from each tube. The pellet in each tube was resuspended in 40mL of PBS + Tween 80 and centrifuged for 10 minutes at 4°C, 4000 r.p.m. After centrifugation, the supernatant from each was removed once again and the pellets were resuspended in 2mL of PBS + Tween 80 and mixed by inversion. The mixture in both tubes were pipetted into 40 1.5mL eppendorf tubes in 100µL quantities. The eppendorf tubes were labeled with red stickers and transferred to the -80°C freezer.

2.9 Synthesis of AuNPs

2.9.1 Synthesis of citrate-stabilised gold nanoparticles

The procedure used to synthesis citrate-stabilised gold nanoparticles (AuNPs) was adapted from leong *et al.* (85).

First, 228.8mg of HAuCl_4 was dissolved in 700mL of distilled water (0.33mg/mL). The aqueous solution was heated to reflux in a scratch-free round-bottomed flask. The solution was divided into two round-bottomed flasks each containing 350mL of the solution. 300mg of sodium citrate was dissolved in 10.2mL of distilled water. This was added in a single portion to one of the flasks containing 350mL of HAuCl_4 solution to give an Au:citrate ratio of 1:3.5. 214mg of sodium citrate was dissolved in 10.2mL of distilled. This was added in a single portion to the other flask containing 350mL of HAuCl_4 solution to give an Au:citrate ratio of 1:2.5.

The temperature was maintained at reflux for 30 minutes, during which time a deep red and deep red/purple colouration formed in the flasks containing an Au:citrate ratio of 1:3.5 and 1:2.5, respectively. The mixtures were allowed to cool over a period of 1 hour. Assuming complete reduction of the HAuCl_4 into the particles, the total gold concentration in the final solution was 0.16mg/mL.

2.9.2 Synthesis of 5nm citrate-coated gold nanoparticles

The experimental procedure for the synthesis of 5nm citrate-coated gold nanoparticles was adapted from leong *et al* (85).

19.8mg of HAuCl_4 was dissolved in 240mL of distilled water (0.08mg/mL) at room temperature. To this was added 13.8mg of trisodium citrate (0.05mmol) dissolved in 223mL of distilled water, giving a final concentration of 0.21mmol/L. 5mL of an ice cold 0.1M (0.5mmol, 18.5mg) solution of NaBH_4 was added to the gold/citrate solution and stirred at room temperature overnight. Assuming complete reduction of the HAuCl_4 to gold particles, the total gold concentration in the final solution was 0.04mg/mL.

2.10 Nanoparticle characterisation

2.10.1 UV-Visible Spectroscopy

200 μL samples of the three citrate-stabilized gold nanoparticle solutions were pipetted into separate wells on a 96-well plate and scanned for UV-Visible analysis in a microplate reader, absorbance was measured between 450nm and 700nm in 1nm steps for all samples. BioTek Synergy HT and BioTek Epoch microplate readers were used.

2.10.2 Dynamic Light Scattering (DLS)

Three separate vials, each containing one of the three citrate-stabilized gold nanoparticle solutions, were prepared for Dynamic Light Scattering Analysis. DLS was conducted using a Malvern Zetasizer instrument. A water control was used. Scattered light was detected at 25°C and the Z-average size measured.

2.11 Synthesis of polymer-coated nanoparticles

2.11.1 General procedure

The three citrate-stabilized gold nanoparticles were coated separately with pDMAEMA and pHEA polymers with the four different degrees of polymerisation (DP 10, 25, 50 and 100) using the following procedure adapted from leong *et al* (85):

10mg of the polymer was added to a falcon tube, and dissolved in 1mL of milliQ water (8 tubes in total). This was refrigerated overnight. After, 100µL of the polymer solution was transferred each into three 1.5mL eppendorf tubes. To each tube 1mL of the 5nm, 1:2.5 (Au:citrate) or 1:3.5 (Au:citrate) citrate-stabilized gold nanoparticle solutions was added. The eppendorf tubes were left at room temperature for 30 minutes. To remove excess polymer, all of mixtures were centrifuged at for 20 minutes at 20,000 r.p.m. After, the supernatants were carefully decanted and the particles were re-dispersed in 1mL milliQ water. The tubes were further centrifuged for another 20 minutes at 13,000 r.p.m. Again, the supernatants were discarded and the particles were dispersed in 1mL of high quality water. Assuming complete incorporation of the citrate-coated gold particles into the final polymer-coated particles the total concentration of gold in the final solution was 8.3mM, 1.6mg/mL. This was carried out for every polymer.

2.11.2 Functionalising nanoparticles with pDMAEMA:pHEA polymers

Aqueous solutions of pDMAEMA and pHEA polymers were prepared by dissolving 10mg of each in 1mL of high-purity water. In separate 1.5mL eppendorf tubes the following ratios of pDMAEMA:pHEA (%) were set up: 100:0 (100µL pDMAEMA, 0µL pHEA), 75:25 (75µL pDMAEMA, 25µL pHEA), 50:50 (50µL pDMAEMA, 50µL pHEA), 25:75 (25µL pDMAEMA, 75µL pHEA), 0:100 (0µL pDMAEMA, 100µL pHEA). These were set up for all the polymers (20 tubes altogether). All pDMAEMA:pHEA combinations were the of the same DP i.e. pDMAEMA DP 10 would be mixed with pHEA DP 10, and pDMAEMA DP 50

combined with pHEA DP 50 etc.

Three sets of the 20 different combinations of mixtures above were prepared (total of 60 tubes). To each tube in the first set was added 1.5mL of the 1:2.5 AuNP solution. To each tube in the second set was added 1mL of the 1:3.5 AuNP solution. To each tube in the third set was added 1mL of the 5nm AuNP solution. All tubes were incubated at room temperature for 30 minutes. The mixtures were then centrifuged for 20 minutes at 8000 r.p.m. The supernatant from each tube was then removed and the pellets of the 1:2.5 and 1:3.5 AuNP mixtures were re-dispersed in 1mL high-quality water. The pellets of the 5nm AuNP mixtures were dispersed in 400mL high quality water using centrifuge filters. The total concentration of gold in these final solutions was 0.4mg/mL.

2.12 Stability Testing

2.12.1 Saline stability

To a clear 96-well plate, 50 μ L of H₂O was added to all the wells excluding column 1. 100 μ L of 1M NaCl in H₂O was added to each well in column 1. This was then serially diluted across the 96-well plate by transferring 50 μ L of NaCl into the next well until column 11 (11 dilutions and one H₂O control in the last well of each row) to give a final concentration of 1mmol/L. The extra 50 μ L in the wells of column 11 was discarded to equalize the volume. 50 μ L of the 1:2.5 AuNP solution, 1:3.5 AuNP solution or the 5nm AuNP was added to the wells of a row.

Three other 96-well plates were prepared with dilutions of NaCl as described above. To each row on all three plates, 50 μ L of a different polymer-coated AuNP compound was added. All plates were transferred to a plate reader and absorbance spectra attained for each sample between 450nm and 700nm in steps of 10nm. Normalized absorbance = A_{700}/A_{450} .

2.12.2 Stability in growth media

Three 96-well plates were prepared with different media. Plate 1 – LB, plate 2 – 7H9GT, plate 3 – PBS (control). 50 μ L of media was added to all wells of the plate. Then the following was added: columns 1-5 rows A-D 50 μ L polymer-coated 5nm AuNPs, columns 1-5 rows E-H 50 μ L polymer-coated 1:3.5 AuNPs, column 8-12 rows A-D 50 μ L polymer-coated 1:2.5 AuNPs. Plates were transferred to three separate plate readers and

absorbance measurements between 450nm and 700nm were taken every hour for 24 hours. Absorbance values for each compound in each well were normalized by A_{700}/A_{450} .

2.13 Synthesis of 2nm polymer-coated AuNPs

The following procedure was adapted from Parry *et al* (86).

Solutions of HAuCl_4 , pDMAEMA DP 100, pHEA DP 100, and NaBH_4 were prepared. 15mg of HAuCl_4 was dissolved in 75mL of water (0.5mM concentration). 60mg of pDMAEMA DP 100 was dissolved in 765 μL of water. 45mg pHEA DP 100 was dissolved in 765 μL of water. 30mg of NaBH_4 was dissolved in 15.5mL of water (50mM concentration).

2nm nanoparticles were synthesized and directly functionalized with 100% pDMAEMA DP 100, 50:50 pDMAEMA:pHEA DP 100, and 100% pHEA DP 100. Three tubes were set up. In tube 1, 0.5mL of pDMAEMA DP 100 solution and 25mL of HAuCl_4 solution were combined. In tube 2, 25mL of HAuCl_4 solution, 0.25mL of pDMAEMA DP 100 solution and 0.25mL of pHEA DP 100 solution were combined. In tube 3, 25mL of HAuCl_4 and 0.5mL of pHEA DP 100 were combined. Each of the mixtures was treated with 5mL NaBH_4 solution while stirred. An immediate colour change from yellow to pale brown was observed in all cases. Stirring continued for 1 hour, after which the solutions were purified by centrifugal filtration for 10 minutes at 7500 r.p.m. After centrifugation each solution was made up to 1.5mL with water. Solutions were then transferred to separate 1.5mL eppendorf tubes.

2.14 REMA Assays

2.14.1 General procedure

200 μL of sterile water was dispensed into the wells on the outer edge of a clear, sterile flat-bottomed 96-well plate to prevent evaporation. 50 μL of 7H9GT or LB was added to all wells except those on the outer edge and column 2. 100 μL of each compound (polymer or AuNP conjugates) was added to the wells of column 2, rows B-G. An antibiotic control was included: AMP for *E. coli*, TCN for *P. putida* and RIF/INH for *M. smegmatis*. Two-fold dilutions of the compounds were prepared directly in the plate by transferring 50 μL of each compound into the next well until column 10. The extra 50 μL of solution in each well of column 10 was discarded to equalize the total volume in each well across the plate. A sterile negative control was included – no compound was transferred to column 11, only media. 50 μL of bacterial culture was added to all the wells except the outer edge.

Plates were covered with tin foil and incubated for a specific length of time: 24 hrs for *M. smegmatis*, 16/18 hrs for *E. coli* and *P. putida* in static incubation at 37°C, 37°C and 30°C, respectively. Following incubation, 25µL of Resazurin solution was added to all wells excluding the outer edge. Plates were returned to static incubation for 24 hrs (*M. smegmatis*) or ~90 minutes (*E. coli* and *P. putida*). Plates were inspected for a change in colour from blue to pink. The minimal inhibitory concentration (MIC) was defined as the lowest concentration of the compound that prevented a colour change.

Figure 2.1 shows a representative REMA assay set-up.

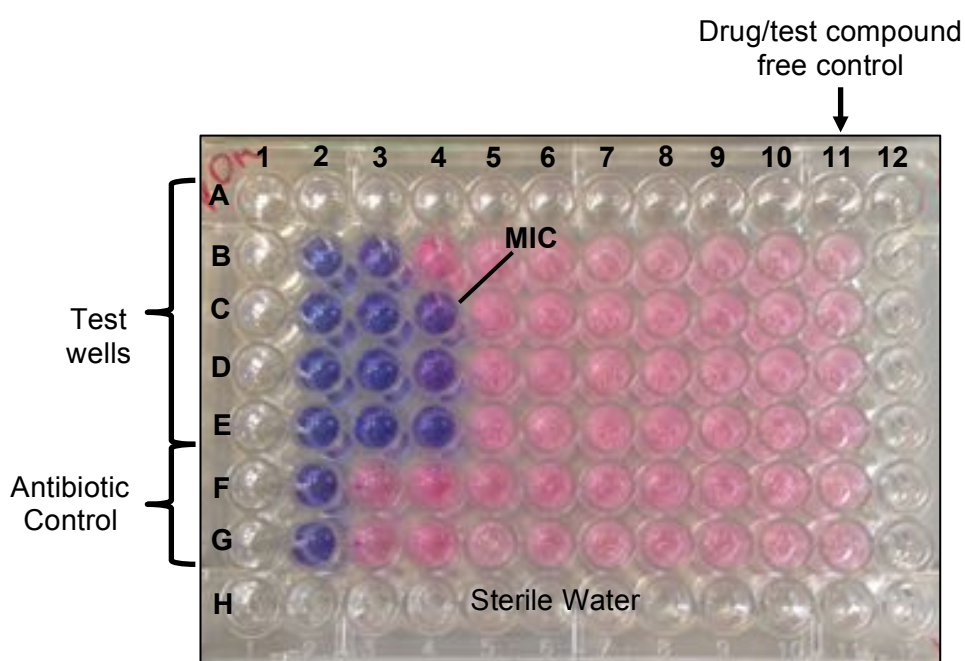


Figure 2.1. Representative 96-well plate format for screening compounds to determine minimum inhibitory concentration. MIC is the concentration of solution in the last well to turn blue across the plate (shown).

2.14.2 Screening known antibiotics for antimicrobial activity

100µL of 1 frozen aliquot of *M. smegmatis* was thawed and dissolved in 2.4mL of 7H9GT. 1mL of this was combined with 9mL of 7H9GT in a 15mL falcon tube for a 1 in 10 dilution. 10-fold serial dilutions were prepared in two 15mL falcon tubes, each containing 9mL of 7H9GT media, by transferring 1mL from one falcon tube into the next. This produced three different dilutions of inoculum: 1 in 10, 1 in 100 and 1 in 1000. A 1 in 100 dilution was also prepared made directly from the 2.4mL culture by transferring 50µL of culture to 4.95mL of 7H9GT.

100µL of *E. coli* overnight culture was transferred to 500mL LB broth and grown to an OD₆₀₀ of ~0.4. The culture was diluted 1 in 10 by transferring 200µL of the culture to 1.8mL LB in a 15mL falcon tube. Two 10-fold serial dilutions of the 1 in 10 dilution were prepared in two other 15mL falcon tubes each containing 1.8mL LB, by transferring 200µL from one tube to the next. This was repeated for *P. putida* in parallel.

REMA assays were carried out as described in **2.15.1 General procedure** to assess antimicrobial activity of AMP against *E. coli*, TCN against *P. putida* and RIF/INH against *M. smegmatis*. Assays were replicated as necessary.

2.14.3 Testing antimicrobial activity of polymers and novel compounds

REMA was used to investigate the antimicrobial activity and determine MIC values for all of the polymers and the polymer-coated AuNP conjugate compounds synthesized prior. These were test for activity against *E. coli*, *P. putida* and *M. smegmatis* in separated assays. Each bacteria was diluted 100 fold by transferring 100µL of bacterial culture to 9.9mL of media. 96-well plates were set up as described in **2.15.1 General procedure**.

N.B. REMA assays were replicated by Dr Richards in parallel throughout.

2.15 Determining CFU/mL

The Miles and Misra method was used to determine the number of colony-forming units per mL (CFU/mL) in a particular bacterial dilution used for REMA assay (87). CFU procedures were performed in parallel with REMA. 1 in 10, 1 in 100 and/or 1 in 1000 of dilutions of bacteria were prepared from liquid culture. After, 10-fold serial dilutions (10^{-1} – 10^{-8}) of the dilution culture were prepared in eppendorf tubes by transferring 20µL from one tube to the next, each containing 1.8mL of media. An inoculum of 100µL from each 10-fold dilution was pipetted as a drop on a sector of an LB agar plate. This procedure was adjusted for *M. smegmatis*. 100µL of inoculum from each 10-fold dilution was pipetted onto the whole agar plate and spread across the plate using an L-shaped spreader. The inocula were allowed to dry before sealed with tin foil and transferred to static incubation. Plates were incubated for a specific length of time to allow colonies to grow: 24 hours for *E. coli* and *P. putida*, 48/72 hours for *M. smegmatis*. After incubation, plates were inspected and all visible colonies counted. CFU/mL was determined using the following equation:

CFU/mL = (no. of colonies x dilution factor)/volume plated (mL)

N.B. Each CFU procedure was replicated by Dr Richards in parallel throughout.

2.16 Blood Toxicity Assays

Polymer-blood solutions were prepared by combining 250 μ L of ovine blood with 250 μ L of polymer (10mg/mL) in a 1.5mL eppendorf tube. This was carried out for all of the polymers, pDMAEMA and pHEA DP 10, 25, 50 and 100. PBS and H₂O controls were prepared in the same way. Blood-AuNP conjugate compound solutions were prepared by combining 125 μ L of ovine blood with 125 μ L of the compound (Au concentration 0.4mg/mL). PBS control was prepared by combining 100 μ L of ovine blood with 100 μ L PBS in an eppendorf tube. H₂O control was prepared in the same way.

2.16.1 Haemagglutination assay

25 μ L of a polymer-blood/polymer-compound solution was added to 25 μ L of PBS in a clear, sterile, round-bottomed 96-well plate. To this plate 25 μ L of PBS/blood, H₂O/blood and PEI/blood solutions were also added to the plate as controls for this assay. The plate was incubated at room temperature for 1 hour and plates inspected for haemagglutination. Photos of these were then taken. Observations were compared to those of the controls incubated with PBS (negative control for haemagglutination), H₂O (haemagglutination observed) and polyethyleneimine (PEI) (positive control for haemagglutination). This was carried out for every polymer, and for 2nm DP 100 50% pDMAEMA, 2nm DP 100 100% pDMAEMA, 5nm 100% pDMAEMA DP 10, 25, 50 and 100 AuNP-conjugate compounds. Assays were completed in replicates of three.

2.16.2 Haemolysis assay

Haemolysis of ovine blood was examined by incubation with the polymers and polymer-coated AuNP conjugate compounds for one hour at room temperature. Each compound-blood solution was serially diluted by 1 in 4 in PBS in 1.5mL eppendorf tubes. Each dilution was then centrifuged at 5000 r.p.m for 5 minutes. Pictures of the supernatant and pellet formed, after centrifugation, were taken. 90 μ L of PBS was added to as many wells as necessary on a clear, round-bottomed 96-well plate. To each well containing PBS 10 μ L of supernatant from each tube was dispensed. Haemolysis was determined by measuring the absorbance at 450nm of 10 μ L of the supernatant in 90 μ L PBS. Incubation with PBS buffer was set as a negative control for haemolysis and incubation with pure H₂O was a positive

control for haemolysis. % Haemolysis was calculated using the equation below.

$$\% \text{ Haemolysis} = [(A_{\text{polymer}} - A_{\text{PBS}})/(A_{\text{H}_2\text{O}} - A_{\text{PBS}})] \times 100\%$$

This was carried out for all polymer-blood solutions and blood-AuNP conjugate compound solutions used for the haemagglutination assay. Assays were completed in replicates of three.

2.17 2nm compounds: further testing

2.17.1 Minimum bactericidal concentration (MBC) Assay

Prior to completing the assays the following were prepared:

E. coli and *P. putida* from glycerol frozen stock were grown in 50mL LB to an OD₆₀₀ of ~0.4. Each bacterial culture was diluted 1 in 100 by inoculating 9.9mL of LB in a 15mL falcon tube with 100µL of culture.

40 x MIC of ampicillin was prepared by diluting 100mg/mL stock in water by serially diluting 1 in 100 followed by a 1 in 4 dilution to achieve a final concentration of 250µg/mL.

40 x MIC of tetracycline was prepared by diluting 10mg/mL stock in LB by serially diluting 1 in 100 followed by a 1 in 3 dilution to achieve a final concentration of 31.2µg/mL.

The 2nm compounds were concentrated to 40 x MIC by Dr Richards by conducting centrifugation as necessary. Final concentrations of these compounds are shown in Table 2.1.

Table 2.1. 40 x MIC of 2nm AuNP conjugate compounds.

Bacteria	Compound 40 x MIC (mg/mL)	
	2nm 100% pDMAEMA DP 100	2nm 50% pDMAEMA DP 100
<i>E. coli</i>	0.5	1
<i>P. putida</i>	2	8

A sterile, clear 96-well plate was set-up like that for a REMA assay. 200µL of distilled water was added to all wells of the outer edge of the plate. To all wells of columns 3-11, rows B-D, LB media was added. To the empty wells (column 2, rows B-D) 100µL 40 x MIC of 2nm compound/antibiotic was added. The compounds were serially diluted 1 in 2 across the plate by transferring 50µL into the next well until column 10. The extra 50µL in the wells of column 10 was discarded. 50µL of the 1 in 100 dilution of *E. coli* or *P. putida* culture was added to the wells containing the antimicrobial compounds and media.

- a) Row B compound – 40 x MIC 2nm 100% pDMAEMA DP 100 (0.5mg/mL for *E. coli* and 2mg/mL for *P. putida*).
- b) Row C compound – 40 x MIC 2nm 50:50 pDMAEMA:pHEA DP 100 (1mg/mL for *E. coli* and 8mg/mL for *P. putida*).
- c) Row D antibiotic controls – 40 x MIC ampicillin (250µg/mL) for *E. coli* and 40 x MIC tetracycline (31.2µg/mL) for *P. putida*.

Plates were then incubated for 24 hours at 37°C for *E. coli* and 30°C for *P. putida*. Following incubation for both plates all 3 x 10µL from each well containing antimicrobials and bacteria were pipetted onto a sector LB agar and allowed to dry. The plates were transferred to static incubation for 72 hours at 37°C for plates containing *E. coli* and 30°C for plates containing *P. putida*. After incubation the plates were inspected visually for any colony growth; the lowest concentration of the antimicrobial to yield no colonies was determined to be the MBC.

2.17.2 Turbidity Assay

Two 96-well plates were set-up, one for *E. coli* and *P. putida* as described for the MBC assay. The only modification to the procedure was the concentration polymer-coated 2nm AuNPs and antibiotic controls used. For this assay the concentration of the 2nm 100% pDMAEMA DP 100 and 2nm 50:50 pDMAEMA:pHEA DP 100 was 0.4mg/mL. The concentrations of ampicillin and tetracycline used were 25µg/mL and 100µg/mL, respectively. Plates with *P. putida* or *E. coli* were incubated at 30°C and 37°C, respectively, with shaking for ~18hrs. After incubation plates were put into a plate reader and absorbance at 600nm measured, three absorbance readings were taken for each well containing antimicrobials and bacteria and the mean of these three readings calculated.

2.17.3 Time-Kill Curve Assay

Two 96-well plates were set-up, one for *E. coli* and one for *P. putida*. To all the wells in row A columns 1-6, 50µL 2 x MIC of 2nm 100% pDMAEMA DP 100 was added (0.025mg/mL for *E. coli* and 0.1 mg/mL for *P. putida*). To all the wells in row B columns 1-6, 50µL 2 x MIC of 2nm 50:50 pDMAEMA:pHEA DP 100 was added (0.05mg/mL for *E. coli* and 0.4mg/mL for *P. putida*). Six wells for six different time points: t(mins) = 15, 30, 60, 180, 300 and 1080 (18 hours). *E. coli* and *P. putida* cultures grown to an OD₆₀₀ of ~0.4 were diluted 1 in 100 by inoculating 9.9mL of LB media with 100µL of culture. 50µL of the diluted

E. coli culture was added to all the wells containing the polymer-coated nanoparticles on one plate and 50µL of the diluted *P. putida* culture to all the wells containing polymer-coated nanoparticles to the other plate. The plate containing *E. coli* was incubated at 37°C and the plate containing *P. putida* was incubated at 30°C.

At each time point the plates were removed from incubation. 20µL of the bacteria/compound mixture from the first well (i.e. A1 t(mins) = 15) was added to 180µL of LB in a 1.5mL eppendorf tube to give a 10⁻¹ dilution. Plates were then returned to incubation as quickly as possible for the length of time required before the next time point. The 10⁻¹ dilution was then serially diluted 1 in 10 across 7 other 1.5mL eppendorf tubes (8 total), each containing 180µL of LB, by transferring 20µL into the next eppendorf until 10⁻⁸ was reached (8th eppendorf tube). The extra 20µL from the 8th eppendorf was discarded. 100µL of each dilution was pipetted onto a sector of an LB agar plate.

This procedure above was carried out for both *E. coli* and *P. putida* at each time point. All LB agar plates were incubated overnight at 37°C for *E. coli* and 30°C for *P. putida*. Following incubation, the plates were inspected and the number of colonies at each dilution for every time point counted and CFU/mL calculated using the formula below:

CFU/mL = (no. of colonies x dilution factor)/volume plated (mL)

Log₁₀CFU/mL was calculated and plotted over time.

3. Results and Discussion

The results of this study focus on comparing the antimicrobial activity of pDMAEMA polymers to the antimicrobial activity of novel polymer-coated gold nanoparticle conjugate compounds against the three bacterial species: *E. coli*, *P. putida* and *M. smegmatis*.

M. smegmatis is a Gram-positive, non-pathogenic surrogate for *M. tuberculosis* (88–90). The highly infectious nature of MDR *M. tuberculosis* restricts its use for large scale screening of probable drug candidates therefore sensitivity profiles of other mycobacteria including *Mycobacterium phlei*, *Mycobacterium fortuitum* and *M. smegmatis*, have been determined against anti-TB drugs, rifampicin and isoniazid (91). *M. smegmatis* exhibited the most similar profile to MDR-TB and demonstrated 100% specificity and 78% sensitivity vis-à-vis MDR-TB in anti-TB compound test screens (91). Taking this into account, *M. smegmatis* can be used as a ‘surrogate’ for TB in scientific experiments. This means that novel compounds with the ability to inhibit *M. smegmatis* growth could have the potential to serve as next generation antibiotics to treat challenging pathogens such as MDR-TB and XDR-TB, in future.

E. coli TOP10 and *P. putida* KT2440 are Gram-negative, non-pathogenic strains, safe to use and easy to grow in the lab. *E. coli* is able to reproduce and grow very rapidly, doubling its population approximately every half hour (92). *E. coli* and *P. putida* are both widely used as experimental models. They were used in this project to compare the activity of the polymers and novel conjugate compounds against these Gram-negative strains to the activity against *M. smegmatis*. Any significant antimicrobial activity shown against *E. coli* and/or *P. putida* means that the novel compounds could have uses as future antimicrobial agents for pathogenic Gram-negative bacteria related to these strains i.e. *Pseudomonas aeruginosa* and drug-resistant *E. coli*.

3.1 Establishing viable bacteria and antibiotic activity

Colony-forming unit is used to determine the number of viable bacteria in a particular bacterial sample. Cultures of *E. coli*, *P. putida* and *M. smegmatis* were diluted 10-fold, 100-fold and 1000-fold. These were then serially diluted by 10-fold to a final dilution of 10^{-8} and plated on LB agar. The Miles and Misra method was used to calculate colony-forming unit/mL (CFU/mL) for each bacterial dilution, for all three species of bacteria (Table 3.1).

This method was used to determine CFU/mL because it's relatively faster and easier to process than other methods and produces less bacterial contamination at the working surface (93). It was difficult to count individual colonies of *M. smegmatis* on LB agar plates due to the aggregative nature of the bacteria and its tendency to clump. Pipetting mixtures, containing *M. smegmatis* culture, up and down helped to prevent such clumping by disbursing the bacteria in the media. Additionally, the plating method used to count visible colonies was adjusted for *M. smegmatis* by plating out each dilution onto individual LB agar plates for each dilution and spreading the dilution mixture across the whole plate. Using this method, it was easier to inspect and count individual colonies.

Table 3.1. MIC and CFU/mL values for *E. coli*, *P. putida* and *M. smegmatis* treated with known antibiotics. * Diluted directly from culture, not serially diluted.

Bacteria	Dilution	Antibiotic	MIC ($\mu\text{g/ml}$)	CFU/mL
<i>E. coli</i>	1:10	Ampicillin	6.25	6.9×10^6
	1:100		6.25	1.1×10^6
<i>P. putida</i>	1:10	Tetracycline	1.56	1.17×10^9
	1:100		0.78	4.5×10^6
<i>M. smegmatis</i>	1:10	Rifampicin	0.16	Uncountable
	1:100*		5-1.25	3.7×10^6

REMA assays were performed to determine minimum inhibitory concentration (MIC) for known antibiotics ampicillin, tetracycline and rifampicin against *E. coli*, *P. putida* and *M. smegmatis*, respectively (Table 3.1). The MIC is the lowest concentration of an antimicrobial that will inhibit visible growth of a microorganism (94). For REMA, resazurin reagent was used to determine cell viability and therefore identify the MIC. In its oxidized state resazurin is blue in colour. Viable, metabolically active cells reduce resazurin to resorufin, which is a pink colour, using oxidoreductases (Fig. 3.1) (95). If an antibiotic agent has successfully inhibited growth, there is no colour change and resazurin remains blue.

REMA assays testing rifampicin were initially unsuccessful; cells were alive at all concentrations of the antibiotic. The assay was repeated using fresh working stocks of rifampicin. *M. smegmatis* was diluted 100-fold directly from culture by transferring 100 μL of culture to 9.9mL 7H9GT rather than being serially diluted from an initial 10-fold dilution. Isoniazid activity was also tested against *M. smegmatis* but no results were obtained due to insufficient activity and inability to attain MIC values, despite repeating the assay three times. Results produced by assays using 1000-fold bacterial dilutions are not shown due to inconsistencies in colony numbers and, in some cases, no colony growth.

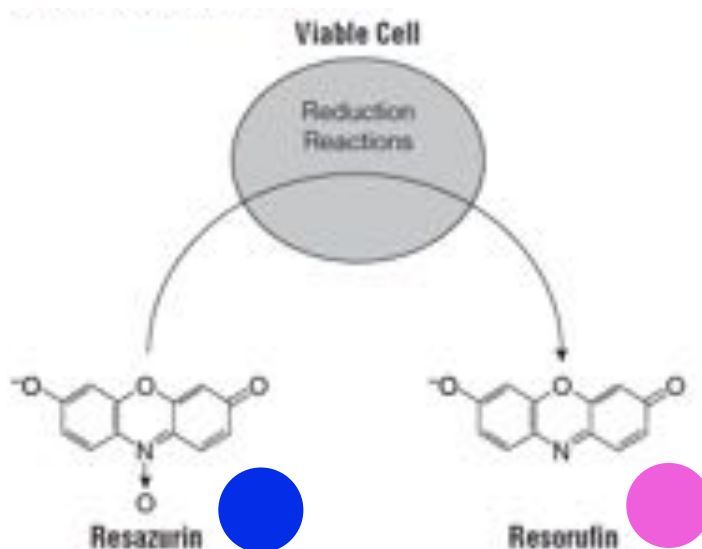


Figure 3.1. Conversion of resazurin to resorufin by metabolically active cells. Resazurin solution is a blue colour but viable live cells reduce resazurin to resorufin (pink) by oxidoreductase enzymes (95).

Results from CFU/mL were used to optimize the MIC values for ampicillin, tetracycline and rifampicin. A 100-fold dilution was the dilution factor of choice as this yielded the most consistent results with a sufficient number of viable bacteria. 10-fold dilutions often yielded too many colonies on LB agar; colonies would often overlap and were difficult to count accurately. *M. smegmatis* colonies grown from a 10-fold dilution mixture could not be counted due to the vast number of overlapping, aggregated colonies on a single plate. These antibiotics were used as positive controls for subsequent REMA assays to investigate the antimicrobial activity of the pDMAEMA and pHEA polymers, and novel polymer-AuNP conjugate compounds.

3.2 Polymers and nanoparticles

3.2.1 Polymer synthesis

Our aim was to focus on enhancing the activity of a known cationic polymer that has previously shown to have antimicrobial properties, by immobilization onto gold nanoparticles.

Dr Sarah-Jane Richards provided the polymers, pDMAEMA and pHEA, throughout this project. Dr Richards has previously synthesized and worked with these polymers before in prior research (96). Other scientists have documented the antimicrobial potential of pDMAEMA polymers. These are known cationic polymers with an ability to disrupt

bacterial cytoplasmic membranes and eventually cause bacterial cell death (80). These polymers are relatively easy to synthesize and have also demonstrated relatively good biocompatibility, a property useful in the development of novel therapeutics (83).

To prevent gold nanoparticles from aggregating in solution a stabilizing agent is required. PHEA polymers are non-charged, non-interacting polymers with extensive stabilizing properties. Previous work by Richards *et al.* has shown that incorporation of pHEA on the gold nanoparticles surface leads to good gold nanoparticle stabilization (96). Polyethylene glycol (PEG) methacrylate is another non-ionic stabilizer and has been used to stabilize nanoparticles such as silver nanoparticles in previous research (97). However, pHEA was chosen for its water solubility and non-thermo-responsive behavior, unlike PEG methacrylates (96). Thermo-responsive polymers, such as PEG, show sharp changes in properties as a result of a small or modest change in temperature (98). These polymers exhibit a volume phase transition at a certain temperature, which causes a sudden change in the solvation state of the polymer (98). The pHEA polymers do not display this type of behavior and can therefore resist changes in solvation even when incubated at different temperatures during REMA.

Dr Richards used reversible-addition fragmentation chain transfer (RAFT) polymerization to prepare the polymers. RAFT is a controlled/living free radical polymerization that provides precisely controlled polymer molecular weights with narrow dispersities. Additionally the use of RAFT polymerization renders each polymer with a trithiocarbonate end-group installed at the ω -terminus (Fig. 3.2). This allows for direct immobilization onto gold nanoparticles due to the affinity of sulfur for gold surfaces. RAFT is generally considered one of the best strategies to obtain functional polymeric systems for defined applications (99). Four different degrees of polymerization (DP 10, 25, 50 and 100) were targeted for each monomer during synthesis of the pDMAEMA and pHEA polymers in order to determine whether molecular weight had any effect on antimicrobial activity. Figure 3.2 shows the structures of pDMAEMA and pHEA.

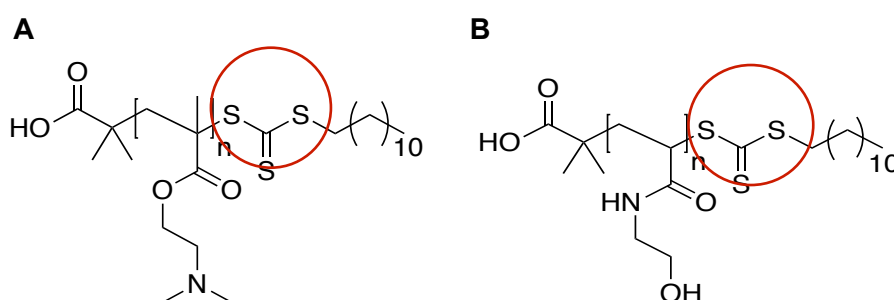


Figure 3.2. Chemical structures of (A) pDMAEMA and (B) pHEA. n = the chain length determined by the degree of polymerisation (DP). Trithiocarbonate ends highlighted by red circles. (Structures provided by Dr Richards).

3.2.2 Synthesis and characterization of AuNPs

Citrate-stabilized AuNPs were synthesized to provide platforms on which to immobilize the previously synthesized pHEA and pDMAEMA polymers. Gold nanoparticles have gained significant interest in scientific research due to their high stability, biological compatibility, easy surface functionalization, and controllable morphology and size dispersion (72). AuNPs were synthesized using the standard citrate/HAuCl₄ reduction approach (100). The Au₃₊ ions are reduced to gold neutral atoms by the citrate in the solution. The solution becomes supersaturated as more and more gold atoms form and the gold gradually starts to precipitate (101). Gold nanoparticles vary from red to purple in colour depending on their size (Fig. 3.3) therefore a colour change is observed from gold to red/purple as the gold nanoparticles form. The size of the nanoparticles is dependent on the ratio of Au: citrate. NaBH₄, a stronger reducing agent, was used to obtain nanoparticles with a diameter <10nm.

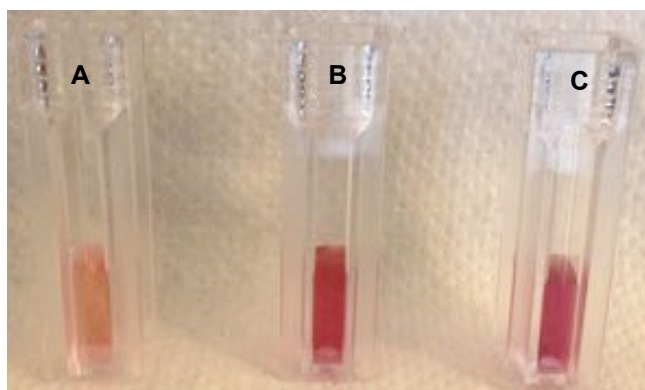


Figure 3.3. Colouration of gold nanoparticles with different dimensions. (A) Light red solution – 5nm. **(B)** Deep red solution – 1:3.5 Au: citrate. **(C)** Deep red/purple solution – 1:2.5 Au: citrate.

Gold nanoparticles exhibit a distinct optical feature that is often referred to as localized surface plasmon resonance (LSPR), an optical phenomena generated by light when it interacts with conductive nanoparticles that are smaller than the incident wavelength (102). The electric field of incident light excites electrons in the conduction band of gold nanoparticles resulting in localized plasmon oscillations with a resonant frequency (102). LSPR of gold nanoparticles results in a strong absorbance band in the visible spectrum region that can then be measured by UV-Visible spectroscopy (103). The LSPR spectrum is dependent on the size and shape of the gold nanoparticles therefore different LSPR spectra can be used to characterize gold nanoparticles of varying sizes.

Dynamic light scattering (DLS) is an analytical tool that is often used to measure the hydrodynamic size of nanoparticles in a liquid environment (104). Gold nanoparticles are capable of scattering light at or near their surface plasmon resonance wavelength (104). DLS measures the light scattered from a laser that passes through the nanoparticles and the modulation of scattered light intensity as a function of time is analyzed and the size of the particles determined (105).

Following synthesis, the nanoparticles were characterized using UV-Visible spectroscopy to provide estimations of their dimensions. Results from UV-Vis (Fig. 3.4) identified nanoparticles in the range 5-36nm. Tabular material from Haiss *et al* (106) was used to determine the size of the nanoparticles from UV-Vis spectra by comparing the absorbance at the surface plasmon resonance peak (A_{spr}) for each AuNP spectrum to known numerical data (106). Using this method, the 1:2.5 Au:citrate nanoparticles were determined to have a diameter of ~36nm. The 5nm and 16nm AuNPs were determined by the ratio of absorbance at the A_{spr} to the absorbance at 450nm (A_{450}) and the ratio value compared to known reference values (106).

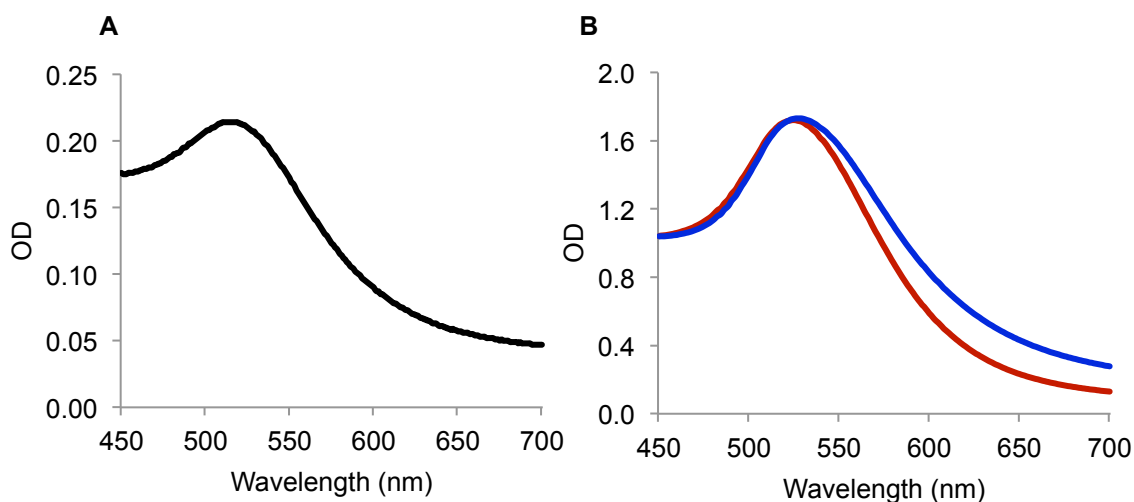


Figure 3.4. UV-Visible Spectra. (A) Mean maximum OD at ~513nm, nanoparticles size ~5nm. **(B)** Red line – mean maximum OD at ~524nm, nanoparticle size ~16nm, blue line – mean maximum OD at ~526nm, nanoparticle size ~36nm.

Figure 3.4 shows that as the nanoparticle size increases the wavelength of the surface plasmon resonance (mean maximum peak) related absorption shifts to the right giving a waveform that is longer. Table 3.2 summarizes findings from UV-Vis. DLS was unsuccessful and results produced were erroneous. The samples of AuNP solution used for DLS analysis may have been too concentrated and perhaps should have been diluted down. If a sample is too concentrated, it will cause multiple scattering or viscosity effects

meaning that the measured size of the nanoparticles in the sample are inaccurate (107). It is possible that other factors such as the presence dust may have interfered with the DLS analysis.

Table 3.2. Citrate-stabilised gold nanoparticles used in this project and determination of size. (Table provided by Dr Richards).

Particle	Citrate: Au	NaBH ₄ : Au	λ_{SRP} (nm)	A_{SPR}/A_{450}	Diameter (nm)	
					DLS	UV - Vis
Au₅	1	10	510	1.26	Error	5
Au₁₆	3.5	-	524	1.65	Error	16
Au₃₆	2.5	-	526	N/A	Error	36

The overall aim here was to synthesize gold nanoparticles of varying dimensions (small, medium and larger nanoparticles) and this was successful. These gold nanoparticles were then later modified with pDMAEMA and pHEA polymers to create a repertoire of novel conjugate compounds for investigation.

3.2.3 Polymer-coated AuNPs

The next step, following the synthesis of the gold nanoparticles, was to immobilize the polymers onto the pre-formed gold nanoparticles. Polymers were immobilized by mixing polymer with nanoparticles in solution, incubating at room temperature followed by centrifugation to remove excess polymer. The AuNPs were coated separately with pDMAEMA and pHEA. The trithiocarbonate end-group on the ω -terminus of both polymers allows pDMAEMA and pHEA to bind to the surface of the gold nanoparticles. This is because gold nanoparticles have a high affinity for thiol derivatives (108).

Three different sized nanoparticles, four pDMAEMAs (DP 10, 25, 50 and 100) and four pHEAs (DP 10, 25, 50 and 100) gave a total of 24 novel conjugate compounds. The antimicrobial activity, if any, of these compounds against *E. coli*, *P. putida* and *M. smegmatis* was later investigated using REMA.

3.3 Stability

3.3.1 Saline stability

Salt-induced aggregation of metal nanoparticles occurs frequently due to shielding of the negative charges on the gold nanoparticles by NaCl ions (a strong electrolyte), which then allows the particles to approach and aggregate into large clumps in solution (109). The

aggregation of the AuNPs has an effect on their optical properties, which can be used to monitor gold nanoparticle stability upon addition of NaCl solution at varying concentrations. To minimize aggregation, the surface of the gold nanoparticles can be modified with various ligands.

Saline stability was monitored by measuring absorbance between 450nm and 700nm of the AuNPs before and after functionalization with polymers. All pHEA-coated AuNPs showed higher stability compared to the non-functionalized citrate-stabilized particles. Some of the nanoparticles, in particular the 16nm nanoparticles, displayed poor long-term stability but when coated with pHEA the particles remained stable indefinitely. This indicated that the pHEA-functionalized nanoparticles would be capable of remaining stable in saline environments such as LB broth, 7H9GT and PBS. This is important as these media were used for other assays including REMA and blood toxicity assays. On the other hand, pDMAEMA-coated AuNPs were less stable than AuNPs prior to functionalization.

When gold nanoparticles aggregate they eventually fall out of solution rendering them useless for antimicrobial or blood toxicity testing, therefore stabilizing gold nanoparticles in solution was crucial. Results from saline stability testing show that in order to achieve successful stabilization incorporation of pHEA is required into the final AuNP conjugate compounds.

3.3.2 Stability in growth media

Saline stability testing showed that functionalizing the gold nanoparticles with pHEA improved stability. However, pDMAEMA is required to confer antimicrobial activity. Taking this into account, citrate-stabilized gold nanoparticles were functionalized with various ratios of pDMAEMA:pHEA (%) on their surface in order to assess whether these conjugate compounds had long term stability in growth media. Using three citrate-stabilized gold nanoparticles, four pDMAEMA, four pHEA polymers, five different ratios of pDMAEMA:pHEA % (0:100, 25:75, 50:50, 75:25, 100:0), 60 different compounds were obtained. These compounds were mixed with samples of LB, 7H9GT and PBS media (control) and absorbance measured between 450nm and 700nm. Absorbance measurements were normalized (A_{700}/A_{450}) and the change in absorbance at 700nm was calculated for every single compound (Fig 3.5).

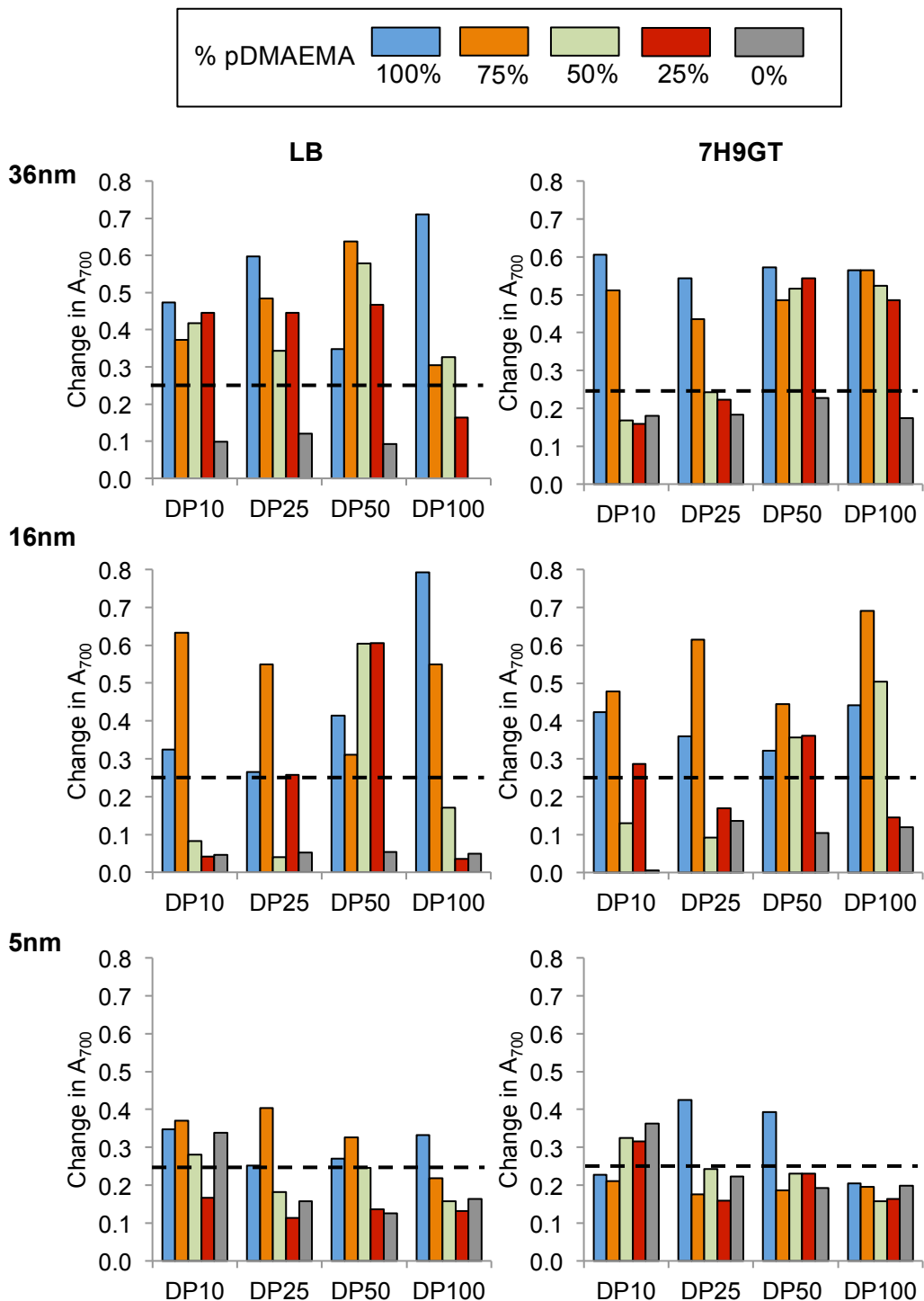


Figure 3.5. Stability of polymer-gold nanoparticle compounds in LB and 7H9GT. Change in absorbance at 700nm for 36nm, 16nm and 5nm polymer-coated gold nanoparticles in LB and 7H9GT. Broken line – threshold for stability is a change in A_{700} of 0.25. Above this value – compound is unstable, below this value – compound is stable.

Figure 3.5 summarizes the results from stability testing. A threshold was set to identify unstable and stable compounds. A change in $A_{700} > 0.25$ meant that the compounds were unstable in that particular media whereas a change in $A_{700} < 0.25$ meant that compounds were stable. All of the compounds were stable in PBS (the control). Figure 3.5 shows that

overall the larger nanoparticles (36nm) were generally less stable than the smaller nanoparticles (5nm). Additionally, as the percentage of pDMAEMA on the nanoparticle surface decreases but the percentage of pHEA increases, the compounds become increasingly more stable in both 7H9GT and LB. There appears to be no pattern between the stability of compounds coated with polymers at different degrees of polymerization, across the board. This suggests that stability is primarily associated with the composition of the pDMAEMA:pHEA (%) on the gold nanoparticle surface. Results from stability testing demonstrate that incorporating pHEA into the final polymer-AuNP conjugate compounds improves their stability in LB and 7H9GT.

Results show that smaller nanoparticles are generally more stable therefore nanoparticles with dimensions of 2nm were synthesized and functionalized directly with the polymers. This added to the repertoire of novel conjugate compounds to be tested using REMA.

3.4 Results from REMA

3.4.1 Polymers

REMA was used to test the antimicrobial activity of pDMAEMA and pHEA alone prior to immobilization onto AuNPs. Polymers were used with a starting concentration of 10mg/mL. No pHEA polymer showed any antimicrobial activity at any concentration against *M. smegmatis*, *P. putida* and *E. coli*. This was predicted because pHEA polymers have no charge and are generally non-interacting. The purpose of these polymers is to enhance the stability of the gold nanoparticles, already shown, and do not confer antimicrobial properties.

Conversely, all pDMAEMA polymers, DP 10, 25, 50 and 100, displayed antimicrobial activity against all three bacteria (Fig. 3.6). At a starting concentration of 10mg/mL all pDMAEMA polymers at all concentrations across the 96-well plate killed *M. smegmatis* therefore no MIC could be extracted from this assay. The assay was repeated with a starting concentration of 0.1mg/mL pDMAEMA.

Results from REMA (Table 3.3) (see Appendix A for photos of REMA plates) show that pDMAEMA was most effective in inhibiting the growth of *M. smegmatis* compared to the Gram-negative bacteria as evidenced by lower minimum inhibitory concentrations (MIC = 0.025 mg/mL). The MIC values for *P. putida* were up to 25 x MIC for *M. smegmatis* treated with the same polymer. Also, MIC values for *E. coli* were up to 12 x MIC of those for *M.*

smegmatis treated with same polymer. The growth inhibition activity of pDMAEMA DP 10, 25, 50 and 100 against *M. smegmatis* was the same based on MIC values. MIC values for DP 25, 50 and 100 were identical for both *E. coli* and *P. putida*. These results show that, in general, the variation in chain length does not influence the extent of antimicrobial activity demonstrated by the polymers.

Table 3.3. Antimicrobial activity of pDMAEMA polymers DP 10, 25, 50 and 100.

pDMAEMA	Minimum inhibitory concentration (mg/mL)		
	<i>E. coli</i>	<i>P. putida</i>	<i>M. smegmatis</i>
DP 10	0.08	0.63	0.025
DP 25	0.31	0.31	0.025
DP 50	0.31	0.31	0.025
DP 100	0.31	0.31	0.025

Previous literature has reported the use of pDMAEMA as an antimicrobial surface coating for the growth inhibition of both Gram-negative and Gram-positive bacteria such as *E. coli* and *Bacillus subtilis*, respectively (84). Additionally, pDMAEMA has previously been incorporated into antimicrobial copolymers to inhibit the growth of *E. coli* and *S. aureus* (84). The mode of action of pDMAEMA has been shown to be similar to that of other cationic biocides and involves adsorption to the bacterial cell surface through electrostatic interactions and disruption of the cytoplasmic membrane through hydrophobic interactions, eventually causing cell death (84).

We have shown here that pDMAEMA polymers also display significant antimicrobial activity against *M. smegmatis* mycobacteria as well as Gram-negative bacteria. Results show that pDMAEMA has better growth inhibitory activity against *M. smegmatis* when compared to activity against the Gram-negatives, based on MIC values. It's possible that the cationic pDMAEMA is capable of forming stronger electrostatic interactions with the mycobacterial cell surface due to the high content of lipids on the mycobacterial cell surface. Perhaps pDMAEMA has a stronger affinity for a mycobacterial cytoplasmic protein. Mode of action can only be determined by performing further experiments, such as membrane permeability assays. In any case, the success of pDMAEMA in the growth inhibition of *M. smegmatis* means pDMAEMA is a promising candidate in the development of a novel antimicrobial agent against *M. tuberculosis*, in particular, against drug-resistant strains of Mtb. This is crucial in an era where novel therapeutic agents are prerequisite to combatting antimicrobial resistance.

3.4.2 Polymer-coated AuNPs

To investigate whether immobilization of pDMAEMA onto the gold nanoparticles results in enhanced antimicrobial activity, the AuNPs were modified with different percentages of pDMAEMA and pHEA on their surfaces. This helped to determine the most suitable combination of polymers on the gold nanoparticle surface to confer sufficient antimicrobial activity without compromising the stability of the polymer-AuNP conjugate compounds. Over 80 different compounds were screened for bacterial growth inhibition using REMA. The compounds with the lowest MIC values across technical repeats were selected (Table 3.4) (see Appendix B for photos of REMA plates). MIC was calculated based on concentration of total Au integrated into the polymer-coated gold nanoparticles, as we were unable to quantify the exact concentrations of the nanoparticles in the compound.

Table 3.4. Antimicrobial activity of 8 different polymer-AuNP conjugate compounds.

Compound	Minimum inhibitory concentration (mg/mL)		
	<i>E. coli</i>	<i>P. putida</i>	<i>M. smegmatis</i>
2nm DP 100 100% pDMAEMA	0.0125	0.025	No activity
2nm DP 100 50% pDMAEMA	0.025	0.2	No activity
5nm DP 100 100% pDMAEMA	0.1	0.1	No activity
5nm DP 50 100% pDMAEMA	0.1	0.2	No activity
16nm DP 100 100% pDMAEMA	1.6	No activity	1.6
16nm DP 50 100% pDMAEMA	1.6	No activity	1.6
16nm DP 25 100% pDMAEMA	1.6	1.6	1.6
16nm DP 10 100% pDMAEMA	1.6	1.6	1.6

The majority of the 80 conjugate compounds tested displayed poor activity against all three bacteria. The 36nm gold nanoparticle conjugate compounds performed the worst in REMA testing, displaying little to no activity. One of the reasons for this lack of antimicrobial activity was due to poor stability in growth media. The particles had a tendency to aggregate and fall out of solution making them useless for purpose.

Overall, results from REMA show that the smaller, 2nm and 5nm (see Appendix C for photos of REMA plates), nanoparticle conjugate compounds displayed better (MIC values $\leq 0.2\text{mg/mL}$) antimicrobial activity than the 16nm AuNP conjugates (MIC = 1.6mg/mL). Furthermore, functionalizing the 2nm gold nanoparticles with pDMAEMA enhanced (on a per-polymer basis) their activity against *E. coli* and *P. putida* compared to non-conjugated pDMAEMA. Immobilization reduced MIC values by up to a factor of 25 (comparing 2nm 100% DP 100 MIC = 0.025mg/mL to pDMAEMA DP 100 MIC = 0.31mg/mL). Conversely, immobilization of pDMAEMA did not show improved activity against *M. smegmatis* compared to non-conjugated pDMAEMA. The MIC values for the 16nm AuNP conjugates are 64x higher than the MIC values for pDMAEMA alone. Furthermore, all, but 1, of the 8 compounds were functionalized with 100% pDMAEMA on their surface. Incorporation of pHEA increased the stability of the compounds but reduced antimicrobial activity.

These results show that immobilization of pDMAEMA on the nanoparticle surface leads to increased antimicrobial activity against *E. coli* and *P. putida* but not against *M. smegmatis*. Polymer immobilization on the nanoparticle surface may expose more polymer ligands to the bacterial cell surface. This may result in an increase in the electrostatic interactions formed between the bacterial cell surface and the pDMAEMA on the gold nanoparticle surface. Additionally, immobilization may increase the cationic density and induce a clustering effect around the bacterial cells. The higher density charge may result in the formation of stronger electrostatic interactions. The lack of improved activity against *M. smegmatis* is dubious. It is possible that the lipid-rich cell wall of the mycobacteria acts as a barrier against these novel compounds but not against pDMAEMA free in solution. The conjugate compounds may be too “bulky” to move across the mycobacterial cell membrane.

3.5 2nm compounds: other results

MIC values deduced from REMA revealed that conjugate compounds, 2nm DP 100 100% pDMAEMA and 2nm DP 100 50:50 (pDMAEMA:pHEA), had better antimicrobial activity against *E. coli* and *P. putida*. In order to further characterize the antibacterial activity of these compounds a MBC, a time-kill curve assay and turbidity assay were performed.

3.5.1 MBC

The Minimum Bactericidal Concentration (MBC) assay is typically performed as an adjunct to the MIC. The MIC is the lowest concentration at which the compounds will inhibit the

growth of *E. coli* and *P. putida*. In this case, the antimicrobial compound is bacteriostatic. On the other hand, the MBC is the lowest concentration at which an antibacterial agent will kill the target bacteria. In this case, the antimicrobial agent is bactericidal.

An MBC assay was set up and performed in a similar way to that of a REMA assay. For this assay, the two 2nm conjugate compounds were used with a starting concentration of 40 x MIC and serially diluted. After incubating the compounds with *E. coli* or *P. putida*, bacterial-compound solutions in each well were plated onto LB agar. Viable cells were counted at each dilution. The lowest concentration at which no growth of bacterial colonies was observed is the MBC (values based on Au integrated into the compound). Table 3.5 summarizes results from MBC assay.

Table 3.5. Minimum bactericidal concentration (MBC) of 2nm AuNP conjugate compounds.

Compound	MBC (mg/mL)	
	<i>E. coli</i>	<i>P. putida</i>
2nm DP100 100% pDMAEMA	0.5	1.0
2nm DP100 50% pDMAEMA	1.0	4.0
Ampicillin	0.0625	-
Tetracycline	-	0.0039

The assay was only performed once and replicated by Dr Richards in parallel. There were discrepancies between the two replicates. The first replicate plates for *E. coli* showed some colony growth at 40 x MIC for both 2nm compounds (2nm 100% pDMAEMA MBC = 0.5mg/mL, 2nm 50% pDMAEMA = 1.0mg/mL) but most were killed. The assay must be repeated in future in order to attain more reliable MBC values.

3.5.2 Time-kill curve

The MIC approach provides only limited information on the kinetics of a particular compound but does not provide information on the rate of bactericidal activity and whether increasing antimicrobial concentrations can enhance this rate (110). Time-kill curve assays assess the time it takes for a particular antimicrobial agent to begin killing the bacteria. *E. coli* and *P. putida* were separately incubated with both of the 2nm conjugate compounds for six different lengths of time: t(hours) = 0.25, 0.50, 1, 3, 5 and ~18. At each time point a sample of bacterial/compound solution was removed and serially diluted 10-fold to a final dilution of 10^{-8} and plated onto LB agar. Viable counts were calculated to give CFU/mL and time-kill curves were plotted with \log_{10} CFU/mL against time (Fig. 3.6).

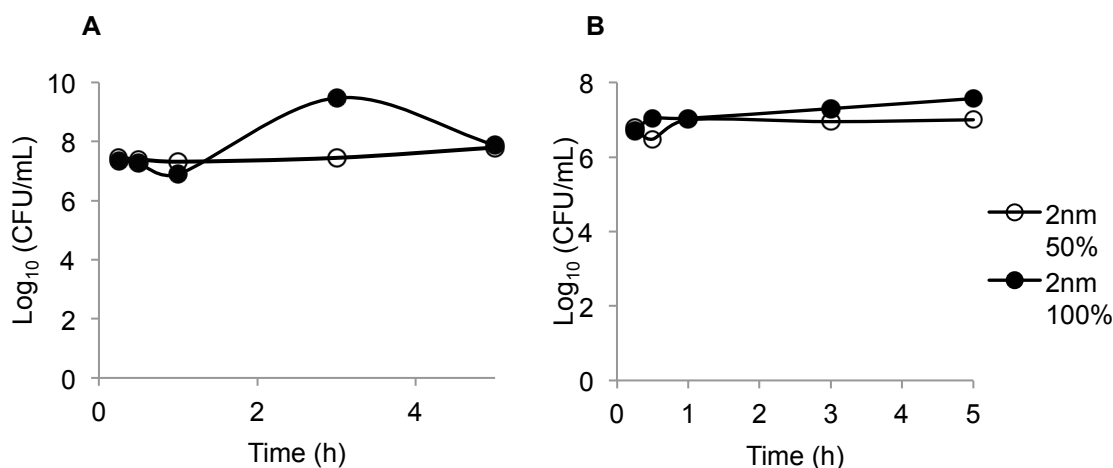


Figure 3.6. Time-kill curves. (A) *E. coli* (B) *P. putida* time-kill curves over a period of 5 hours. % pDMAEMA DP 100.

2nm AuNPs 100% pDMAEMA exhibit killing activity against *E. coli* after 3hrs incubation with $\sim 2\log_{10}$ decrease between 3 hrs and 5 hrs (Fig. 3.6A). No other killing activity can be distinguished from the time-kill curves. After 18 hours, too many colonies had grown on all plates and could not be counted therefore the sixth time point, $t=18\text{hrs}$, is not shown in Figure 3.6. The compounds may have begun to kill the bacteria somewhere between 5 and 18hrs after incubation. This assay was only carried out once and requires replicating to attain more reliable results and a better understanding of killing activity.

Time-kill curve is an effective assessment of antimicrobial activity and can help distinguish how long an antimicrobial begins to work. Subsequent pharmacokinetic-pharmacodynamic analysis may provide more meaningful information about the interactions between the bacteria and antimicrobial compound (110). Results from time-kill curves can help determine and optimize the dosage profile of antimicrobials. This is very important should these compounds be developed into future therapeutic drugs that are administered to patients.

3.5.3 Turbidity

Turbidity is the cloudiness or haziness of a fluid that is caused by suspended solids, usually invisible to the naked eye (111). The greater the number of bacterial cells in a suspension the greater the turbidity. Turbidity can therefore be used to determine the lowest concentration at which the antimicrobial compound prevents the appearance of turbidity, providing further information of antibacterial activity.

The 2nm conjugate compounds were mixed with *E. coli* or *P. putida* culture and LB media on a 96-well plate. Absorbance was measured at 600nm and plotted against concentration. The greater the turbidity of a solution, the higher the absorbance measurement should be (Fig. 3.7). Higher concentrations of an antimicrobial should result in less turbidity and therefore a decrease in A_{600} with increasing concentration should be observed.

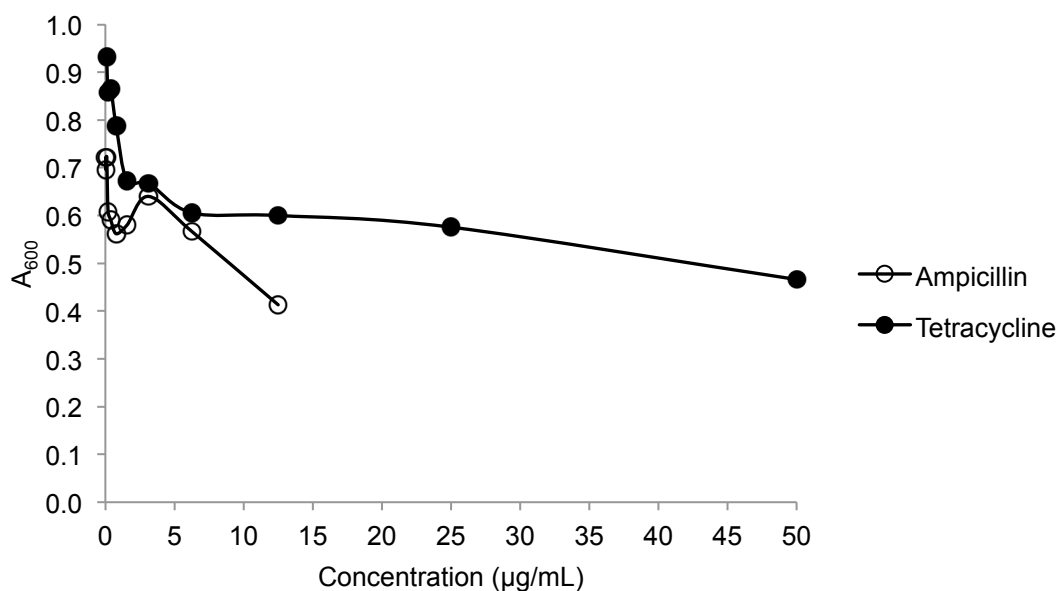


Figure 3.7. Turbidity of bacteria treated with antibiotics, ampicillin or tetracycline. A_{600} mean values ($n=2$) for *E. coli* treated with ampicillin and *P. putida* treated with tetracycline.

Figure 3.7 shows that as the concentration of ampicillin and tetracycline increases the turbidity decreases. There is a sharp decrease in turbidity as concentration reaches the MIC but the rate of decrease in turbidity slows down after MIC is reached. This is because cells are more able to grow at antibiotic concentrations lower than the MIC.

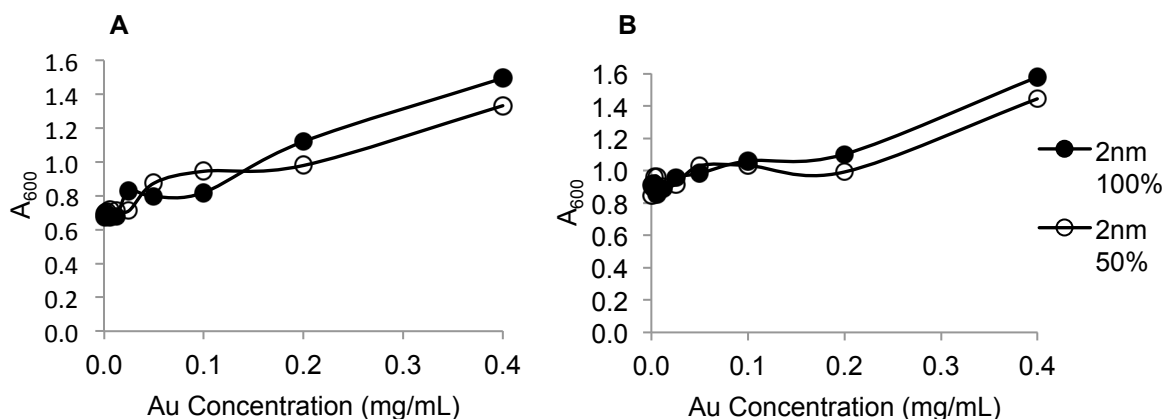


Figure 3.8. Turbidity of bacteria treated with 2nm AuNP conjugate compounds. A_{600} mean values ($n=2$) for (A) *E. coli* and (B) *P. putida* treated with varying concentrations of 2nm AuNP conjugate compounds. % pDMAEMA DP 100.

Figure 3.8 shows that turbidity increases as the concentration of gold incorporated into the conjugate compounds also increases. 2nm AuNPs are distinctly brown-coloured. The colour of the nanoparticles interfered with the turbidity measurements. This type of assay is not an effective way of assessing the antimicrobial activity of gold nanoparticle conjugate compounds and does not relay any valuable information, in this case.

3.6 Blood toxicity results

3.6.1 Haemagglutination assay

Haemagglutination tests were performed using ovine blood. Samples of the blood were mixed with the polymers and the 2nm and 5nm polymer-coated AuNPs.

Haemagglutination refers to the clumping of red blood cells. These cells are particularly useful targets of blood toxicity testing because they are readily available and agglutination is observable using the naked eye (112). The agglutination of sheep erythrocytes was used as a model to assess the interactions between the compounds and eukaryotic red blood cells. The polymers and polymer-coated nanoparticles were serially diluted by 1 in 4 and mixed with ovine blood on a clear 96-well plate. This assay was completed in replicates of three and all plates were observed after 30 minutes at room temperature. The presence or absence of haemagglutination was determined by visual comparisons to the positive control (polyethyleneimine – PEI) and negative control (PBS) (Fig. 3.9).

The haemagglutination titer is the lowest concentration of a compound that causes haemagglutination. Results shown by Figure 3.9 show that haemagglutination only occurs at the highest concentrations of the compounds; 10mg/mL for polymers, and 0.4mg/mL for the polymer-AuNP conjugate compounds. These relatively high concentrations would not be used for antibacterial treatment, as the MIC values determined by REMA were much lower; polymer MICs varied between 0.025-0.31mg/mL while nanoparticle compound MICs varied between 0.0125-0.2mg/mL. The absence of haemagglutination at lower concentrations indicates that the polymers and the novel polymer-coated AuNPs are not cytotoxic to sheep erythrocytes. This means that these compounds are unlikely to be toxic to red blood cells in other mammals i.e. humans. Absence of haemagglutination at most concentrations further highlights the suitability of these compounds as possible candidates in the development of novel antimicrobial agents for therapeutic applications.

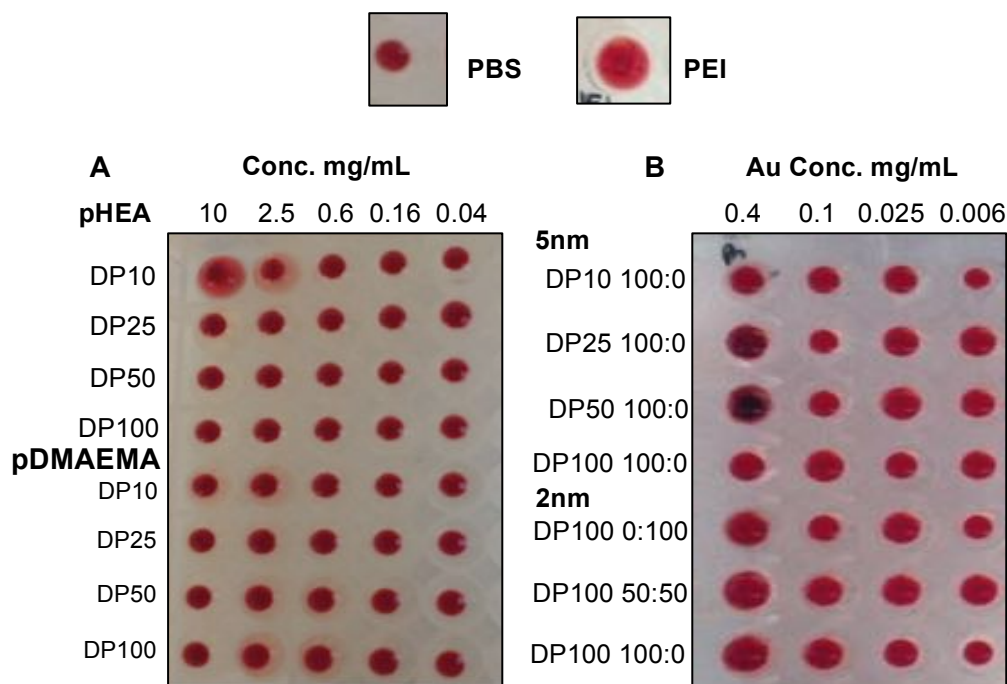


Figure 3.9. Haemagglutination assay results. Visual haemagglutination results for (A) pHEA and pDMAEMA polymers alone, (B) 5nm and 2nm conjugate compounds, ratios shown are pDMAEMA:pHEA (%). PBS (negative) and PEI (positive) controls shown above.

3.6.2 Haemolysis assay

Haemolysis is the rupturing of the red blood cell membrane resulting in the release of haemoglobin and other internal components of the cells into the surrounding fluid. Haemolysis induced toxicity to mammalian cells would be a major drawback to any future clinical development of the novel compounds synthesized in this project into therapeutic antimicrobial agents. The cationic pDMAEMA, and nanoparticles coated with this polymer could lead to cytotoxic, pro-inflammatory effects and haemolysis, especially if the positive charge on the polymer is too high (113).

All pDMAEMA and pHEA polymers, 2nm and 5nm polymer-coated AuNPs were evaluated to determine if they are haemolytic. The compounds were incubated with ovine blood for at least 1 hour, after which mixtures were centrifuged to pellet the blood cells. Following centrifugation, % haemolysis was calculated by measuring the absorbance of the supernatant at 450nm in order to determine the haemoglobin leaching due to lysis. Absorbance values were compared to those of PBS and H₂O controls whereby PBS = 0% lysis and H₂O = 100% lysis. Assays were completed in replicates of three for all compounds tested. Figure 3.10 shows the percentage lysis, relative to the controls, of the polymers at the range of concentrations used in REMA assays.

Figure 3.11 shows the percentage lysis of the 2nm and 5nm polymer-coated nanoparticles at the range of concentrations used in REMA.

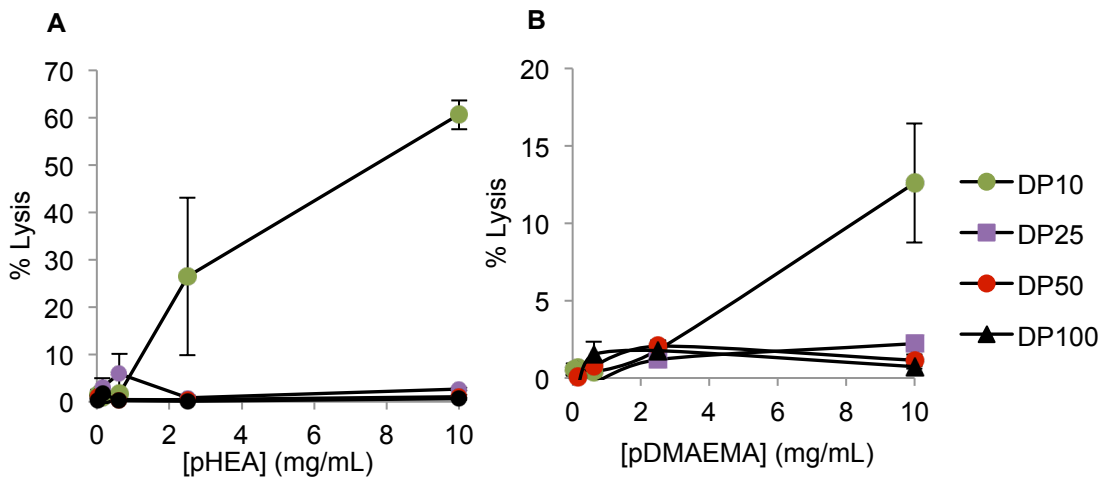


Figure 3.10. Percentage haemolysis of ovine blood exposed to pDMAEMA and pHEA. Mean % lysis (n=3) relative to 0% lysis and 100% lysis. Error bars show standard error.

We can see that polymers at the highest concentration tested caused the most lysis. PDMAEMA and pHEA DP 10 were especially lytic at higher concentrations. There was relatively little to no lysis at lower concentrations. Higher values of standard error seen for pDMAEMA DP 10 and pHEA DP 10 may be due to contamination between samples or disruption of the pellet during removal of the supernatant, causing it to re-disperse in the solution. The pDMAEMA DP 10 polymer showed greater % lysis (~61%) than the pHEA DP 10 polymers (~13%). This is probably due to the positive charge present on the pDMAEMA polymers. The increased positive charge at high concentrations may disrupt the erythrocyte membrane and exert a haemolytic effect. At lower concentrations the charge is not strong enough to have this effect.

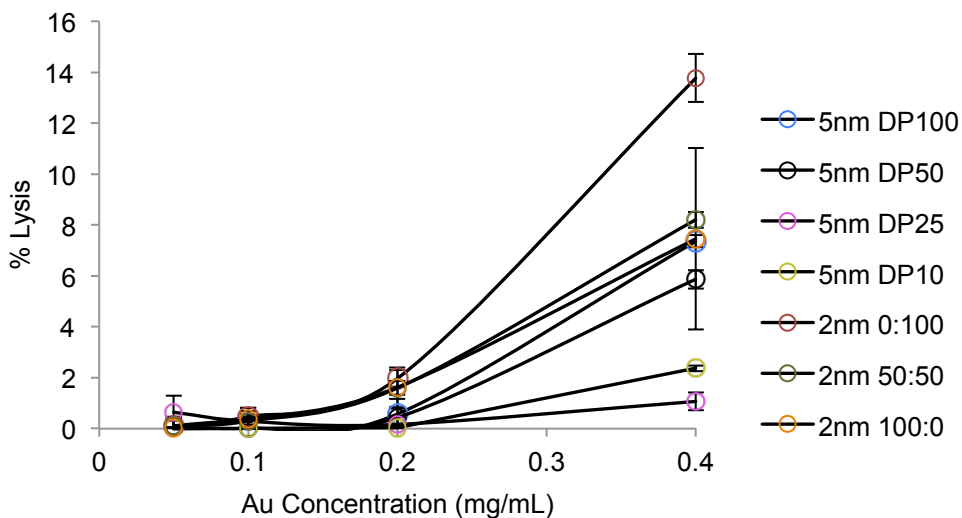


Figure 3.11. Percentage haemolysis of ovine blood exposed to 5nm and 2nm AuNP conjugate compounds. Mean % lysis (n=3) relative to 0% and 100% lysis. Ratios - pDMAEMA:pHEA (%). All 5nm compounds were coated with 100% pDMAEMA. Error bars show standard error.

The percentage of haemolysis was greatest at the highest concentration of the compounds. At lower concentrations there is relatively little to no lysis caused by any of the compounds. An increase in % lysis is observed at concentrations above 0.2mg/mL. These concentrations are up to 16x higher than MIC values obtained for the compounds during antimicrobial testing. Figure 3.12 shows photos of the blood-compound mixtures after centrifugation for 5 minutes to pellet the intact red blood cells.

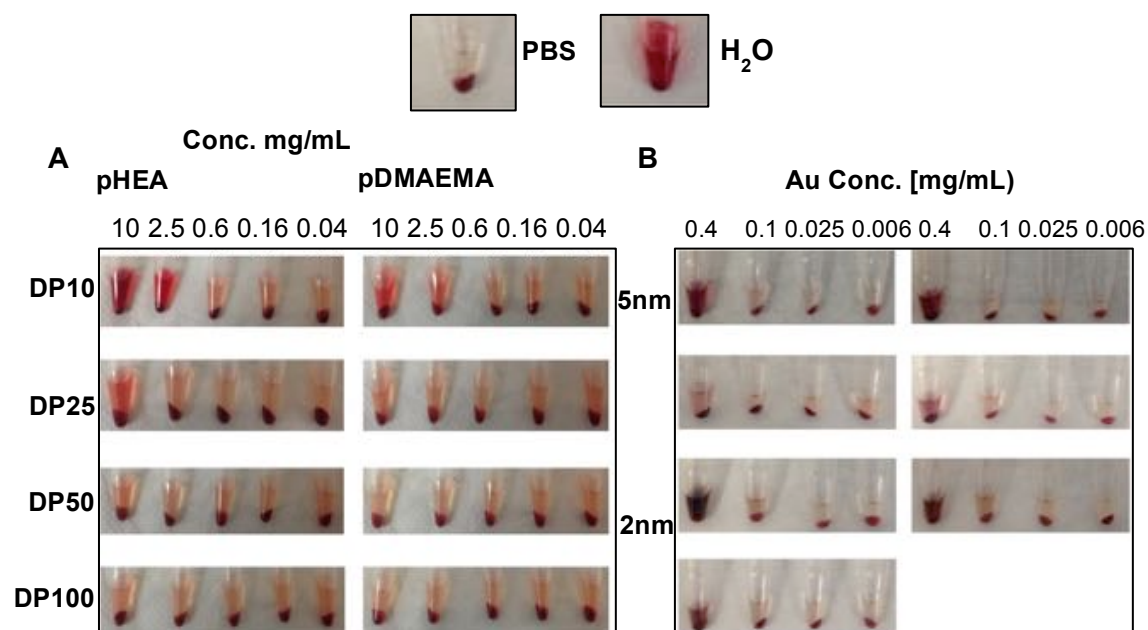


Figure 3.12. Visual haemolysis. (A) Ovine blood and polymer mixtures 3 hours after centrifugation for 5 minutes. (B) Ovine blood and nanoparticle compound mixtures 3 hours after centrifugation for 5 minutes. Ratios – pDMAEMA:pHEA (%). Ovine blood mixed with controls: PBS (no lysis) and H₂O (lysis), shown above.

Overall, the polymers and the polymer-coated nanoparticles do not induce haemolysis in ovine blood cells. We can predict that these compounds would not induce haemolysis in other mammalian red blood cells such as those of humans. This further highlights the therapeutic potential of these compounds as future clinical antimicrobial agents.

3.7 Summary of results

Results from REMA and blood toxicity have been summarised in Tables 3.6-3.7.

Table 3.6. Summary of results from REMA and blood toxicity testing for pDMAEMA and pHEA polymers. X = no haemagglutination observed at any concentration.

Polymer or antibiotic	MIC (mg/mL)			Haemolysis at highest concentration (%)	Haemagglutination titer (mg/mL)
	<i>E. coli</i>	<i>P.putida</i>	<i>M. smegmatis</i>		
pHEA DP10	-	-	-	61	10
PHEA DP25	-	-	-	3	X
pHEA DP50	-	-	-	1	X
pHEA DP100	-	-	-	1	X
pDMAEMA DP10	0.08	0.63	0.025	13	X
pDMAEMA DP25	0.31	0.31	0.025	2	X
pDMAEMA DP50	0.31	0.31	0.025	1	X
pDMAEMA DP100	0.31	0.31	0.025	1	X
Rifampicin	-	-	0.005	-	-
Ampicillin	0.00625	-	-	-	-
Tetracycline	-	0.00078	-	-	-
CFU/mL	7.8-13.0 $\times 10^6$	1.0-1.01 $\times 10^6$	3.1-5.8 $\times 10^6$		

Table 3.7. Summary of results from REMA and blood toxicity testing for 2nm and 5nm gold nanoparticle conjugate compounds. X = no haemagglutination observed at any concentration.

Compound	MIC (mg/mL)		Haemolysis at highest concentration (%)	Haemagglutination titer (mg/mL)
	<i>E. coli</i>	<i>P. putida</i>		
5nm DP10 100% pDMAEMA	No activity	No activity	7	X
5nm DP25 100% pDMAEMA	0.1	0.2	6	0.4
5nm DP50 100% pDMAEMA	0.1	0.2	1	0.4
5nm DP100 100% pDMAEMA	0.1	0.1	2	X
2nm DP100 100% pDMAEMA	0.0125	0.05	14	X
2nm DP100 50:50	0.025	0.2	8	X
2nm DP100 100% pHEA	No activity	No activity	7	X
Ampicillin	0.00625	-		
Tetracycline	-	0.00078		
CFU/mL	9.4-9.8 $\times 10^6$	2.6-6.1 $\times 10^6$		

4. Conclusion

4.1 Summary

Overall, the results from this project show that cationic pDMAEMA polymers, with different degrees of polymerization, have antimicrobial properties that allows them to inhibit the growth of *M. smegmatis*, *E. coli* and *P. putida*. The polymers were most effective at inhibiting the growth of *M. smegmatis* vs. the Gram-negative bacteria based on comparisons between MIC values extracted from REMA assessment. The non-charged pHEA polymers did not display any antimicrobial activity but were important in stabilizing the gold nanoparticles in solution. However, reducing the percentage of pDMAEMA on the nanoparticle surface and increasing the percentage of pHEA resulted in a reduction in antimicrobial activity.

Immobilization of the pDMAEMA polymers onto the gold nanoparticle surface enhances (on a per-polymer basis) their antimicrobial activity against *E. coli* and *P. putida*. However, this was not observed for *M. smegmatis*. In fact most of the conjugate compounds exhibited little to no improvement in activity compared to mobilized pDMAEMA in solution. These results demonstrate that immobilization is a good tool to enhance the antimicrobial activity of the cationic polymers against Gram-negative bacteria but not the mycobacteria.

The larger nanoparticles were generally unstable in growth media therefore smaller nanoparticles are a better platform for polymer immobilization. Based on comparisons between MIC values, *E. coli* and *P. putida* were more susceptible to 2nm AuNPs coated with pDMAEMA 100% and pDMAEMA 50% compared to the larger nanoparticle-conjugates. Further assessment of the antimicrobial activity of these compounds demonstrated that turbidity assays are not an effective method of bactericidal assessment due to the colouration of the gold nanoparticles. Additionally, time-kill curves demonstrated little information about the killing activity of the compounds over time therefore these assays require replication and assessment over a longer periods of time with increased frequency of measurements during that time.

To test their therapeutic potential, the polymers and the 2nm and 5nm polymer-coated gold nanoparticle compounds were subjected to blood toxicity testing. It was observed that polymers and conjugate compounds were only haemolytic at very high concentrations and

no haemagglutination was observed except for some of the compounds at very high concentrations, as well.

In conclusion, some of the novel pDMAEMA-AuNP conjugate compounds have demonstrated enhanced antimicrobial activity against *E. coli* and *P. putida*, compared to pDMAEMA alone. No improved antimicrobial action was observed against *M. smegmatis* therefore these conjugate compounds would not make suitable candidates in the future development of novel anti-TB agents as was originally hoped. Nonetheless, *M. smegmatis* was more susceptible to mobilized pDMAEMA than both *E. coli* and *P. putida*. Therefore, this may pave the way to developing pathways of using and modifying pDMAEMA as a candidate in TB-drug discovery and perhaps combining pDMAEMA with other compounds aside from nanoparticles (i.e. copolymers). The polymer-coated AuNP compounds may be able to inhibit the growth of other Gram-negative bacteria that are of medical and clinical relevance such as drug-resistant *E. coli* and *P. aeruginosa*, an opportunistic bacterium that is responsible for a variety of nosocomial infections, untreatable by current antibiotics. Additionally, these compounds are not cytotoxic *in vitro* and have the potential to be developed into future therapeutic agents with further and more extensive research.

4.2 Future recommendations

It is recommended that MBC and time-kill curve assays be replicated for the 2nm conjugate compounds. Additionally, the overall concentration of the conjugate compounds must be calculated by determining the grafting density of the polymer on the AuNP. This can be achieved using X-Ray photoelectron microscopy, potentially thermogravimetric analysis (TGA) and inductively coupled plasma mass spectrometry (ICP-MS). Calculation of the concentration of the whole conjugate compound will allow more accurate MIC values to be extracted.

It is also important to carry out further toxicity assays. These may include assessing the exposure effect of the conjugate compounds on the generation of reactive oxygen species (ROS) and on platelet aggregation in subsets of mammalian cells. This will provide further assessment of the extent to which these novel polymer-AuNP conjugates may have therapeutic applications.

The compounds should be tested against other strains of Gram-negative bacteria to determine whether they have broad-spectrum or specific activity. It would be interesting to assess if these compounds exhibit any activity against Gram-positive bacteria as well.

Furthermore, it is important to determine the mode of action of these compounds in order to understand how they exert a cytotoxic effect and how they are selective in their activity against bacterial cells. Understanding the mode of action can help to determine the specificity of these compounds and how they can be enhanced. It is already known that cationic ligands have the potential to disrupt cell membranes therefore membrane permeability assays are good place to begin assessing the mode of action. Additionally, transmission electron microscopy (TEM) may be used to gain further insight into the interactions between the conjugate compounds and the bacterial cells. It would be interesting to note how the mode of action varies between these novel compounds and conventional small-molecule antibiotics. Perhaps by understanding the mode of action, the reasons behind the lack of improved activity against the mycobacteria may become clearer.

Once the activity and cytotoxicity of these novel compounds are well characterized, these compounds must be optimized in ways that will improve their activity and render them efficacious at levels deemed safe and effective for therapeutic applications. In an era where antimicrobial resistance is a rapidly growing concern, the development of novel drug therapies is paramount. This research and future work based around the concepts presented in this project will bring the scientific community closer to combatting one of the biggest health concerns of the 21st century.

References

1. Nieme R. Brief History of Mycobacterium tuberculosis' Etiology | Intellectual Ventures Laboratory [Internet]. 2014 [cited 2016 Apr 4]. Available from: <http://www.intellectualventureslab.com/invent/brief-mtb-history>
2. Smith I. *Mycobacterium tuberculosis* pathogenesis and molecular determinants of virulence. Clin Microbiol Rev [Internet]. 2003;16(3):463–96. Available from: <http://cmr.asm.org/content/16/3/463.short>
3. Mandal A. History of Tuberculosis [Internet]. 2014 [cited 2016 Apr 8]. Available from: <http://www.news-medical.net/health/History-of-Tuberculosis.aspx>
4. Burdass D. Tuberculoses: Can the spread of this killer disease be. Soc Gen Microbiol. 2009;27(1):1–11.
5. Cole ST. Comparative and functional genomics of the Mycobacterium tuberculosis complex. Microbiology. 2002;148(Pt 10):2919–28.
6. Timeline - TB Alert [Internet]. [cited 2016 Apr 5]. Available from: <http://www.tbalert.org/about-tb/tb-in-time/tb-timeline/>
7. Parida SK, Kaufmann SHE. Novel tuberculosis vaccines on the horizon. Curr Opin Immunol [Internet]. Elsevier Ltd; 2010;22(3):374–84. Available from: <http://dx.doi.org/10.1016/j.coi.2010.04.006>
8. Daniel TM. The history of tuberculosis. Respir Med. 2006;100(11):1862–70.
9. Glaziou P, Falzon D, Floyd K, Raviglione M. Global epidemiology of tuberculosis. Semin Respir Crit Care Med. 2013;34(1):3–16.
10. Donald PR, van Helden PD. The Global Burden of Tuberculosis — Combating Drug Resistance in Difficult Times. N Engl J Med [Internet]. 2009;360(23):2393–5. Available from: <http://www.nejm.org/doi/full/10.1056/NEJMp0903806> \n <http://www.nejm.org.proxy1.cl.msu.edu/doi/full/10.1056/NEJMp0903806> \n <http://www.nejm.org.proxy1.cl.msu.edu/doi/pdf/10.1056/NEJMp0903806>
11. WHO Global Report 2015 [Internet]. WHO. 2015 [cited 2016 May 18]. Available from: http://www.who.int/tb/publications/global_report/gtbr15_main_text.pdf
12. Sulis G, Roggi A, Matteelli A, Raviglione MC. Tuberculosis: Epidemiology and control. Mediterr J Hematol Infect Dis. 2014;6(1).
13. Guidelines for the Use of Antiretroviral Agents in HIV-1-Infected Adults and Adolescents [Internet]. Aids Info. 2012 [cited 2016 May 18]. Available from: https://aidsinfo.nih.gov/contentfiles/lvguidelines/glchunk/glchunk_27.pdf
14. Luetkemeyer A. Tuberculosis and HIV [Internet]. HIV InSite. 2013 [cited 2016 May

- 18]. Available from: <http://hivinsite.ucsf.edu/InSite?page=kb-05-01-06>
15. Film | True Vision [Internet]. 2014 [cited 2016 May 20]. Available from: <http://truevisiontv.com/films/details/251/tb-return-of-the-plague>
 16. WHO | The five elements of DOTS. World Health Organization; [cited 2016 May 18]; Available from: <http://www.who.int/tb/dots/whatisdots/en/>
 17. WHO. What is DOTS ? 1999;
 18. Analysis of a success story: Implementation of DOTS strategy in China | GiveWell [Internet]. [cited 2016 May 18]. Available from: <http://www.givewell.org/international/technical/programs/DOTS/China>
 19. WHO | The End TB Strategy. World Health Organization; [cited 2016 May 18]; Available from: <http://www.who.int/tb/strategy/end-tb/en/>
 20. Mandal A. Tuberculosis Transmission [Internet]. News-Medical. 2013 [cited 2016 May 18]. Available from: <http://www.news-medical.net/health/Tuberculosis-Transmission.aspx>
 21. Niemi R. Overview of Tuberculosis Pathogenesis | Intellectual Ventures Laboratory [Internet]. 2014 [cited 2016 May 18]. Available from: <http://www.intellectualventureslab.com/invent/overview-of-tuberculosis-pathogenesis>
 22. Nunes-Alves C, Booty MG, Carpenter SM, Jayaraman P, Rothchild AC, Behar SM. In search of a new paradigm for protective immunity to TB. *Nat Rev Microbiol* [Internet]. Nature Publishing Group; 2014;12(4):289–99. Available from: <http://dx.doi.org/10.1038/nrmicro3230>
 23. Secondary pulmonary tuberculosis [Internet]. 2014 [cited 2016 May 19]. Available from: <http://www.pathologyatlas.ro/secondary-pulmonary-tuberculosis-pathology.php>
 24. Symptoms and causes - Tuberculosis - Mayo Clinic [Internet]. [cited 2016 May 18]. Available from: <http://www.mayoclinic.org/diseases-conditions/tuberculosis/symptoms-causes/dxc-20188557>
 25. TB Skin Test (Mantoux Test) [Internet]. Northwest Territories Health and Social Services. [cited 2016 May 18]. Available from: <http://www.hss.gov.nt.ca/health/diseases-conditions/tuberculosis/tb-skin-test-mantoux-test>
 26. TB Tests | Skin test, sputum & other types of TB test [Internet]. [cited 2016 May 18]. Available from: <http://www.tbfacts.org/tb-tests/>
 27. Desikan P. Sputum smear microscopy in tuberculosis: Is it still relevant? *Indian J Med Res*. 2013;137(3):442–4.
 28. Gaillard F. Pulmonary tuberculosis | Radiology Case | Radiopaedia.org [Internet].

- [cited 2016 May 19]. Available from: <http://radiopaedia.org/cases/pulmonary-tuberculosis-29>
29. Todar K. Tuberculosis [Internet]. [cited 2016 May 18]. Available from: <http://textbookofbacteriology.net/tuberculosis.html>
 30. Details - Public Health Image Library (PHIL) [Internet]. 2005 [cited 2016 May 19]. Available from: <http://phil.cdc.gov/phil/details.asp?pid=5789>
 31. Cole ST, Brosch R, Parkhill J, Garnier T, Churcher C, Harris D, et al. Deciphering the biology of *Mycobacterium tuberculosis* from the complete genome sequence. *Nature*. 1998;393(6685):537–44.
 32. Sakamoto K. The Pathology of *Mycobacterium tuberculosis* Infection [Internet]. *Veterinary Pathology*. 2012 [cited 2016 May 18]. p. 423–39. Available from: <http://vet.sagepub.com/content/49/3/423.full.pdf>
 33. Gebhardt H, Meniche X, Tropis M, Krämer R, Daffé M, Morbach S. The key role of the mycolic acid content in the functionality of the cell wall permeability barrier in *Corynebacterineae*. *Microbiology*. 2007;153(5):1424–34.
 34. Marrakchi H, Lanéelle MA, Daffé M. Mycolic acids: Structures, biosynthesis, and beyond. *Chem Biol*. 2014;21(1):67–85.
 35. Kaiser GE. BIOL 230 Lecture Guide - Acid-Fast Cell Wall [Internet]. 2008 [cited 2016 May 19]. Available from: <http://faculty.cbcemd.edu/courses/bio141/lecguides/unit2/control/u1fig11.html>
 36. Jankute M, Cox JAG, Harrison J, Besra GS. Assembly of the *Mycobacterial* Cell Wall. *Annu Rev Microbiol* [Internet]. 2015;69:405–23. Available from: <http://www.annualreviews.org/doi/abs/10.1146/annurev-micro-091014-104121>
 37. Rajni, Rao N, Meena LS. Biosynthesis and Virulent Behavior of Lipids Produced by *Mycobacterium tuberculosis*: LAM and Cord Factor: An Overview. *Biotechnol Res Int*. 2011;2011:274693.
 38. Riley LW. Microbiology and pathogenesis of tuberculosis [Internet]. 2011 [cited 2016 May 18]. Available from: http://cursoenarm.net/UPTODATE/contents/mobipreview.htm?18/6/18529?source=see_link
 39. Peterson JW. Bacterial Pathogenesis [Internet]. University of Texas Medical Branch at Galveston; 1996 [cited 2016 May 18]. Available from: <http://www.ncbi.nlm.nih.gov/books/NBK8526/>
 40. Todar K. Tuberculosis Virulence [Internet]. [cited 2016 May 18]. Available from: http://textbookofbacteriology.net/tuberculosis_3.html
 41. Saita N, Fujiwara N, Yano I, Soejima K. Trehalose 6 ,6'-Dimycolate (Cord Factor) of *Mycobacterium tuberculosis* Induces Corneal Angiogenesis in Rats. *Infect Immun*.

- 2000;68(10):5991–7.
42. Elamin AA, Stehr M, Singh M. The Cord Factor : Structure , Biosynthesis and Application in Drug Research – Achilles Heel of Mycobacterium tuberculosis ? Underst Tuberc New Approaches To Fight Against Drug Resist. 2012;(May):187–206.
 43. Chan J, Fan X, Hunter SW, Brennan PJ, Bloom BR. Lipoarabinomannan, a possible virulence factor involved in persistence of Mycobacterium tuberculosis within macrophages. Infect Immun. 1991;59(5):1755–61.
 44. Protein Kinase C Signaling | Cell Signaling Technology [Internet]. [cited 2016 May 18]. Available from:
<http://www.cellsignal.com/common/content/content.jsp?id=pathways-kinase-c>
 45. Isakov N, Altman A. Regulation of immune system cell functions by protein kinase C. Front Immunol [Internet]. 2013 Jan [cited 2016 Apr 16];4:384. Available from:
<http://www.pubmedcentral.nih.gov/articlerender.fcgi?artid=3831523&tool=pmcentrez&rendertype=abstract>
 46. Scherr N, Honnappa S, Mueller P, Jayachandran R, Win- F, Pieters J, et al. Structural basis for the specific inhibition of protein kinase G , a virulence factor of Mycobacterium tuberculosis. 2007;104(41).
 47. Cimino M, Thomas C, Namouchi A, Dubrac S, Gicquel B, Gopaul DN. Identification of DNA binding motifs of the mycobacterium tuberculosis phop/phor two-component signal transduction system. PLoS One. 2012;7(8):1–12.
 48. López M, Sly LM, Luu Y, Young D, Cooper H, Reiner NE. The 19-kDa Mycobacterium tuberculosis protein induces macrophage apoptosis through Toll-like receptor-2. J Immunol. 2003;170(5):2409–16.
 49. da Silva PEA, Palomino JC. Molecular basis and mechanisms of drug resistance in Mycobacterium tuberculosis: Classical and new drugs. J Antimicrob Chemother. 2011;66(7):1417–30.
 50. Timmins GS, Deretic V. Mechanisms of action of isoniazid. Mol Microbiol. 2006;62(5):1220–7.
 51. Isoniazid. [cited 2016 May 20]; Available from:
<http://www.drugbank.ca/drugs/DB00951>
 52. Zhang Y, Wade MM, Scorpio A, Zhang H, Sun Z. Mode of action of pyrazinamide: Disruption of Mycobacterium tuberculosis membrane transport and energetics by pyrazinoic acid. J Antimicrob Chemother. 2003;52(5):790–5.
 53. Zhang Y, Shi W, Zhang W, Mitchison D. Mechanisms of Pyrazinamide Action and Resistance. Microbiol Spectr [Internet]. 2014 Aug [cited 2016 May 20];2(4):MGM2–0023 – 2013. Available from:

- <http://www.pubmedcentral.nih.gov/articlerender.fcgi?artid=4268777&tool=pmcentrez&rendertype=abstract>
54. Kolyva A, Karakousis P. Old and new TB drugs: Mechanisms of action and resistance. *Underst Tuberc - New Approaches to Fight Against Drug Resist* [Internet]. 2012;210–32. Available from:
http://cdn.intechopen.com/pdfs/28840/InTech-Old_and_new_tb_drugs_mechanisms_of_action_and_resistance.pdf
 55. Streptomycin. [cited 2016 May 20]; Available from:
<http://www.drugbank.ca/drugs/DB01082>
 56. Chapter 6 Treatment of Tuberculosis Disease. *Tuberculosis*. 2013;139–88.
 57. Arbex MA, Varella MDCL, Siqueira HR De, Mello FAF De. Antituberculosis drugs: Drug interactions, adverse effects, and use in special situations. Part 1: First-line drugs. *J Bras Pneumol*. 2010;36(June):626–40.
 58. Nachegea JB, Chaisson RE. Tuberculosis drug resistance: a global threat. *Clin Infect Dis*. 2003;36(Suppl 1):S24–30.
 59. D'ambrosio L, Centis R, Sotgiu G, Pontali E, Spanevello A, Migliori GB. New anti-tuberculosis drugs and regimens: 2015 update. *ERJ Open Res* [Internet]. 2015;1:10–2015. Available from: <http://ow.ly/LnJER>
 60. England NHS. Clinical Commissioning Policy : Bedaquiline and Delamanid for defined patients with MDR-XDR-TB. :1–19.
 61. Gupta R, Geiter LJ, Wells CD, Gao M, Cirule A, Xiao H. Delamanid for Extensively Drug-Resistant Tuberculosis. *N Engl J Med*. Massachusetts Medical Society; 2015 Jul 16;373(3):291–2.
 62. Mahajan R. Bedaquiline: First FDA-approved tuberculosis drug in 40 years. *Int J Appl basic Med Res* [Internet]. 2013 Jan [cited 2016 Mar 31];3(1):1–2. Available from:
<http://www.pubmedcentral.nih.gov/articlerender.fcgi?artid=3678673&tool=pmcentrez&rendertype=abstract>
 63. Lessem BE, Mckenna L. Bedaquiline. *TAG Treat Action Gr*. 2013;1–8.
 64. Rice LB. Progress and challenges in implementing the research on ESKAPE pathogens. *Infect Control Hosp Epidemiol*. 2010;31 Suppl 1(November 2010):S7–10.
 65. Boucher HW, Talbot GH, Bradley JS, Edwards JE, Gilbert D, Rice LB, et al. Bad bugs, no drugs: no ESKAPE! An update from the Infectious Diseases Society of America. *Clin Infect Dis* [Internet]. 2009;48(1):1–12. Available from:
<http://www.ncbi.nlm.nih.gov/pubmed/19035777>
 66. O'Neill J. Antimicrobial Resistance : Tackling a crisis for the health and wealth of

- nations. *Rev Antimicrob Resist.* 2014;(December):1–16.
67. Miller K. Drug-Resistant E.Coli Infections On the Rise [Internet]. 2015 [cited 2016 May 18]. Available from: <https://uk.news.yahoo.com/drug-resistant-ecoli-infections-are-on-the-rise-194436499.html>
 68. O'Neill J. Securing New Drugs for Future Generations : the Pipeline of Antibiotics. 2015;(May).
 69. Seil JT, Webster TJ. Antimicrobial applications of nanotechnology: Methods and literature. *Int J Nanomedicine.* 2012;7:2767–81.
 70. Jain S, Hirst DG, O'Sullivan JM. Gold nanoparticles as novel agents for cancer therapy. *Br J Radiol* [Internet]. 2012;85(1010):101–13. Available from: <http://www.pubmedcentral.nih.gov/articlerender.fcgi?artid=3473940&tool=pmcentrez&rendertype=abstract>
 71. Mody V V, Siwale R, Singh A, Mody HR. Introduction to metallic nanoparticles. *J Pharm bioallied Sci.* 2010;2(4):282–9.
 72. Shen L. Gold Nanoparticles [Internet]. 2008 [cited 2016 May 18]. Available from: http://www.chemistry.illinois.edu/research/inorganic/seminar_abstracts/2008-2009/Shen.Abstract.pdf
 73. Li X, Wang L, Fan Y, Feng Q, Cui FZ. Biocompatibility and toxicity of nanoparticles and nanotubes. *J Nanomater.* 2012;2012.
 74. Abou El-Nour KMM, Eftaiha A, Al-Warthan A, Ammar RAA. Synthesis and applications of silver nanoparticles. *Arab J Chem.* 2010;3(3):135–40.
 75. Conn PM. Imaging and Spectroscopic Analysis of Living Cells: Optical and Spectroscopic Techniques [Internet]. Academic Press; 2012 [cited 2016 May 18]. 506 p. Available from: <https://books.google.com/books?id=fOHw6YBnpdAC&pgis=1>
 76. Zhou Y, Kong Y, Kundu S, Cirillo JD, Liang H. Antibacterial activities of gold and silver nanoparticles against *Escherichia coli* and *Bacillus Calmette-Guérin*. *J Nanobiotechnology* [Internet]. 2012;10(1):19. Available from: <http://www.biomedcentral.com/10/1/19>
 77. Gifford JC, Bresee J, Carter CJ, Wang G, Melander RJ, Melander C, et al. Thiol-modified gold nanoparticles for the inhibition of *Mycobacterium smegmatis*. *Chem Commun (Camb)* [Internet]. 2014;50(100):15860–3. Available from: <http://www.ncbi.nlm.nih.gov/pubmed/25350535>
 78. Osbaugh N. The Efficacy and Specificity of Gold Nanoparticles as Antibiotics for *Klebsiella pneumoniae*. 2015;
 79. Moore LE, Ledder RG, Gilbert P, McBain AJ. In vitro study of the effect of cationic biocides on bacterial population dynamics and susceptibility. *Appl Environ Microbiol.* 2008;74(15):4825–34.

80. Mei L, Zhang X, Wang Y, Zhang W, Lu Z, Luo Y, et al. Multivalent polymer-Au nanocomposites with cationic surfaces displaying enhanced antimicrobial activity. *Polym Chem* [Internet]. 2014;5(8):3038–44. Available from: <http://pubs.rsc.org/en/Content/ArticleLanding/2014/PY/c3py01578e>
81. Samal SK, Dash M, Van Vlierberghe S, Kaplan DL, Chiellini E, van Blitterswijk C, et al. Cationic polymers and their therapeutic potential. *Chem Soc Rev*. 2012;41(21):7147.
82. Agarwal S, Zhang Y, Maji S, Greiner A. PDMAEMA based gene delivery materials. *Mater Today* [Internet]. 2012 Sep [cited 2016 May 3];15(9):388–93. Available from: <http://www.sciencedirect.com/science/article/pii/S1369702112701657>
83. Verbaan FJ, Crommelin DJ., Hennink WE, Storm G. *Polymeric Gene Delivery: Principles and Applications* [Internet]. CRC Press; 2004 [cited 2016 May 20]. 704 p. Available from: <https://books.google.com/books?id=5pemd0DWUjUC&pgis=1>
84. Rawlinson L-AB, Ryan SM, Mantovani G, Syrett JA, Haddleton DM, Brayden DJ. Antibacterial effects of poly(2-(dimethylamino ethyl)methacrylate) against selected gram-positive and gram-negative bacteria. *Biomacromolecules* [Internet]. American Chemical Society; 2010 Feb 8 [cited 2016 May 25];11(2):443–53. Available from: <http://dx.doi.org/10.1021/bm901166y>
85. leong NS, Brebis K, Daniel LE, O'Reilly RK, Gibson MI. The critical importance of size on thermoresponsive nanoparticle transition temperatures: gold and micelle-based polymer nanoparticles. *Chem Commun* [Internet]. 2011;47(42):11627–9. Available from: <http://dx.doi.org/10.1039/C1CC15171A>
86. Parry AL, Clemson NA, Ellis J, Bernhard SS., David BG, Cameron NR. “Multicopy Multivalent” Glycopolymer-stabilised Gold Nanoparticles as Potential Synthetic Cancer Vaccines – Supporting Information. *J Am Chem Soc*. 2003;2004.
87. Bio-Resource: CFU: Colony Forming Unit & Calculation [Internet]. [cited 2016 May 28]. Available from: <http://technologyinscience.blogspot.co.uk/2011/11/cfu-colony-forming-unit-calculation.html#.V0oMWVfSNg0>
88. Reyrat JM, Kahn D. *Mycobacterium smegmatis*: an absurd model for tuberculosis? *Trends Microbiol* [Internet]. 2001 Oct [cited 2016 May 23];9(10):472–4. Available from: <http://www.ncbi.nlm.nih.gov/pubmed/11597444>
89. Tyagi JS, Sharma D. *Mycobacterium smegmatis* and tuberculosis. *Trends Microbiol* [Internet]. 2002 Feb [cited 2016 May 23];10(2):68–9. Available from: <http://www.ncbi.nlm.nih.gov/pubmed/11827806>
90. Mishra AK, Driessen NN, Appelmek B, Besra GS. Lipoarabinomannan and related glycoconjugates: structure, biogenesis and role in *Mycobacterium tuberculosis* physiology and host-pathogen interaction. *FEMS Microbiol Rev* [Internet]. 2011 Nov

- [cited 2016 May 13];35(6):1126–57. Available from:
[http://www.pubmedcentral.nih.gov/articlerender.fcgi?artid=3229680&tool=pmcentrez
&rendertype=abstract](http://www.pubmedcentral.nih.gov/articlerender.fcgi?artid=3229680&tool=pmcentrez&rendertype=abstract)
91. Chaturvedi V, Dwivedi N, Tripathi RP, Sinha S. Evaluation of *Mycobacterium smegmatis* as a possible surrogate screen for selecting molecules active against multi-drug resistant *Mycobacterium tuberculosis*. *J Gen Appl Microbiol* [Internet]. 2007 Dec [cited 2016 May 23];53(6):333–7. Available from:
<http://www.ncbi.nlm.nih.gov/pubmed/18187888>
 92. *Escherichia coli* (E. coli) as a Model Organism or Host Cell - Video & Lesson Transcript | Study.com [Internet]. [cited 2016 May 23]. Available from:
<http://study.com/academy/lesson/escherichia-coli-e-coli-as-a-model-organism-or-host-cell.html>
 93. Determination of Bacterial CFU Using “Miles And Misra Technique” [Internet]. [cited 2016 May 23]. Available from: <http://www.biotechnologyforums.com/thread-2028.html>
 94. Andrews JM. Determination of minimum inhibitory concentrations. *J Antimicrob Chemother* [Internet]. 2001 Jul 1 [cited 2015 Jan 2];48(suppl 1):5–16. Available from: http://jac.oxfordjournals.org/content/48/suppl_1/5.short?rss=1&ssource=mfc
 95. Promega. CellTiter-Blue Assay Protocol. 2016; Available from:
http://www.promega.co.uk/~media/files/resources/protocols/technical_bulletins/101/celltiter-blue_cell_viability_assay_protocol.pdf
 96. Richards S-J, Gibson MI. Optimization of the Polymer Coating for Glycosylated Gold Nanoparticle Biosensors to Ensure Stability and Rapid Optical Readouts. *ACS Macro Lett* [Internet]. American Chemical Society; 2014 Oct 21 [cited 2016 May 24];3(10):1004–8. Available from: <http://dx.doi.org/10.1021/mz5004882>
 97. Shkilnyy A, Soucé M, Dubois P, Warmont F, Saboungi M-L, Chourpa I. Poly(ethylene glycol)-stabilized silver nanoparticles for bioanalytical applications of SERS spectroscopy. *Analyst* [Internet]. The Royal Society of Chemistry; 2009 Sep 17 [cited 2016 May 24];134(9):1868–72. Available from:
<http://pubs.rsc.org/en/content/articlehtml/2009/an/b905694g>
 98. Gandhi A, Paul A, Sen SO, Sen KK. Studies on thermoresponsive polymers: Phase behaviour, drug delivery and biomedical applications. *Asian J Pharm Sci* [Internet]. 2015 Apr [cited 2016 Feb 17];10(2):99–107. Available from:
<http://www.sciencedirect.com/science/article/pii/S1818087614000634>
 99. Tebaldi ML, Leal DA, Montoro SR, Petzhold C. Synthesis of stimuli-sensitive copolymers by RAFT polymerization: potential candidates as drug delivery systems. *Mater Res* [Internet]. Materials Research; 2014 Aug [cited 2016 May 24];17:191–6.

Available from: http://www.scielo.br/scielo.php?script=sci_arttext&pid=S1516-14392014000700031&lng=en&nrm=iso&tlng=en

100. Kimling J, Maier M, Okenve B, Kotaidis V, Ballot H, Plech A. Turkevich method for gold nanoparticle synthesis revisited. *J Phys Chem B* [Internet]. American Chemical Society; 2006 Aug 17 [cited 2015 Mar 5];110(32):15700–7. Available from: <http://dx.doi.org/10.1021/jp061667w>
101. J. Turkevich; P.C. Stevenson; J. Hiller. Synthesis of Gold Nanoparticles Turkevich method. *Discuss Faraday Soc.* 1951;11:55–75.
102. Petryayeva E, Krull UJ. Localized surface plasmon resonance: nanostructures, bioassays and biosensing--a review. *Anal Chim Acta* [Internet]. 2011 Nov 7 [cited 2016 Mar 8];706(1):8–24. Available from: <http://www.sciencedirect.com/science/article/pii/S0003267011011196>
103. Introduction to Gold Nanoparticle Characterization - Cytodiagnosics [Internet]. [cited 2016 May 24]. Available from: <http://www.cytodiagnosics.com/store/pc/Introduction-to-Gold-Nanoparticle-Characterization-d3.htm>
104. Jans H, Liu X, Austin L, Maes G, Huo Q. Dynamic light scattering as a powerful tool for gold nanoparticle bioconjugation and biomolecular binding studies. *Anal Chem* [Internet]. 2009 Nov 15 [cited 2016 May 24];81(22):9425–32. Available from: <http://www.ncbi.nlm.nih.gov/pubmed/19803497>
105. Tomaszewska E, Soliwoda K, Kadziola K, Tkacz-Szczesna B, Celichowski G, Cichomski M, et al. Detection limits of DLS and UV-Vis spectroscopy in characterization of polydisperse nanoparticles colloids. *J Nanomater.* 2013;2013.
106. Haiss W, Thanh NTK, Aveyard J, Fernig DG. Determination of Size and Concentration of Gold Nanoparticles from UV – Vis Spectra Determination of Size and Concentration of Gold Nanoparticles from UV - Vis Spectra. 2015;79(October):4215–21.
107. Farrell E, Brousseau J. Guide for DLS sample preparation. Brookhaven Instruments. 2014;1(631):1–3.
108. Dewi MR, Laufersky G, Nann T. A highly efficient ligand exchange reaction on gold nanoparticles: preserving their size, shape and colloidal stability. *RSC Adv* [Internet]. The Royal Society of Chemistry; 2014 Jul 30 [cited 2016 May 6];4(64):34217. Available from: <http://pubs.rsc.org/en/content/articlehtml/2014/ra/c4ra05035e>
109. Teacher Guide EXPERIMENT C – COLORIMETRIC GOLD NANOSENSOR. 2013;(233433):1–17.
110. Müller M, Dela Peña A, Derendorf H. Issues in Pharmacokinetics and

Pharmacodynamics of Anti-Infective Agents: Distribution in Tissue. *Antimicrob Agents Chemother.* 2004;48(5):1441–53.

111. What is Turbidity? [Internet]. [cited 2016 May 25]. Available from:
<http://www.lamotte.com/en/blog/test-factors/91-what-is-turbidity>
112. Costabile M. Determining the reactivity and titre of serum using a haemagglutination assay. *J Vis Exp* [Internet]. 2010;(35):1–2. Available from:
<http://www.pubmedcentral.nih.gov/articlerender.fcgi?artid=2818707&tool=pmcentrez&rendertype=abstract>
113. Francolini I. *Biofilm-based Healthcare-associated Infections, Volume 2* [Internet]. Springer; 2014 [cited 2016 May 25]. 195 p. Available from:
<https://books.google.com/books?id=cAFNBQAAQBAJ&pgis=1>

Appendices

Appendix A – REMA Assays with Polymers

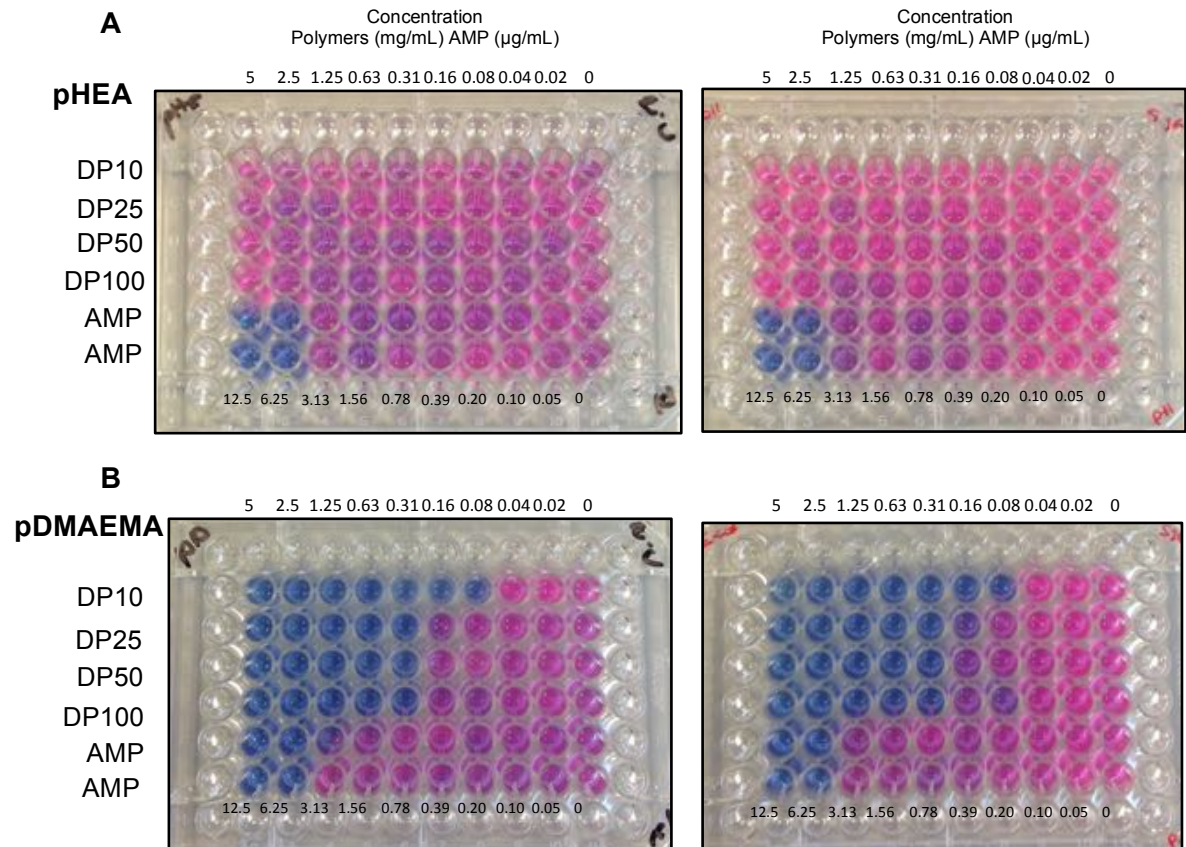


Figure A1. REMA assays with polymers and *E. coli*. (A) pHEA polymers DP 10, 25, 50 and 100. Left (replicate 1), right (replicate 2). (B) pDMAEMA polymers DP 10, 25, 50 and 100. Left (replicate 1), right (replicate 2).

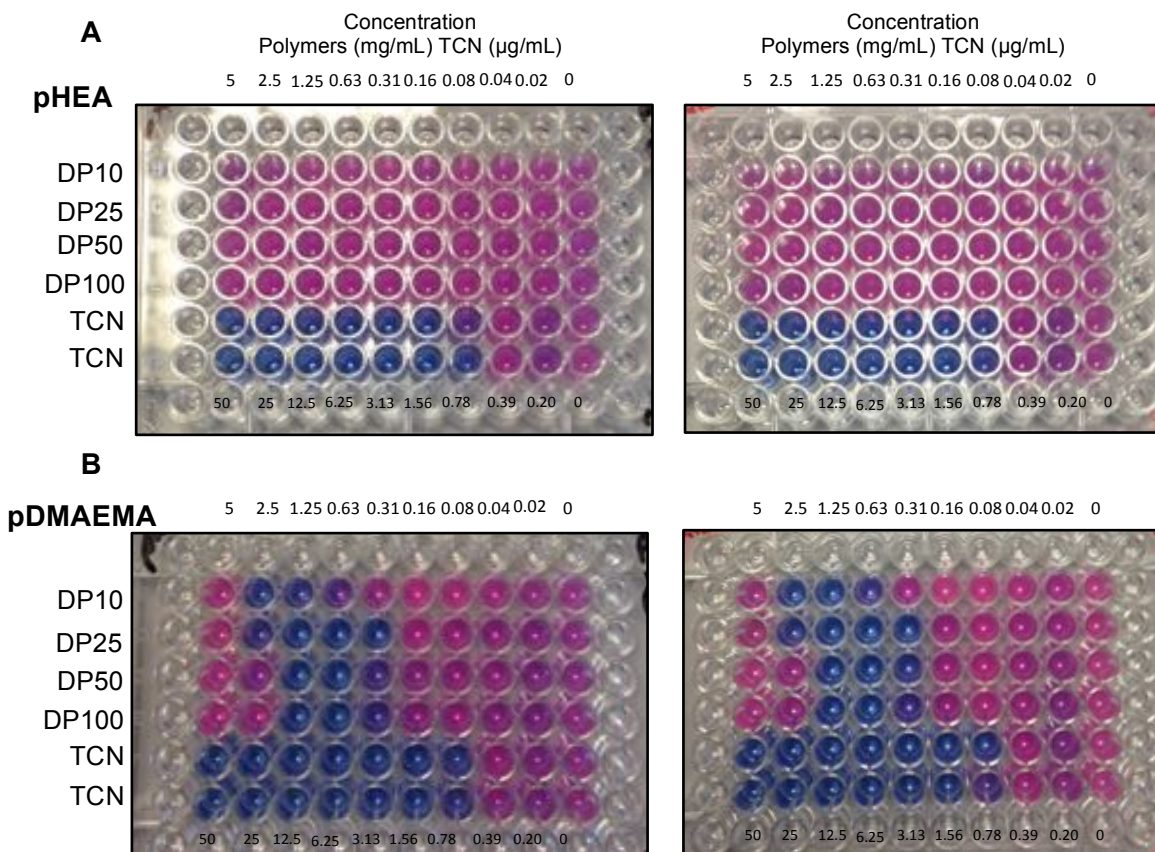


Figure A2. REMA assays with polymers and *P. putida*. (A) pHEA polymers DP 10, 25, 50 and 100. Left (replicate 1), right (replicate 2). (B) pDMAEMA polymers DP 10, 25, 50 and 100. Left (replicate 1), right (replicate 2).

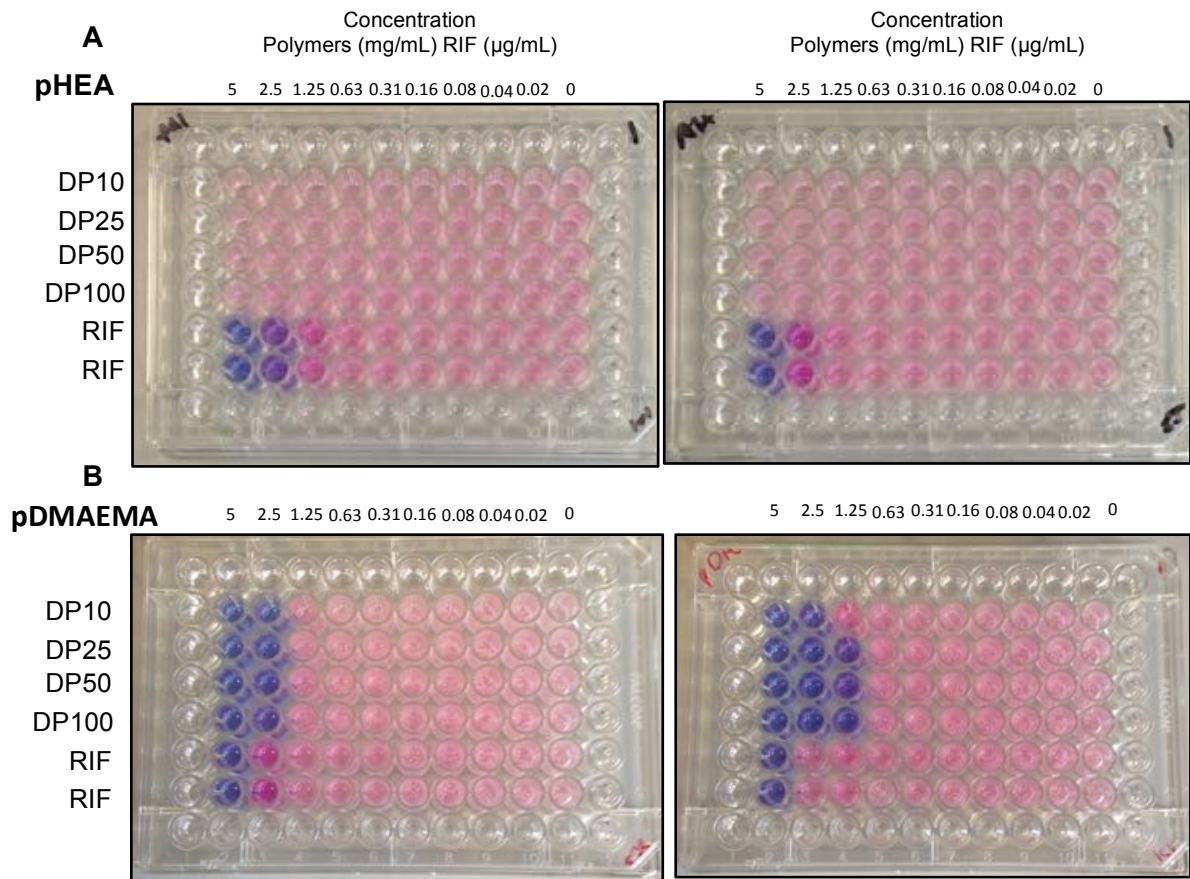


Figure A3. REMA assays with polymers and *M. smegmatis*. (A) pHEA polymers DP 10, 25, 50 and 100. Left (replicate 1), right (replicate 2). (B) pDMAEMA polymers DP 10, 25, 50 and 100. Left (replicate 1), right (replicate 2).

Appendix B – REMA Assays with 15nm polymer-coated AuNP compounds

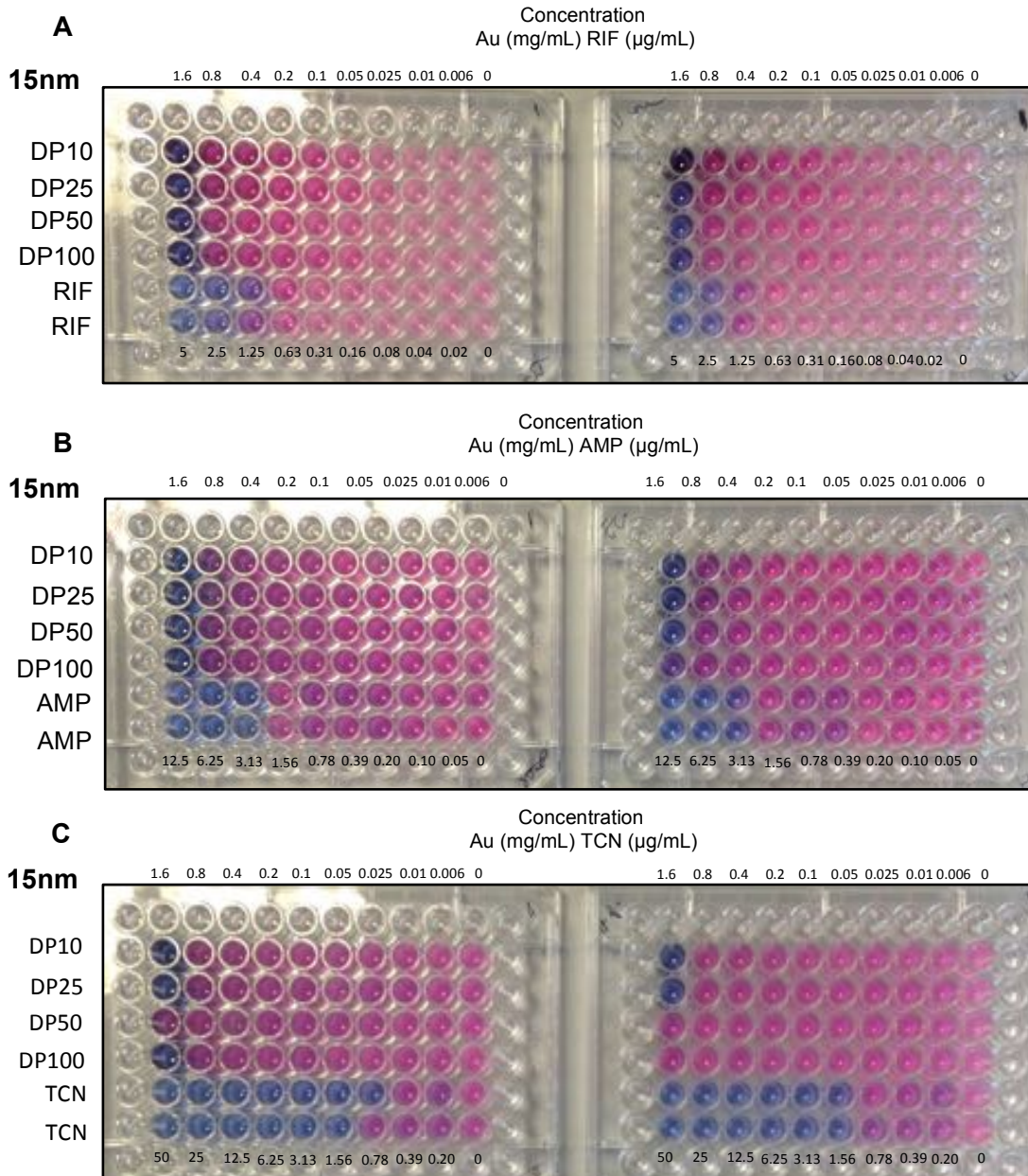


Figure B1. REMA assays with 15nm 100% pDMAEMA-coated nanoparticles. (A) *M. smegmatis*. (B) *E. coli*. (C) *P. putida*. Left – first replicates, right – second replicates.

Appendix C – REMA Assays with 2nm and 5nm polymer-coated AuNP compounds

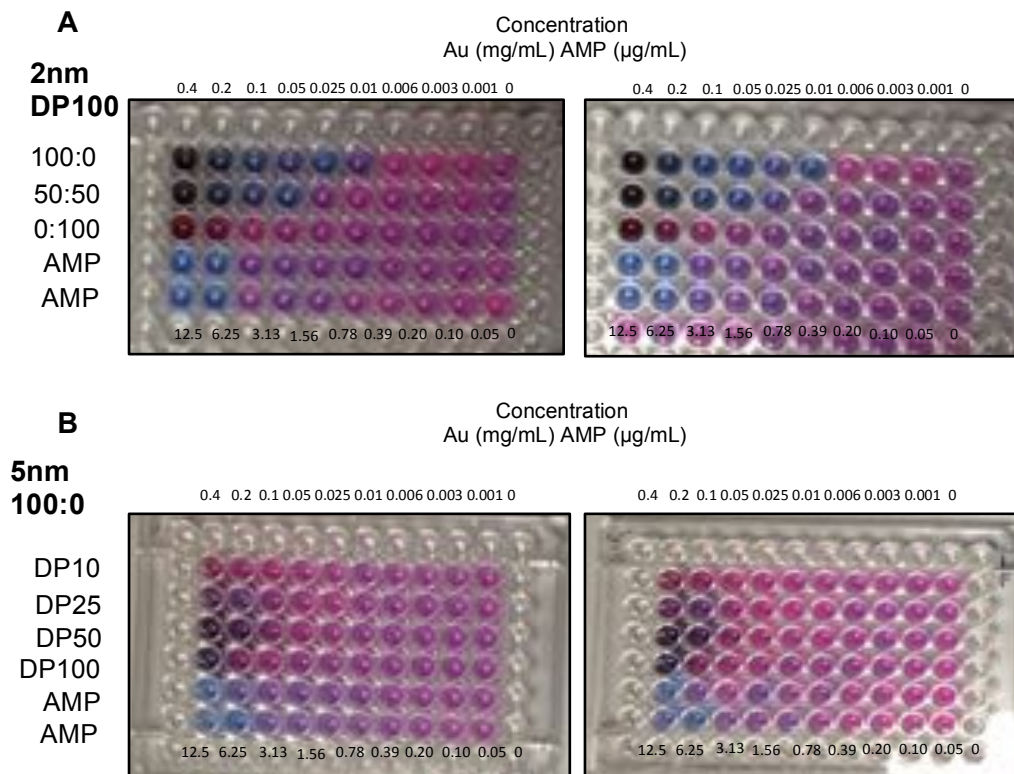


Figure C1. REMA assays with polymer-AuNP conjugates and *E. coli*. (A) 2nm polymer-AuNPs. (B) 5nm polymer-AuNPs. Left – first replicates, right – second replicates.

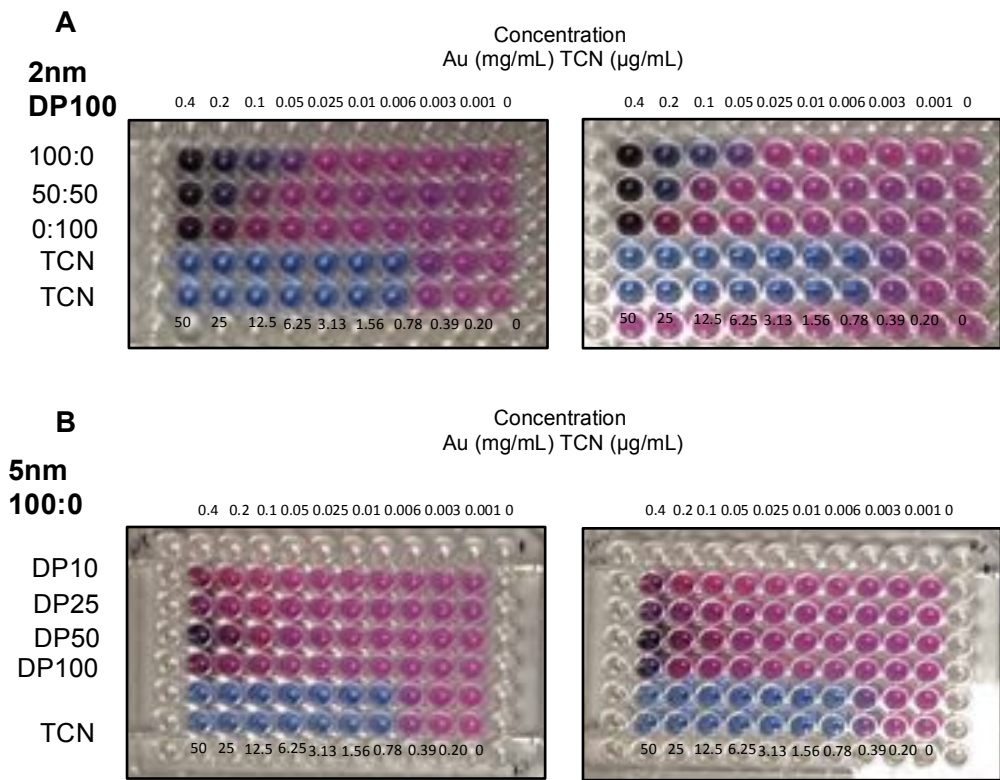


Figure C1. REMA assays with polymer-AuNP conjugates and *P. putida*. (A) 2nm polymer-AuNPs. (B) 5nm polymer-AuNPs. Left – first replicates, right – second replicates.